

**REPUBLIC OF TURKEY  
YILDIZ TECHNICAL UNIVERSITY  
GRADUATE SCHOOL OF NATURAL AND APPLIED SCIENCES**

**THERMOELASTIC STABILITY ANALYSIS OF SOLIDIFICATION  
OF PURE METALS ON A COATED PLANAR MOLD OF FINITE  
THICKNESS: EFFECTS OF THE COATING LAYER**

**MEHMET HAKAN DEMİR**

**Ph.D THESIS  
DEPARTMENT OF MECHANICAL ENGINEERING  
PROGRAM OF MACHINE THEORY AND CONTROL**

**ADVISER  
PROF. DR. FARUK YİĞİT**

**İSTANBUL, 2016**

**REPUBLIC OF TURKEY**  
**YILDIZ TECHNICAL UNIVERSITY**  
**GRADUATE SCHOOL OF NATURAL AND APPLIED SCIENCES**

**THERMOELASTIC STABILITY ANALYSIS OF SOLIDIFICATION  
OF PURE METALS ON A COATED PLANAR MOLD OF FINITE  
THICKNESS: EFFECTS OF THE COATING LAYER**

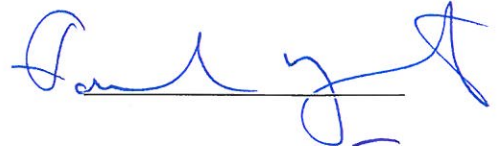
A thesis submitted by Mehmet Hakan DEMİR in partial fulfillment of the requirements for the degree of **DOCTOR OF PHILOSOPHY** is approved by the committee on 29.04.2016 in Department of Mechanical Engineering, Machine Theory and Control Program

**Thesis Adviser**

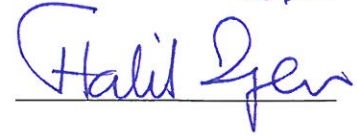
Prof.Dr. Faruk YİĞİT  
Yıldız Technical University

**Approved By the Examining Committee**

Prof.Dr.Faruk YİĞİT  
Yıldız Technical University



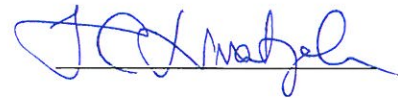
Prof.Dr. Halil ÖZER, Member  
Yıldız Technical University



Prof.Dr. Muammer KALYON, Member  
Istanbul Commerce University



Prof.Dr. Haydar LİVATYALI, Member  
Yıldız Technical University



Prof.Dr. Ata MUĞAN, Member  
Istanbul Technical University



## ACKNOWLEDGEMENTS

---

First of all, I would like to thank my advisor Dr. Faruk YİĞİT for his continuous guidance, support and patience. His constant support and commitment to my intellectual development made this work possible. Working with Dr. Yiğit was one of my most precious experiences in my life. His technical knowledge and constructive criticism can be noticed in every part of this dissertation.

I also wish to acknowledge the insights, suggestions and helpful comments of my committee members Professor Halil ÖZER and Professor Muammer KALYON.

I also would like to thank TÜBİTAK for their doctoral fellowship support during my doctorate.

I am deeply indebted to my mother, my father and my sister for their love and encouragement.

At the end I would like to express my deep gratitude to my wife, the one who supported me in every step of my doctorate with patience and encouragement.

April, 2016

Mehmet Hakan DEMİR

## TABLE OF CONTENTS

---

	Page
LIST OF SYMBOLS .....	viii
LIST OF ABBREVIATIONS.....	x
LIST OF FIGURES .....	xi
LIST OF TABLES.....	xiv
ABSTRACT.....	xv
ÖZET .....	xviii
CHAPTER 1	
1.1 Motivation .....	21
1.2 Literature Review .....	24
1.2.1 Heat Conduction Problem with Phase Change .....	24
1.2.1 Determination Stress Field .....	32
1.2.2 Thermoelastic Stability Analysis .....	35
1.2.3 Mold Coating.....	42
1.3 Industrial Application Areas .....	46
1.4 Thesis Overview .....	48
1.5 Contributions of the Thesis .....	50
CHAPTER 2	
HEAT CONDUCTION PROBLEM .....	52
2.1 Introduction.....	52
2.2 Formulation of the Problem .....	53
2.3 The Perturbation Analysis.....	56
2.4 Solution of the Heat Conduction Problem .....	62
2.4.1 Solution for Zeroth-Order Thermal Problem .....	62

2.4.2 Solution for First-Order Thermal Problem.....	63
CHAPTER 3	
DETERMINATION OF STRESS FIELDS .....	67
3.1 Introduction.....	67
3.2 Solution Procedure.....	67
3.3 Determination of Zeroth Order Stress Field.....	71
3.3.1 Particular Solution $((\sigma_0^i)^p)$ .....	71
3.3.2 Homogeneous Solution $((\sigma_0^i)^h)$ .....	72
3.3.3 Complete Solution $(\sigma_0^i)$ .....	72
3.4 Determination of first order stress field .....	73
3.4.1 Particular Solution $((\sigma_1^i)^p)$ .....	73
3.4.2 Homogeneous Solution $((\sigma_1^i)^h)$ .....	75
3.4.3 Complete Solution $\sigma_1^i$ .....	78
CHAPTER 4	
NUMERICAL SOLUTION.....	84
4.1 Dimensionless Presentation .....	84
4.2 Solution Method.....	88
CHAPTER 5	
STABILITY ANALYSIS OF THERMOELASTIC CONTACT.....	90
5.1 Introduction.....	90
5.2 Effects of the System Parameters.....	90
5.2.1 Effects of thermal conductivity of coating material.....	91
5.2.2 Effect of thickness of the mold coating layer, $(U)$ .....	99
5.2.3 Effect of zeroth order thermal contact resistances at shell/coating and coating/mold interfaces $(R$ and $R_m)$ .....	111
5.2.4 Effect of wavelength $(\lambda)$ .....	121
5.3 A case study .....	122
5.3.1 Properties of selected materials.....	122
5.3.2 Effect of coating layer material .....	124
5.3.3 Effect of Thickness of the Coating Layer .....	130
5.3.4 Effect of Coupling Rates .....	137

## CHAPTER 6

SUMMARY AND CONCLUSIONS .....	143
6.1 Summary .....	143
6.2 Conclusions .....	144
6.3 Future Works.....	147
REFERENCES .....	149
CURRICULUM VITAE.....	161

## LIST OF SYMBOLS

---

$u$	thickness of the mold
$h$	thickness of the coating layer
$Q$	heat flux
$K$	thermal conductivity
$L$	latent heat
$R^T$	thermal contact resistance at shell/coating interface
$R_m^T$	thermal contact resistance at coating/mold interface
$m$	wave number
$P$	contact pressure
$p$	value of the contact pressure
$T$	temperature
$t$	time
$T_m$	melting temperature
$s$	solidified shell thickness
$x,y$	Cartesian coordinates
$E$	Young's modulus
$R'$	sensitivity of contact resistance to contact pressure at shell/coating interface
$R'_m$	sensitivity of contact resistance to contact pressure at coating/mold interface
$g$	residual stress function
$f$	displacement potential function
$H$	dimensionless thickness of the mold
$U$	dimensionless thickness of the coating layer
$S$	dimensionless shell thickness
$X,Y$	dimensionless Cartesian coordinates
$\beta$	dimensionless time
$\bar{T}$	dimensionless temperature
$\bar{Q}$	dimensionless heat flux
$\bar{P}$	dimensionless contact pressure
$G$	dimensionless residual stress function
$R$	dimensionless thermal contact resistance at shell/coating interface
$R_m$	dimensionless thermal contact resistance at coating/mold interface
$\bar{R}'$	dimensionless sensitivity of contact resistance to contact pressure at shell/coating interface
$\bar{R}'_m$	dimensionless sensitivity of contact resistance to contact pressure at coating/mold interface
$\lambda$	wavelength
$\zeta_1$	thermal conductivity ratio between solidified shell and coating materials
$\zeta_2$	thermal conductivity ratio between coating and mold materials

$\rho$	density
$\alpha$	thermal expansion coefficient
$\nu$	Poisson's ratio
$\sigma$	stress
$\delta$	thermal distortivity
$\emptyset$	displacement potential function
$\Phi$	Airy stress function

#### Superscript

b,c,d	coating layer, solidified shell and mold, respectively
p	particular solution
h	homogeneous solution

#### Subscript

0,1	zeroth and first order quantities, respectively
-----	---



## **LIST OF ABBREVIATIONS**

---

ALE	Arbitrarian Lagrangian Eulerian
FEM	Finite Element Method
HTC	Heat Transfer Coefficient
PF	Phase Field

## LIST OF FIGURES

	Page
Figure 1.1	A photograph of uneven shell growth during aluminum casting ..... 22
Figure 1.2	Closed loop mechanism during the solidification process ..... 23
Figure 1.3	Uncoupled process block diagram..... 36
Figure 1.4	Coupled process block diagram..... 36
Figure 2.1	Geometry of the system ..... 53
Figure 2.2	Typical experimental results for the variation of thermal contact resistance with contact pressure ..... 56
Figure 2.3	Reducing order of the problem by using linear perturbation method..... 57
Figure 5.1	Comparison of the developed model with the limiting case in Yigit [107] ..... 91
Figure 5.2	Maximum amplitude of perturbation in solidification front as a function of $\zeta_1$ for selected values of coating thickness and $\zeta_3$ when $\bar{R}' = -1$ , $\bar{R}'_m = -1$ ..... 92
Figure 5.3	Maximum amplitude of perturbation in solidification front as a function of $\zeta_1$ for selected values of coating thickness and $\zeta_3$ when $\bar{R}' = -100$ , $\bar{R}'_m = -1$ ..... 93
Figure 5.4	Maximum amplitude of perturbation in solidification front as a function of $\zeta_1$ for selected values of coating thickness and $\zeta_3$ when $\bar{R}' = -1$ , $\bar{R}'_m = -100$ ..... 94
Figure 5.5	Maximum amplitude of perturbation in solidification front as a function of $\zeta_1$ for selected values of coating thickness and $\zeta_3$ when $\bar{R}' = -100$ , $\bar{R}'_m = -100$ ..... 95
Figure 5.6	Maximum amplitude of perturbation in solidification front as a function of $\zeta_1$ for selected values of coating thickness and $\zeta_2$ when $\bar{R}' = -1$ , $\bar{R}'_m = -1$ ..... 96
Figure 5.7	Maximum amplitude of perturbation in solidification front as a function of $\zeta_1$ for selected values of coating thickness and $\zeta_2$ when $\bar{R}' = -100$ , $\bar{R}'_m = -1$ ..... 97
Figure 5.8:	Maximum amplitude of perturbation in solidification front as a function of $\zeta_1$ for selected values of coating thickness and $\zeta_2$ when $\bar{R}' = -1$ , $\bar{R}'_m = -100$ ..... 98
Figure 5.9	Maximum amplitude of perturbation in solidification front as a function of $\zeta_1$ for selected values of coating thickness and $\zeta_2$ when $\bar{R}' = -100$ , $\bar{R}'_m = -100$ ..... 99
Figure 5.10	Perturbation in solidification front as a function of $S_0(\beta)$ for selected values of $U$ when $\bar{R}' = -1$ , $\bar{R}'_m = -1$ , $\zeta_1 = 0.1$ , $\zeta_2 = 0.1$ ..... 100

Figure 5.11	Perturbation in solidification front as a function of $S_0(\beta)$ for selected values of $U$ when $\bar{R}' = -1, \bar{R}'_m = -1, \zeta_1 = 2, \zeta_2 = 0.1$ .....	101
Figure 5.12	Perturbation in solidification front as a function of $S_0(\beta)$ for selected values of $U$ when $\bar{R}' = -1, \bar{R}'_m = -1, \zeta_1 = 0.1, \zeta_2 = 2$ .....	102
Figure 5.13	Perturbation in solidification front as a function of $S_0(\beta)$ for selected values of $U$ when $\bar{R}' = -1, \bar{R}'_m = -1, \zeta_1 = 2, \zeta_2 = 2$ .....	103
Figure 5.14	Perturbation in solidification front as a function of $S_0(\beta)$ for selected values of $U$ when $\bar{R}' = -100, \bar{R}'_m = -1, \zeta_1 = 0.1, \zeta_2 = 0.1$ .....	104
Figure 5.15	Perturbation in solidification front as a function of $S_0(\beta)$ for selected values of $U$ when $\bar{R}' = -100, \bar{R}'_m = -1, \zeta_1 = 2, \zeta_2 = 0.1$ .....	105
Figure 5.16	Perturbation in solidification front as a function of $S_0(\beta)$ for selected values of $U$ when $\bar{R}' = -100, \bar{R}'_m = -1, \zeta_1 = 0.1, \zeta_2 = 2$ .....	106
Figure 5.17	Perturbation in solidification front as a function of $S_0(\beta)$ for selected values of $U$ when $\bar{R}' = -100, \bar{R}'_m = -1, \zeta_1 = 2, \zeta_2 = 2$ .....	107
Figure 5.18	Perturbation in solidification front as a function of $S_0(\beta)$ for selected values of $U$ when $\bar{R}' = -1, \bar{R}'_m = -100, \zeta_1 = 0.1, \zeta_2 = 0.1$ .....	108
Figure 5.19	Perturbation in solidification front as a function of $S_0(\beta)$ for selected values of $U$ when $\bar{R}' = -1, \bar{R}'_m = -100, \zeta_1 = 2, \zeta_2 = 0.1$ .....	109
Figure 5.20	Perturbation in solidification front as a function of $S_0(\beta)$ for selected values of $U$ when $\bar{R}' = -1, \bar{R}'_m = -100, \zeta_1 = 0.1, \zeta_2 = 2$ .....	109
Figure 5.21	Perturbation in solidification front as a function of $S_0(\beta)$ for selected values of $R$ when $H = 4, U = 0.5, \bar{R}' = -1, \bar{R}'_m = -1, \zeta_1 = 0.1, \zeta_2 = 0.1$ and $R_m = 0.01$ .....	112
Figure 5.22	Perturbation in solidification front as a function of $S_0(\beta)$ for selected values of $R$ when $H = 4, U = 0.5, \bar{R}' = -1, \bar{R}'_m = -1, \zeta_1 = 2, \zeta_2 = 0.1$ and $R_m = 0.01$ .....	113
Figure 5.23	Perturbation in solidification front as a function of $S_0(\beta)$ for selected values of $R$ when $H = 4, U = 0.5, \bar{R}' = -1, \bar{R}'_m = -1, \zeta_1 = 0.1, \zeta_2 = 2$ and $R_m = 0.01$ .....	113
Figure 5.24	Perturbation in solidification front as a function of $S_0(\beta)$ for selected values of $R$ when $H = 4, U = 0.5, \bar{R}' = -1, \bar{R}'_m = -1, \zeta_1 = 2, \zeta_2 = 2$ and $R_m = 0.01$ .....	114
Figure 5.25	Perturbation in solidification front as a function of $S_0(\beta)$ for selected values of $R$ when $H = 4, U = 0.5, \bar{R}' = -100, \bar{R}'_m = -1, \zeta_1 = 0.1, \zeta_2 = 0.1$ and $R_m = 0.01$ .....	115
Figure 5.26	Perturbation in solidification front as a function of $S_0(\beta)$ for selected values of $R$ when $H = 4, U = 0.5, \bar{R}' = -100, \bar{R}'_m = -1, \zeta_1 = 2, \zeta_2 = 0.1$ and $R_m = 0.01$ .....	116
Figure 5.27	Perturbation in solidification front as a function of $S_0(\beta)$ for selected values of $R$ when $H = 4, U = 0.5, \bar{R}' = -100, \bar{R}'_m = -1, \zeta_1 = 0.1, \zeta_2 = 2$ and $R_m = 0.01$ .....	117
Figure 5.28	Perturbation in solidification front as a function of $S_0(\beta)$ for selected values of $R$ when $H = 4, U = 0.5, \bar{R}' = -100, \bar{R}'_m = -1, \zeta_1 = 2, \zeta_2 = 2$ and $R_m = 0.01$ .....	118
Figure 5.29	Perturbation in solidification front as a function of $S_0(\beta)$ for selected values of $R_m$ when $H = 4, U = 0.5, \bar{R}' = -1, \bar{R}'_m = -1, \zeta_1 = 0.1, \zeta_2 = 0.1$ and $R = 0.01$ .....	119

Figure 5.30	Perturbation in solidification front as a function of $S_0(\beta)$ for selected values of $R_m$ when $H = 4$ , $U = 0.5$ , $\bar{R}' = -100$ , $\bar{R}'_m = -1$ , $\zeta_1 = 0.1$ , $\zeta_2 = 0.1$ and $R = 0.01$ .....	120
Figure 5.31	Effect of the wavelength on the growth of the perturbation when $H = 4$ , $U = 0.5$ , $\zeta_1 = 2$ , $\zeta_2 = 0.1$ , $\bar{R} = 0.5$ , $\bar{R}_m = 0.5$ , $\bar{R}'_h = -300$ and $\bar{R}'_{hm} = -300$ .....	122
Figure 5.32	Perturbation in the solidification front as a function of $s_0(t)$ for various values of $u$ and Al-Fe-Cu material combination when $R' = R'_m = -10^{-14}m^2sec^oC/J.Pa$ .....	131
Figure 5.33	Perturbation in the solidification front as a function of $s_0(t)$ for various values of $u$ and Al-Fe-Cu material combination when $R' = -10^{-12}m^2sec^oC/J.Pa$ , $R'_m = -10^{-14}m^2sec^oC/J.Pa$ .....	132
Figure 5.34	Perturbation in the solidification front as a function of $s_0(t)$ for various values of $u$ and Al-Fe-Cu material combination when $R' = -10^{-14}m^2sec^oC/J.Pa$ , $R'_m = -10^{-12}m^2sec^oC/J.Pa$ .....	133
Figure 5.35	Perturbation in the solidification front as a function of $s_0(t)$ for various values of $u$ and Al-Fe-Cu material combination when $R' = R'_m = -10^{-12}m^2sec^oC/J.Pa$ .....	134
Figure 5.36	Perturbation in the solidification front as a function of $s_0(t)$ for various values of $u$ and Al-Al-Cu material combination when $R' = -10^{-14}m^2sec^oC/J.Pa$ , $R'_m = -10^{-12}m^2sec^oC/J.Pa$ .....	136
Figure 5.37	Perturbation in the solidification front as a function of $s_0(t)$ for various values of $u$ and Al-Al-Cu material combination when $R' = R'_m = -10^{-12}m^2sec^oC/J.Pa$ .....	137
Figure 5.38	Perturbation in the solidification front as a function of $s_0(t)$ for various values of $R'$ and Al-Fe-Cu material combination when $u = 1\text{ mm}$ and $R'_m = -10^{-14}m^2sec^oC/J.Pa$ .....	138
Figure 5.39	Perturbation in the solidification front as a function of $s_0(t)$ for various values of $R'_m$ and Al-Fe-Cu material combination when $u = 1\text{ mm}$ and $R' = -10^{-14}m^2sec^oC/J.Pa$ .....	139
Figure 5.40	Perturbation in the solidification front as a function of $s_0(t)$ for various values of $R'$ and Al-Al-Cu material combination when $u = 1\text{ mm}$ and $R'_m = -10^{-14}m^2sec^oC/J.Pa$ .....	140
Figure 5.41	Perturbation in the solidification front as a function of $s_0(t)$ for various values of $R'$ and Al-Al-Cu material combination when $u = 10\text{ mm}$ and $R'_m = -10^{-14}m^2sec^oC/J.Pa$ .....	141

## LIST OF TABLES

---

Table 5.1	Material properties at fusion temperature.....	123
Table 5.2	Coating material effect on $s_1^m$ , $s_0^m$ and $t^m$ values under different coupling rates for aluminium solidifies on a copper mold with coating of 1 <i>mm</i> thickness.....	125
Table 5.3	Coating material effect on $s_1^m$ , $s_0^m$ and $t^m$ values under different coupling rates for aluminium solidifies on an iron mold with coating of 1 <i>mm</i> thickness.....	128

## ABSTRACT

---

# **THERMOELASTIC STABILITY ANALYSIS OF SOLIDIFICATION OF PURE METALS ON A COATED PLANAR MOLD OF FINITE THICKNESS: EFFECTS OF THE COATING LAYER**

Mehmet Hakan DEMİR

Department of Mechanical Engineering

Ph.D. Thesis

Adviser: Prof. Dr. Faruk YİĞİT

During the solidification process, initially liquid material is started to solidify when its temperature reduce below its melting temperature by heat transfer from its surfaces which are in contact with a surrounding mold. Therefore the solidification process starts with the formation of the solid at the surfaces of the mold and spreads all of the liquid mass as the time progressed. The heat transfer from liquid to mold continues until all liquid mass solidify. If the process is interrupted and remaining liquid is drawn away from the process, some periodic variations are observed on the thickness of the solidified shell. This undulatory structure is seen in the solidification of many metals as inevitable result of cooling. Such uneven undulations are not desirable in the manufacturing because the associated thermal distortions in the solidified shell cause severe cracks in the solidified ingot. Undesirable cracks have significant effects on the strength and microscopic structure of the ingot and according to this the final product has poor quality. If the solidification is not interrupt, at the end of the process the periodic variations at the freezing front tends to die out since the conditions at the liquid/solid interface becomes less dependent upon the conditions at the mold/shell interface due to the increasing of the solidified shell thickness. These non-uniform undulations are occurred as a consequence of the non-uniform heat extraction along the mold/shell interface. There is some thermal resistance at this interface due to the surface roughness and contaminants films. Thermal contact resistance is changed as a function of contact pressure. There is an inverse proportion between the contact pressure and thermal resistance. The non-uniform temperature and stress fields in the solidified material and mold associated with non-uniform heat extraction cause thermal distortions in the casting and mold. Thermal distortions have a great influence on the contact pressure at the shell/mold interface. As it seen the thermal and mechanical problems

must be investigated together and the system behaves like a positive feedback system, therefore it may have potential to being unstable.

The purposes of this thesis are that investigating the instability mechanism in the solidification process during casting of pure metals and improving our knowledge about this thermo-elastic instability mechanism, determining the conditions which eliminate or minimize the profile defects such as cracks in the surface and internal structure of casting product associated with the coupled thermo-mechanic events, analyzing the effects of coating layer and other system parameters on the solidification process and specify the conditions which improve the quality of product. The fluid flow in the melt metal, adjusting the freezing range of the metal, solidification rate of the continuous casting process and superheat of the melted metal affect the non-uniform structure at the moving interface. But researches about the solidification process show that undulations depend considerably the geometry of the mold/shell interface. Mold coating at the mold-shell interface is one of the most important factors controlling the heat transfer and, hence, it has very important role on the solidification rate and development of microstructure. Other advantages of coating layer protecting the mold during the casting process because of expensiveness of the mold manufacturing technology and the additional manufacturing requirements are prevented before the using of final product by controlling the unstable growth of the solidified shell. At the end coating layer affects the quality of casting and provides energy, time and workforce savings. In this study thermal and mechanical problems are coupled through the contact pressure dependent thermal contact resistance at the coating/shell interface. The thermal diffusivities of the mold, coating and solidified shell materials are assumed infinitely large. The physical meaning of this assumption is that the thermal capacities of the materials of the mold, coating and shell are zero. This assumption is correct at the beginning of the solidification since the materials properties have no significant effects on the process and it allows us to solve the heat conduction problem analytically because the temperature distributions in the each layer changes linearly in space coordinate. The model is restricted to the solidification of pure metals and the solidification occurs at a distinct temperature. Therefore, there is a sharp interface between solid and liquid phases, no mushy zone occurs. For modeling the changes in the heat flux drawn from the lower surface of the mold, small spatial perturbations are added and amplitude of this perturbation are much small than its wavelength. The liquid initially at its melting temperature and the liquid phase is assumed to be at constant hydrostatic pressure. The determination of the stress distribution in the solidified layer is very complex, because the material is continually being solidified while the solid is in a deformed state, and therefore the final cast product exhibits residual stress, even after the temperature has been reduced to zero. Linear constitutive model has been employed which assumes the behavior of the solidified material to be elastic during solidification. Thermo-elastic displacement potential and Airy stress function are used to obtain particular solution and homogeneous solutions of the stress fields in each layer, respectively. Linear perturbation method is used to obtain the governing equations of solidification problem on coated planar mold of finite thickness. Two-dimensional problem is modelled with two one dimensional problem called as zeroth and first order problem. Zeroth order solution is the nonlinear unperturbed solution of the problem. As long as the perturbation is small compared with the zeroth order values, the perturbation will be linear. The zeroth and first order problems involve fields varying in only one spatial dimension and time, they are considerably easier to implement and more efficient computationally than a full two-dimensional numerical solution of the solidification problem. After the modeling of thermal and mechanical problems with

respect to thermal and mechanical boundary conditions, two second-order differential equations with variable coefficients which involving amplitude of perturbation at the moving interface, its time derivative, residual stress and its derivative with respect to mean shell thickness. The problem solve in dimensionless form for generality of the solution. These equations are written in state-space form and solving simultaneously with the given initial conditions. A variable step variable-order predictor-corrector algorithm is used to solve this stiff problem. The effects of the system parameters such as thickness of the coating layer and mold, thermal conductivity ratio between the solidified shell material and coating material, thermal conductivity ratio between the coating material and mold material, coupling between thermal and mechanical problems at the interfaces between solidified shell, coating and mold on the growth of the solidified shell thickness are investigated. The results of this study use in the development of the numerical solution of general problem with adding thermal diffusivities, as well as in providing an initial conditions for the general case and use to control validity of the numerical solution.

**Keywords:** Solidification of pure metals, thermoelastic instability, metal casting, mold coating, phase change problems, linear perturbation method



## ÖZET

### **KATILAŞMA SÜRECİNDE GÖZLEMLENEN KARARSIZLIK MEKANİZMASININ ANALİZİ: KALIP YÜZEYİ KAPLAMA TABAKASININ ETKİLERİ**

Mehmet Hakan DEMİR

Makine Teorisi ve Kontrol Anabilim Dalı

Doktora Tezi

Tez Danışmanı: Prof. Dr. Faruk YİĞİT

Katılma süreci sırasında başlangıçta sıvı halde bulunan malzeme kendisini çevreleyen kalıp ile temas halindeki yüzeylerden gerçekleşen ısı transferi ile sıcaklığının erime sıcaklığının altına düşmesiyle katı hale geçmeye başlar. Bu sebepten katılma süreci kalıp yüzeylerinde oluşan katı oluşumu ile başlar ve tüm sıvı kütlesine yayılarak devam eder. Sıvıdan kalıba olan ısı transferi tüm sıvı katılma sürecine kadar devam eder. Eğer katılma süreci katılma devam ederken kesilip, katılmayan sıvı prosesten uzaklaştırılırsa katılmış malzemenin kalınlığında periyodik değişimler gözlemlenir. Bu dalgalı yapı üniform olmayan soğumanın kaçınılmaz sonucu olarak birçok metalin katılması sırasında görülür. Katılmış kabuğun bu tip düzensiz büyümesi üretimde, bununla ilişkili olan katılmış kabuktaki termal bozunumların katılan parçada ciddi çatlaklar oluşturması nedeniyle istemeyen bir durumdur. Bu çatlaklar katılan malzemenin mukavemetini, mikroskobik yapısını ve buna bağlı olarak katılma sonucu oluşan parçanın kalitesini önemli ölçüde etkilemektedir. Katılma kesilmeyip bitmesi sağlandığında ise katı/sıvı fazları arasındaki periyodik değişimler, katılan malzeme kalınlığının artmasıyla katı/sıvı ara yüzeyindeki koşulların kalıp ile katılmış malzeme arasındaki koşullara olan ilişkisinin azalması nedeniyle zaman ilerledikçe kaybolacaklardır. Katı ve sıvı fazları arasındaki bu üniform olmayan dalgalanmalar kalıp ile katı malzeme arasındaki yüzeyden olan ısı çıkışının düzensiz yapısı sebebiyle ortaya çıkmaktadır. Bu yüzeyde genelde yüzey pürüzlülüğü ve kirlenici filmlere bağlı olarak termal temas dirençleri mevcuttur. Bu termal temas direnci temas basıncına ters orantılı olarak değişir ve basınç artarsa azalma eğilimi gösterir. Prosesten düzensiz ısı çıkışına bağlı olarak hem katılan malzeme hem de kalıp içerisinde üniform olmayan sıcaklık ve gerilme alanlarının oluşur. Bu düzensiz termal

ve gerilme alanları kalıp ve katılaşılan malzemede termal bozunumların meydana gelmesine neden olur ve bu bozunumların kalıp ile katılaşılan malzeme arasındaki yüzeydeki temas basıncı üzerinde büyük etkisi vardır. Temas basıncının değişimi termal temas direncini etkiler ve buna bağlı olarak ısı akısı değişir. Anlaşılacağı gibi bu problemde termal ve mekanik olaylar birbirine bağlı olarak gerçekleşmektedir. Dolayısıyla problemin komple bir sistem olarak incelenmesi gerekmektedir. Bu birbirine bağlı sistem bir pozitif geri besleme mekanizmasına sahiptir ve bu sebepten dolayı kararsız olma potansiyeli bulunmaktadır. Sistem faz değişimli ısı transferi, gerilme alanlarının belirlenmesi ve termoelastik kararlılık analizi olarak üç kısımda incelenir.

Yapılan tezin amacı saf metallerin katılaşması prosesindeki kararsızlık mekanizmasını araştırmak ve bu termoelastik kararsızlık hakkındaki bilgileri arttırmak, birbiriyle bağıntılı termo-mekanik olaylar sonucunda döküm parçasının iç yapısı ve dış yüzeylerinde oluşan çatlaklar gibi profil hatalarını elimine ya da minimize edecek koşulları belirlemek ve kalıp üzerine eklenen kaplama tabakasının ve diğer sistem parametrelerinin katılaşma prosesi üzerindeki etkisini incelemek ve son ürünün kalitesini arttırmak için koşulları belirlemektir. Katı-sıvı ara yüzeyindeki oluşan bu dalgalanmaya, temas basıncının yanında eriyik metal içindeki sıvı akışı, metalin donma aralığının ayarlanması, sürekli döküm prosesleri için katılaşma hızı ve erimiş metalin süper ısıtma derecesi gibi faktörler de etki etmektedir. Yapılan çalışmalar bu dalgalanmanın önemli ölçüde kalıp ile katılaşılan malzeme arasındaki ara yüzeyin geometrisine bağlı olduğunu göstermiştir. Farklı kalıp topografileriyle yapılan deneyler sonucunda bu kalıp/katılaşmış katman arasında oluşan hava boşluklarının oluşma zamanlarının ve yerlerinin seçilerek ya da ayarlanarak daha düzgün bir yapıya sahip katılaşma elde edilebileceği kanıtlanmıştır. Kalıp kaplaması prosesinden olan ısı çıkışını kontrol etmek için en çok kullanılan yöntemlerden biridir. Bu yüzden katılaşma derecesinin ve mikro yapının oluşması üzerinde önemli bir rol oynamaktadır. Kalıp kaplaması tekniği sanayide üretimde sık kullanılan bir tekniktir. Kalıp kaplaması ısı çıkışını kontrolünü sağlayıp daha üniform bir büyüme sağlar ve kalitesi yüksek ürünlerin döküm sürecinden çıkmasına yardımcı olur. Bu da üreticinin oluşan ürünün atılması ya da başka bir amaca yönelik kullanmak için herhangi bir ek işleme gerek kalmamasına yardımcı olur. Böylece zaman, enerji, iş gücü ve malzeme sarfıyatı azaltılmış olur. Ayrıca kalıp üretim teknolojisinin pahalı bir teknoloji olması nedeniyle kaplama katmanının kalıbı koruyucu bir faydası da vardır. Bu çalışmada termal ve mekanik problemler basınca bağlı termal temas direnci aracılığıyla bağıntılı (birleşik) olarak ele alınmıştır. Kalıp, kaplama katlaması ve katılaşmış malzemenin termal difüzyonları sonsuz büyük kabul edilmiştir. Bu kabulün fiziksel olarak kalıp, kaplama ve katılaşmış kabuk malzemelerinin termal kapasitelerinin sıfır olduğu anlamına gelir. Bu kabul prosesin başlangıcında kısa bir evre için malzeme özelliklerinin proses üzerindeki etkisinin çok az olması nedeniyle doğru bir kabuldür ve kalıp, kaplama katmanı ve katılaşmış kabuk içerisindeki sıcaklık dağılımlarının değişimi uzay koordinat sisteminde doğrusal bir hale gelir. Böylece ısı transferi probleminin analitik olarak çözülmesi mümkün olmaktadır. Oluşturulan matematiksel model saf metallerin katılaşması ile sınırlandırılmıştır ve böylece katılaşmanın belirli bir sıcaklık değerinde meydana geldiği ve katı/sıvı arasındaki hareketli ara yüzeyin keskin ve belirgin bir yapıda olduğu varsayılmıştır. Başlangıçta sıvının sıcaklığı erime sıcaklığına eşittir ve sıvı fazın sabit hidrostatik basınca sahip olduğu kabul edilmiştir. Malzemelerin fiziksel özellikleri sıcaklığa bağlı olarak değişmemektedir. Faz değişimli ısı transferi problemi analitik olarak çözülür. Katılaşmış metal içerisindeki gerilme alanlarının belirlenmesi katı deforme olmuş durumda iken katılaşmanın devam etmesi nedeniyle karmaşık bir

işlemdir. Katılma sona erdikten sonra final ürünü kalıcı durum sıcaklığına ulaştığında içerisinde artık gerilmeler içerir. Bu gerilmelerin modellenmesi sırasında katılma sırasında katılan malzemenin elastik davrandığı varsayılan doğrusal yapısal model kullanılmıştır. Katmanlardaki gerilme alanları homojen ve özel çözüm olmak üzere iki kısımdan oluşmaktadır. Özel çözümü bulmak için Termoelastik yerdeğiştirme potansiyeli, homojen çözüm için ise Airy gerilme fonksiyonu kullanılmıştır. Sonlu kalınlığa sahip kaplanmış kalıp üzerinde saf metallerin katılma probleminin modellenmesi için doğrusal pertürbasyon metodu kullanılmıştır. İki boyutlu model bu metot aracılığıyla sıfırıncı ve birinci dereceden problem olmak üzere iki adet tek boyutlu probleme indirgenmiş ve bu problemlerin çözümü iki boyutlu problemin çözümünden daha verimli ve hızlı bir çözüm getirmektedir. Termal ve mekanik problemler sınır koşullarına bağlı olarak modellendikten sonra, birleşik katılma modeli için iki adet değişken katsayılı iki dereceden adi diferansiyel denklem elde edilir. Bu denklemler hareketli arayüzdeki pertürbasyonların genliği ve bu genliğin zamana göre türevi ile katılmış kabukta oluşan artık gerilmeleri ve bu gerilmelerin uzay değişkenine göre birinci ve ikinci dereceden türevlerini içermektedir. Problem çözümün genelleştirilmesi için boyutsuz olarak çözülmüştür. Elde edilen boyutsuz denklemler durum uzayı formunda yazılarak, belirlenen başlangıç koşulları doğrultusunda eş zamanlı olarak çözülür. Bu rijit katılma problemin nümerik çözümü için değişken adımlı değişken dereceli tahmin ve doğrulama algoritması kullanılmıştır. Çözüm elde edildikten sonra kaplama katmanının ve kalıbın kalınlığı, katılan malzeme ile kaplama katmanı malzemesinin termal kondüktivitelerinin oranı, kaplama malzemesi ile kalıp malzemesinin termal kondüktivitelerinin oranı, katmanlar arasındaki yüzeylerdeki termal ve mekanik problemlerin birleşme (coupling) derecesi gibi sistem parametrelerinin katılmış malzeme kalınlığının büyümesi üzerindeki etkileri incelenmiştir. Bu çalışma sonucunda elde edilen sonuçlar daha genelleştirilmiş model olan malzeme termal difüsitelerinin hesaba katıldığı problemin nümerik çözümünde başlangıç koşulu olarak ve bu nümerik çözümün doğruluğunun kontrolünü yapmak amacıyla kullanılacaktır.

**Anahtar Kelimeler:**Saf metallerin katılması, termoelastik kararsızlık, metallerin dökümü, kalıp kaplaması, faz değişimli problemler, doğrusal pertürbasyon metodu

## CHAPTER 1

---

### INTRODUCTION

#### 1.1 Motivation

Solidification problems has a great importance in many engineering applications such as casting of pure metals and alloys, welding, freezing of foods, enzymes and tissues and many others applications. Casting process involves solidification of melted metals and alloys in a surrounding mold. The dimensions of the parts produced by the casting are changed from a few millimeters to a few meters and their weight is varied from a few grams to a few tons. On the other hand casting is suitable method for manufacturing of the products which have internal spaces, complex shapes with curved surfaces or consisting of several parts. The materials, which are hard to processing in machining or have low deformation ability, can be forms only through casting. Because of these obvious advantages, casting has a great importance in manufacturing methods.

For analyzing casting process and the microstructure of the final cast product, it is necessary to investigate the solidification process. During the solidification process, an initially liquid mass of material is started to solidify in the surrounding mold through its temperature reduces below its melting temperature due to heat transfer from its surfaces to mold. Generally solidification process begins with formation of shell in contact with the mold and spreads entire of the liquid mass as time progressed and heat transfer from solidified shell to surrounding mold continues until all liquid mass solidifies. If the solidification process is interrupted and remaining liquid is drawn away from the process, some periodic variations are observed at the moving interface between solid and liquid phases. This undulatory growth of shell is generally occurred due to the observed non-uniform cooling profile during the solidification of most metals. Such uneven undulations at the freezing front are not desirable in the manufacturing process because they will cause severe structural faults in the cast product such as micro and

macro cracks. For example Figure 1.1 shows the photograph of the casting in an interrupted process in which the remaining liquid has been drained away. The sinusoidal variations at the freezing front are seen clearly in this figure. The thickness of the solidified layer exhibits serious periodic non uniformities. These undesirable cracks have significant effects on the strength, microscopic structure, quality and usability of the casting product. Therefore, preventing unstable growth during the solidification is important for saving of energy, time, raw materials and cost. If the solidification is allowed to proceed, these periodical variations tend to die out and a planar surface is observed on the cast. The reason of the disappearing of the undulatory structure is that the conditions at the moving interface between solid and liquid phases becomes less dependent upon the conditions at shell/mold interface due to increasing in shell thickness. The question to be answered is that what the underlying mechanisms are behind occurred growth instability during the casting process.

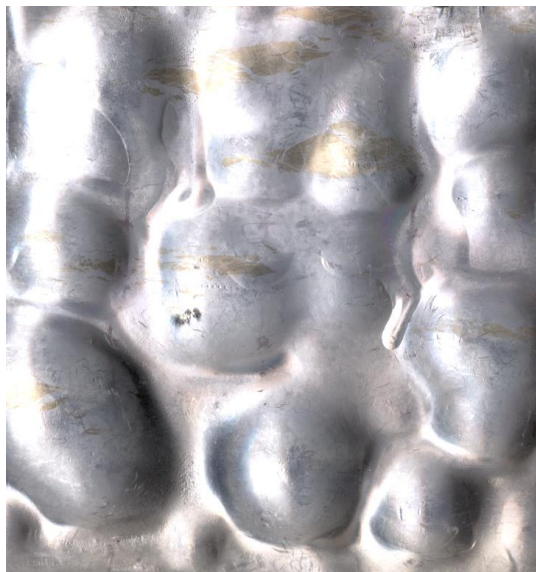


Figure 1.1 A photograph of uneven shell growth during aluminum casting

These non-uniform undulations are occurred as a consequence of the non-uniform heat extraction along the shell/mold interface. Heat transfers from solidified shell to mold by conduction and heat flux rate at the interface between solidified shell and mold is significantly dependent on the conditions at this interface. There are some thermal contact resistances at shell/mold interface due to surface roughness and other contaminant films. These thermal contact resistances are changed as a function of contact pressure. If contact pressure increases at a local region of this surface, thermal contact resistance reduce at this region and therefore, the conducted heat flux at these

regions increases and the melting liquid above this region solidifies faster. Vice versa if the contact pressure decreases, thermal contact resistance increase and inversely the liquid material above the region solidifies slower. Solidifying melting material faster in one region than the other region causes observed undulatory structure at the solid/liquid interface. The non-uniform temperature and stress fields in the solidified material and mold associated with non-uniform heat extraction cause thermal distortions in the casting and mold. Contact pressure changes locally at the shell/mold surfaces depending on these thermal distortions. The closed loop mechanism of the solidification process is shown in Figure 1.2. As it is seen the thermal and mechanical problems must be investigated together and the system behaves like a positive feedback system, therefore it may have potential to being unstable.

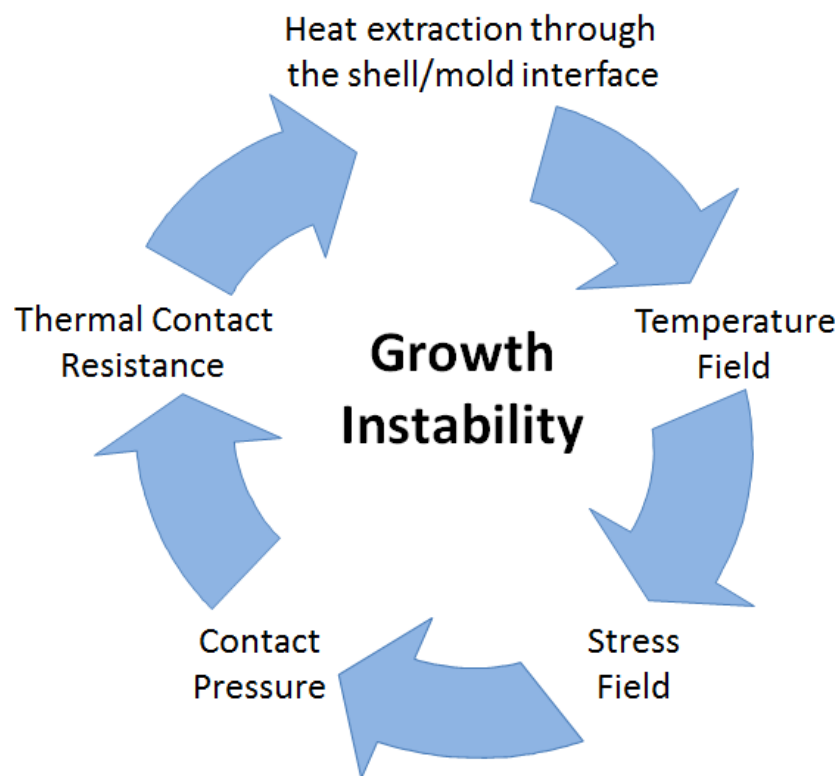


Figure 1.2 Closed loop mechanism during the solidification process

The objective of this study is to investigate the instability mechanism in the solidification process during casting of pure metals and improve our knowledge about this thermo-elastic mechanism. Also we determine the conditions which eliminate or minimize the profile defects such as cracks associated with the coupled thermomechanical events. A high priority in this study is to extend the earlier researches to include the effects of the mold coating layer. The effects of the thermal and

mechanical properties of the coating layer on the growth of the perturbation at the moving interface are investigated in detail. For this purpose the influences of thickness and material of the coating layer, coupling rates at shell/coating and coating/mold interfaces on the growth instability are determined. Case studies in which different shell, coating layer and mold materials combinations are used, are done for applying our model to real material solidification on a coated mold of finite thickness. Additionally the solution of this study will use as initial condition in the solution of full solidification problem which involves the effects of thermal diffusivities of the materials of solidified shell, coating layer and mold.

This system is discussed in three parts as heat conduction problem with phase change, determination of stress fields and analysis of the thermo-elastic instability mechanism. In the following section a review of related previous works will be given including studies on both parts of these studies. The industrial applications of this study are given in section 1.3 with relevant patents. An overview of the thesis is presented in section 1.4 and the original contributions of our work are outlined in section 1.5.

## **1.2 Literature Review**

### **1.2.1 Heat Conduction Problem with Phase Change**

The transient heat transfer problems with phase-change which involve solidification and melting process are called as “phase-change problems” or “moving interface problems” and have great importance in many engineering applications such as purification of metals [1], metal casting and welding processes [2,3], freezing of foods [4], freezing of the proteins of the enzyme and tissue [5], cooling of the electrical components [6] and thermal energy storage systems [7]. The common property of phase change heat transfer problems is a moving interface is occurred between the solid and liquid phases during the solidification or melting process. The interface between the phases is moving as the latent heat is absorbed or released at the interface. Therefore, the dynamics of these types problems are very difficult to investigate and the location of the solid-liquid interface do not known a priori and must calculate as a part of the solution. The morphology of this moving interface varies according to the purity of the solidified material.

Stefan [8] studied on the earliest theoretical works about the solution of the phase change problem in formation of ice. The existence of the solution of a Stefan problem is investigated by Evans [9] and Douglas [10] worked on the uniqueness of the solution of this problem. Since then, despite the many phase change problems are appeared in the literature, the exact solutions of this problem may be obtained just for limited idealized cases containing semi-finite or infinite regions with simple boundary and initial conditions. Junyi and Minyu [11] obtained some exact solutions to the first, second and extended Stefan problems with fractional time derivative in the Caputo sense. The history and some classical solutions to the Stefan problems were well covered in Crank [12] and Hill [13].

Since the nonlinear behavior of this problem superposition principle is not applicable and all cases are evaluated separately. When the exact solution of the full Stefan problem is not calculated analytically, the approximate, semi analytic and numerical methods are developed to solve these problems. For the numerical solution of the problem various approximations are existed in the literature. One of these approximation techniques is Front Tracking Method and it is based on the tracking of the interface between the solid and liquid continuously. Another one is the Lagrangian method in which the variable space grid and variable time steps are used and provide the way to track the moving front explicitly. The obtaining numerical solution by using these or similar approaches is compared with the analytical solution for limiting problems due to controlling the convergence and stability of the numerical solution. Now various methods of solution of phase change problem (Stefan problem or moving boundary problem) are presented briefly as follows.

Barry and Caunce [14] analyzed Stefan type problems with two moving boundaries. The numerical and exact analytical solutions are obtained for linear and nonlinear diffusivities for a variety of parameter ranges and the limitations of the pseudo-steady-state assumption. Song et al. [15] solved the Stefan problem by using an underlying non-uniform rational B-spline based iso-geometric approximation with sharp interface. Due to increase the stability and efficiency of the adopted method, adaptive time stepping, refinement and coarsening of geometry were developed. Reutskiy [16] developed a new meshless numerical technique for the solution of one-dimensional Stefan problems with moving boundaries. The technique is based on the delta shaped functions and the method of approximate fundamental solutions. The results show that



the method has high accuracy for determining the position of the moving boundary. Juric and Tryggvason [17] applied a front tracking method for dendritic solidification problem. The fixed grid in space was used for determining location of moving boundary and the interface heat sources were calculated by using moving grid on the interface. Murray and Landis [18] compared and adapted grid procedure with a fixed grid and showed that grid method determines more accurately the interface position but fixed grid algorithm gives more precise heat distribution in the whole domain. Segal et al. [19] used an adaptive grid method for discretization for the free boundary in two dimensional phase change problem. The movement of the grid in adaptive grid method was introduced into the system equations by use of Arbitrary Lagrangian Eulerian (ALE) approach.

Kutluay et al. [20] applied variable space grid and boundary immobilization techniques based on the explicit finite difference technique to the one-phase classical Stefan problem. Caldwell and Kwan [21] used nodal integral and enthalpy solution of one dimensional Stefan problem and Caldwell et al. [22] extended the previous work by obtaining the solution of the one-dimensional phase change problem by using finite difference methods. They compared the solutions with the previous studies and obtained good agreement between these solutions. Caldwell and Chiu [23] used the heat balance integral method for the numerical solution of one-dimensional Stefan problems with temperature dependent thermal properties. Numerical results were obtained for both cylindrical and spherical geometries. In the second part of the study in [23], Caldwell and Chiu [24] used a special starting procedure for small time. The systems of nonlinear algebraic equations for the coefficients in the small time series were derived for the both cylindrical and spherical geometries. Caldwell and Kwan [25] described and compared several effective methods for the numerical solution of one dimensional Stefan problems for simple geometries including plane, cylindrical and spherical such as including the enthalpy method, boundary immobilization method, perturbation method, nodal integral method and heat balance integral method.

Tarwidi and Pudjaprasetya [26] solved the enthalpy formulated one and two dimensional Stefan problems numerically by using Godunov method. Savovic and Caldwell [27] developed a methodology for solving phase change problem with Dirichlet boundary condition. Finite difference approximation was used to derive temperature distribution, the location of moving interface between the phases and its

velocity. Javierre et al. [28] compared the numerical methods, level set, moving grid and phase field model, used in the cases of melting of pure phase and diffusional solid-state phase transformations in a binary system. They found that the type of the phase transformation considered determines the convenience of the numerical techniques. Voller [29] developed an enthalpy node-jumping method for solution of the one-dimensional Stefan problems under heat conduction. A variable time step and fixed space grid were used to ensure that the moving front is always on a node point and also the problems were solved in an uncoupled form by using this method. Developing technique was applied to a problem of binary alloy solidification. Nedjar [30] used an efficient algorithm based on the finite element method for solving nonlinear phase change heat transfer problems. They considered two problems which are the stationary convection-diffusion problem and the classical transient heat problem. They obtained the mathematical models based upon the enthalpy formulations. Chen et al. [31] presented a simple level set method for solving Stefan problems and they applied this method to dendritic solidification problems. Implicit finite difference scheme was used to solve the equation of heat transfer and the position of the moving interface between the solid and liquid phases was calculated with level set method. Gibou et al. [32] investigated the dendritic solidification of pure melt by using level set approach and numerical results showed that developing method is used on complex interfacial shapes and can simulate many of the physical features of dendritic solidification.

Phase-field (PF) models avoid the need to explicitly track the moving interface. Mackenzie and Robertson [33] investigated the phase-field modeled phase change problem. A moving mesh algorithm was developed for discretization of the equations and existence and uniqueness of the equations was examined. The results show that the developed method is more efficient than fixed grid methods. Other research about the phase-field modelling of the phase change problem is Sun and Beckermann [34]. They developed a method based on the phase-field equation and can track the interface between the phases and different modifications of the phase-field equations were investigated. The accuracy of the present method was demonstrated in several numerical examples for a variety of interface motions and shapes that include singularities, such as sharp corners and topology changes. Voller and Falcini [35] investigated the two different one-phase Stefan problems: in the one of them diffusivity varying as power law of position, in the other problem diffusivity changes as a power

function of the slope. The exact similarity solutions of these problems were calculated and the time exponent in the front position relationship can take values in the range  $[0,1]$  was observed from these solutions. Esen and Kutluay [36] used finite difference approximations for solving Stefan problem with a Neumann-type boundary condition numerically. Enthalpy method was used to modeling the system and numerical results were obtained by the hopscotch technique. Asaithambi [37] developed a numerical method using automatic differentiation technique which obtains a Taylor series expansion of solution and coefficients of the series terms were calculated using recursive formulas derived from the differential equation itself. He applied this method to the heat transfer problem in an ice-water medium. Yang and He [38] solved the phase-change heat transfer problem by combining the heat capacity method and element free Galerkin method. They used a sigmoid function for a continuous and smooth effective heat capacity function for avoiding the error due to the step jump and the influences of adjusting of element-free Galerkin method nodes and parameters relevant with Sigmoid function on the solutions were investigated. Vynnycky and Mitchell [39] developed an algorithm for one dimensional time dependent problem of an evaporating spherical droplet that has a finite extinction time by use of the Keller box finite difference scheme in tandem with boundary immobilization technique. Mitchell and Vynnycky [40] extended the work referred in [39] for the purpose of two- phase moving boundary problem with heat flux boundary conditions using same solution techniques. The second phase appears first only after a finite delay time. They used variable transformations in the numerical algorithm to resolve boundary condition discontinuity and it allows them to determine the time delay until solidification starts and improves the accuracy of the algorithm. Myers and Mitchell [41] developed a solution method for solving Stefan problem based on the heat balance integral method which is called combined integral method. This method is more accurate than the second order, large Stefan number and perturbation solution for a wide of Stefan numbers. The combined integral method breaks down like other integral methods when the boundary temperature approaches zero or oscillates. Zabaras and Ruan [42] studied on the moving and deforming finite element method analysis of two dimensional phase-change problems. The transfinite mapping method was used for mesh generation in the liquid phase and the solid phase was divided into a non-moving element region and a moving region which involves the finite elements near to moving interface. The calculated

solutions were shown good agreement with analytical and numerical solutions in the literature.

Some of the research about Stefan problem consist the effect of the latent heat at the solid-liquid interface. Voller et al. [43] studied on an analytical solution of the Stefan problem with variable latent heat. They governed the equations of one-phase Stefan melting problem for modelling the movement of the shoreline in a sedimentary basin. The results show that latent heat that increases linearly with distance from the origin. Other related articles about the phase-change problem with variable latent heat are referred in the [44, 45].

Natale et al. [46] investigated the one-dimensional two-phase free boundary solidification problem of pure materials with shrinkage and expansion of liquid as it solidifies. Initially the liquid temperature is higher than its melting temperature and the system is adiabatic in a region. They found temperature distributions in the solid and liquid layer and location of the interface between the phases and positions of the two free boundaries (liquid-solid interface and interface due to shrinkage or expansion of liquid) for three different cases involving temperature boundary condition, heat flux boundary condition and convective boundary condition at the interface due to shrinkage or expansion. Zabaras and Mukherjee [47] determined the position of the freezing front and the time dependent temperature field during solidification of pure metal by using boundary element method with time dependent Green's functions and convolution integrals. The results show that developed method is faster, more accurate and without time-step limitations in comparison with other semi-analytical and numerical solutions. Dursunkaya and Nair [48] analyzed the motion of a solidification front by using a semi analytical approach during the solidification of a finite one dimensional medium with boundary temperature with oscillations. The effects of the solid, liquid Stefan numbers and the unsteady boundary temperature variation were investigated and they found that if the initial temperature of the medium is different than melting temperature of the solidified material, reversal of the interface motion is possible. The large solid Stefan number leads to fast interface motion but large liquid Stefan number has opposite effect on the interface motion. Skrzypczak and Wegrzyn-Skrzypczak [49] studied on the mathematical and numerical modelling of the heat transfer problem during solidification of pure metals by using finite element method. They used front tracking method based on the level set method for determining the position of the moving interface. They

applied developed method to two dimensional area at different temperatures on the boundaries to establish the effectiveness of the method for a complex shape of the solidification front.

Caldwell and Kwan [50] used the perturbation method for the solution of Stefan problems with time-dependent boundary conditions. They applied this method to different cases such as melting of ice in the half plane, outward spherical and cylindrical solidification of a saturated liquid. Pedroso and Domoto [51] and Huang and Shih [52] used this method to investigate the solution of the planar solidification of saturated liquid with convection at the wall. The perturbation solutions of the spherical and cylindrical solidification process were derived in Pedroso and Domoto [53], and Stephan and Holzkecht [54]. Yu et al. [55] obtained perturbation solution of planar solidification problem with time dependent heat generation. The effects of heat generation and Stefan number on the growth of the solidification were investigated. Yigit [56] obtained an analytical solution for a two dimensional heat conduction problem with phase change by using linear perturbation method when the temperature at the outer surface of the planar mold was prescribed. The inverse problem was also discussed and the effects of the process parameter such as cold thickness, thermal contact resistance on the growth of the perturbation and the outer temperature of the mold were examined. Yigit [57] used a linear perturbation method for determining the solution of the solidification of pure metal on a sinusoidal mold surface of finite thickness. The governing equations were discretized by using finite difference approach and the effects of the system parameters such as thermal capacities of the shell and mold materials and wavelength of the mold surface on the growth of the perturbation at the solid-liquid interface were investigated for the different combination of the shell and mold materials. A linear perturbation solution was used to obtain approximate analytical and numerical solution of the two-dimensional heat conduction problem by Yigit [58]. The pure material solidified on a planar mold surface and the cooling rate is perturbed by a small spatially sinusoidal heat flux at shell-mold interface. Approximate analytical results were obtained for the solid/melt moving interface as a function of time and for the temperature field in the shell. The approximate analytical solution was compared with a numerical solution, and a very good agreement has been found. The effect of thermal diffusivity of the solidified shell material on the development of the shell thickness was investigated. It was shown that solidified shell materials with higher

thermal diffusivities may result in irregular growth which, generally, causes cracking near the surface. Yigit [59] solved the solidification of pure metal on a planar mold of finite thickness by use of linear perturbation method. Analytical results were obtained for limiting case in which the diffusivities of the mold and shell material are assumed to be infinitely large. Then these analytical results were used to validate the numerical results of model with diffusivities which are calculated by using an explicit finite difference Lagrangian scheme. The influences of thermal diffusivities of materials, thickness of the mold, thermal contact resistance at the mold-shell interface and the thermal conductivity ratio of the material on the growth shell thickness were investigated. The two-dimensional heat conduction equation with phase change was solved by using linear perturbation method in Yigit [60]. The system involved a liquid which is solidified on a sinusoidal mold with finite thickness and both surfaces of the mold follow a sinusoidal lay for which the ratio of the amplitude to the wavelength. The temperature of the bottom of the mold was prescribed as a constant. The thickness of the shell and the temperature distributions in the shell and mold were examined. The inverse phase change problem was solved in which the temperature at the bottom of the mold is found according to the moving interface position. The effects of the system parameters on the growth of the perturbation at the freezing front were investigated. The one dimensional solidification problem with a periodic boundary condition prescribed at the bottom of the mold of finite thickness was solved numerically in Yigit [61]. The finite difference method was used for solution and the temperature distributions in the solidified shell and mold, the position of the moving freezing front and its velocity were calculated. The influences of the Stefan number of the solidified material and thickness of the mold, the thermal conductivity and thermal diffusivity between the shell and mold materials on the growth of the shell and growing velocity of the shell were analyzed. The impact of oscillating mold temperature boundary on the growth of shell thickness is particularly significant at earlier stages of the process and more pronounced for smaller Stefan numbers. Hu and Argyropoulos [62] wrote a peer review paper about most using analytical and numerical techniques for modelling and solving phase-change heat transfer problem during melting and solidification problems. They gave the advantages and disadvantages of each formulation.

The inverse heat conduction problem with phase-change usually refers to the problem of calculating the heat flux and temperature at the boundaries for a given position,

velocity of the interface between the phases or heat flux at this interface. The desired motion and growth of the solidification is important for obtaining desired cast quality, optimizing the time of casting, controlling the liquid feeding to the contracting front. Zabaras et al. [63] developed a method to adjust the motions of moving interface between the solid and liquid phases during the solidification process. In this method, they calculated the boundary heat flux or temperature for a desired motion of the solidification front. A moving and deforming FEM formulation in [42] was used with spatial smoothing and a modification of Beck's future information method to solve this ill-posed design problem. A variety researches for solutions of the inverse one or two phase change problems during the solidification process by using different solution techniques are listed in [64-70].

### **1.2.2 Determination Stress Field**

During the solidification of pure metals or alloys, the thermal stresses may develop. If these developed stresses in the solidified shell and mold have sufficient magnitude, they cause severe defects, such as formation of surface cracks in the final cast. The stress fields in the solid layers are occurred depend on the two factors during solidification of metals. First one of these factors is the external force due to the hydrostatic pressure from the liquid metal and second one is the non-uniform cooling rate in the solidified shell and mold. Some theoretical and experimental studies about development of the stresses during the casting process are mentioned below briefly.

Tien and Koump [71] studied on the stress distributions and displacement in a slab during solidification of metals analytically. The model consisted on elastic horizontal beam with temperature-dependent parameter and different boundary conditions. They investigated the effects of the cooling rate and dimensions of the beam on development of thermal stress and transverse displacement. They found that the stress at the solid-liquid interface depends on the compression to tension during the freezing process for simply supported beam. However the stress at the freezing front is always compressive for built-in ends beam. The stress at the cooling surface was always positive for both models.

Richmond and Tien [72] investigated the mechanical behavior of the solidified material at high temperatures. They used non-linear viscoelastic model without neglecting the pressure of melt for determining stress fields. The viscosity and Young's modulus of the

solidified material changed depending on the temperature and the stresses in the solidified layer and air-gap nucleation time at the shell/mold interface analytically.

Heinlein et al. [73] proposed to solve the heat transfer problem with phase change and the thermal stress problem associated with thermal fields, thermal and elastic strains and viscoplastic flow during the solidification by using boundary element method. In their model, material properties changed with temperature.

Chen et al. [74] investigated the developing thermal stresses in a silicon ingot during a unidirectional solidification numerically. The dynamic front tracking method was used to determine the position of moving interface and thermal stress in the ingot was solved using the displacement based thermo-elastic stress model. They observed the shapes of the freezing interface for different growth velocities and investigate the occurred thermal stress in the ingot for some different times.

Zhang et al. [75] studied on the modelling the meshless solidification process by using finite point method and elastic-plastic analysis mode. They developed integrated meshless thermal-mechanical analysis system and they investigated thermal stress and strain distribution in the cast and mechanism of the off-corner defects formation. They analyzed large deformation case by using same method.

Liu et al. [76] investigated the thermal stress and estimation of hot tearing and residual stress of shaped casting. Rheological model and thermo-elasto-plastic model were used for analyzing the quasi-solid zone and the time after solidification, respectively. The finite element method was used to obtain thermal distribution and the stress analysis based on the finite difference. The accuracy of their model was tested by comparing the experimental and empirical results for casting of steel and iron.

Risso et al. [77] suggested two numerical models for early stages of steel casting process and the thermal stress and plastic strain in the casting ingot was analyzed. Thermo-mechanical problem during the solidification process was solved using these models with Eulerian-Lagrangian procedure and extended plane strain condition with uniform and nonzero axial strain at z-direction. The results of these models for the simulation of a billet continuous casting process were compared and the results match very well.

Meng et al. [78] modeled the continuous casting of steel process to simulate the evolution of temperature field, stress field and strain in the steel cast using finite



element method. The model involved combined elastic-viscoplastic constitutive models for different graded steels and it was validated by submerged split chill tensile test. The developed model was used to predict shrinkage during the casting and the effects of grades on the shrinkage were investigated.

Xue and Wang [79] developed a finite difference based discretization method for solving equations in terms of displacement associated with the thermal distortion. In this method different partial derivatives were added to the boundary conditions to correct the inner control volume's discretized equations coefficients. These coefficients of derived discretized equations were solved by line Gauss-Siedel method and 3-D algorithm using this method was developed to solve thermal stress problem during the casting process.

Sadrossadat and Johansson [80] studied on the effects of modification, superheat temperature and mold properties on residual stresses and microstructure of final cast during solidification of Al-Si-Mn alloy experimentally. Residual stresses were measured by using sectioning method for different designs under different physical parameters effects. The results showed that residual stresses decreases with lowered superheat, temperature and mold hardness and microstructure of the ingot is influenced significantly by changing these parameters.

Uehora et al. [81] studied on the phase field simulations of development of stress to investigate the stress distributions in dendritic microstructures during solidification of alloys. The finite element method was used to solve the coupled thermo-mechanical equations which involved the phase transformation, thermal and stress fields. The mechanical properties of the melt were neglected. The stress distribution in a dendrite is determined and the influences of the morphology of the microstructures on the stresses were investigated.

Farhangi et al. [82] investigated the effects of casting process variables on the residual stress in Ni-base superalloys, IN713C and U500, for the rectangular and triangular shapes samples. They found that increasing melt superheat temperature cause to higher residual stresses and higher level of residual stresses were developed in U500 compared to IN713C at constant melt superheat temperature due to more extended freezing range and mushy solidification behavior of U500. In triangular sample castings, higher levels of residual stresses were developed in triangular sample casting under same conditions.

Uehara [83] used a phase field model for investigating cellular microstructure formation and stress distribution in the binary alloy system. They observed a wavy pattern with tips and bottom edges at solid-liquid interface and occurred stress below these tips has significant magnitude. Also they studied on the effect of the phase transformation on the pattern formation and they found that solidification grows faster at the bottom than the tips until a flat interface is observed at the growing front when transformation is accelerated under the tensile stress.

Thomas et al. [84] developed a mathematical model for determining the generated internal stresses in the steel ingot during the thermal processes. The stress model was formulated for a two dimensional transverse plane at mid-height of the ingot and is a transient, elasto-viscoplastic, finite element analysis of thermal stress field. They applied their model to solidification process, air cooling and reheating process to calculate the thermal stresses. The result showed that while mold corrugations do not have significant effect on temperature field but have an important influence on local stress field variations. The maximum tensile stress generally centered beneath the corrugation ridges.

### **1.2.3 Thermoelastic Stability Analysis**

Thermoelastic stability analysis of solidification of metals is very important for manufacturing process especially casting and welding. Due to the non-uniform heat extraction at the shell/mold interface, uneven shell growth is occurred at the moving interface. This uneven shell growth during the solidification process was observed experimentally in [85-90]. This undulatory growth of the shell causes severe defaults in the final casting such as cracks and it reduces the quality and usability of the casting. [91-94].

Before the summarizing the theoretical studies about observed growth instability during the solidification process, the two different models, which identify the relation between the thermal and mechanical problems in the process, are discussed. As shown in the Figure 1.3 the thermal problem affects the mechanical problem but mechanical problem does not affect the thermal problem in uncoupled model. The temperature distributions in the solid layer affect the thermal stresses, thermal distortion and contact pressure but vice versa these temperature fields are not affected by the stress fields. This model is valid for early stages of the solidification process.



Figure 1.3 Uncoupled process block diagram

Figure 1.4 shows the block diagram of the coupled process. As seen in the figure, the thermal and mechanical problems are affected each other through contact pressure dependent thermal contact resistance. Full stages of the solidification process are represented by using the coupled model.

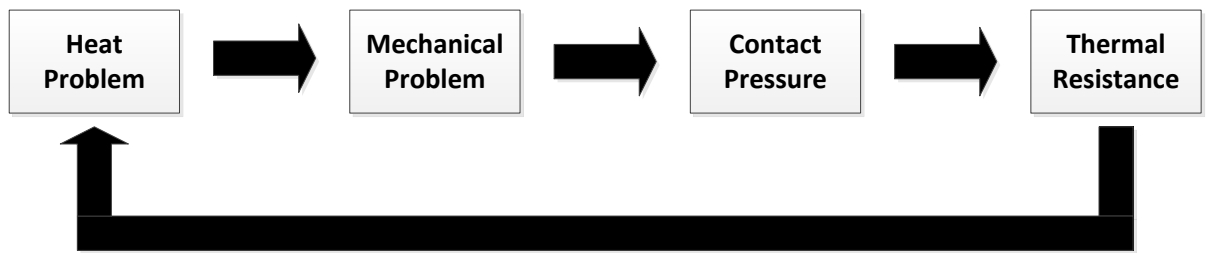


Figure 1.4 Coupled process block diagram

Theoretical works about thermoelastic instability during solidification firstly investigated Richmond and Huang [95] and they showed that the contact pressure decreases at the thinnest sections of the solidified shell, but increases at the thickest section. An air-gap forms at the shell/mold interface when the contact pressure falls down to zero under these thin sections of the shell. Lastly they indicated that increasing in liquid pressure leads to increase the air-gap nucleation time but increasing cooling rate has an opposite effect on this formation time. Li and Barber [96] studied on two dimensional heat conduction problem during solidification of pure metals and they found that a small sinusoidal perturbation in temperature parallel to the plane of the mold and determined corresponding perturbed solution for the temperature field and the motion of the solidified surface. Richmond et al. [97] developed a model for this problem with analyzing non-uniform beam approximation based thermomechanical stresses. The uniform heat flux at the shell/mold interface has a small, spatially sinusoidal perturbation. Their model was valid only for early stages of solidification and they found that if the heat flux increases in a region than associated thermal distortion leads to increase in contact pressure. Therefore the thermomechanical coupled problem behaves like a positive feedback system. Zabaras et al. [98] determined the temperature

and stress field development in a pure metal during the solidification by using front tracking finite element method. The velocity and location of freezing front were determined and the thermal stress field was calculated based on virtual work principle and hypoelastic-viscoplastic constitutive model. The effects of melt pressure, cooling conditions and geometry of continuously cast metal on the occurred residual stresses were investigated and the residual stress for the cylindrical section were compressive in the region close to outer surface and tensile in the region close to the center. Zabaras et al. [99] extended previous work for axially symmetric solidification. The thermal and mechanical properties were changed depending on the temperature and strain rate. The results show that residual stresses are very sensitive to the applied cooling rates and melt pressure has important effect on the air-gap nucleation at shell/mold interface. Li and Barber [100] solved the coupled solidification problem in which thermal and mechanical problems were investigated together through pressure dependent thermal contact resistance at the shell/mold interface. They assumed that the liquid was initially at its melting temperature and thermal capacity of the solidified material was zero. They indicated that coupling between the thermal and mechanical problems at the shell/mold interface causes rapid growth of perturbation at the moving interface.

Yigit et al. [101] extended previous coupled study with taking into account the effect of the thermal capacity of the solidified shell and they used linear perturbation method for modeling the system and the governing equations were solved numerically by using finite difference algorithm. The mold was assumed rigid and the heat flux at the shell/mold interface was prescribed as a constant. The results showed that thermal capacity of the shell has a stabilizing effect on the fully coupled process and its effects are more important at large cooling rate. Yigit and Barber [102] determined the effect of Stefan number on the growth of the shell during solidification on a rigid mold. The thermal and mechanical problems were coupled at the shell/mold interface. They found that Stefan number has a stabilizing effect on the solidification process and the amplitude of the perturbation on the mean shell thickness reaches its maximum value when the solidified shell thickness is about half the wavelength of the perturbation then decays its steady state value. Zabaras and Kang [103] developed a methodology to provide a uniform desired lateral residual stress distribution and a desired uniform temperature distribution by determining the optimum cooling temperature history on the fixed boundary of a unidirectional solidifying cast. A moving finite element method approach was used for the thermal part of the solidification process and an approximate

incremental hypoelastic-viscoplastic model was used for the thermal stress problem. Hector et al. [104] and Li et al. [105] developed uncoupled and coupled models to investigate the growth instability during solidification of pure metal by assuming that the strain rate in the solidifying shell is the sum of elastic, thermal and viscous components, respectively. Therefore, they developed a model for plane strain thermoviscoelasticity and the strain rate relaxation parameter was defined for determining the extent due to viscous creep. They investigated the effect of this parameter on the contact pressure at the shell/mold interface. Hector et al. [106] extended earlier works by considering the solidification of a three phase system and investigated the effect of freezing width on the macro morphology of the solidification front. They used perturbation theory for heat problem and then hypoelastic constitutive law was used to obtain the thermal stresses and strains. They found that at small liquid metal pressure, freezing range width has a destabilizing effect on the growth instability but if liquid metal pressure is increased, freezing range effect becomes opposite. However, the effect of the freezing range on the growth instability diminishes under very high liquid pressure. Yigit [107] developed a coupled model for the solidification of pure metal on a deformable mold of finite thickness with neglecting thermal capacities of the mold and solidified shell materials. They found that the effects of the contact pressure changes depending on the thickness of the mold. For highly distortive mold, two contrary effects are observed such as for small thickness, the mold is flexible and less pressure is needed to straighten it out but for large thickness, mechanical rigidity of the mold increases and the perturbation in contact pressure reduces. But for less distortive mold second effect overcomes the first and then perturbation grows slowly.

The unstable growth of the solidified shell is eliminated or minimized by controlling the heat transfer at the shell/mold interface. One of the most used controlling techniques is using the periodic mold surface topography. Murakami et al. [108] investigated the solidification process on the periodic grooved mold surface experimentally and they found that grooved mold provides more uniform contact along the shell/mold interface. Cracks in the final casting reduce and quality increases due to less uneven shell growth associated with the more uniform heat extraction. Other experimental studies about using different mold surface topographies were done by Anyalebechi [109,110]. He investigated the effects of the wavelength of a grooved mold surface topography and casting speed on the solidification of aluminum alloy in [109]. He observed early stages

of solidification and compared the casting produced on ungrooved and grooved mold surfaces. He found that the grooved mold surface topography has a stabilizing effect on the growth of the perturbation and increase in speed, melt heat and wavelength of the grooves increases the undulatory growth. Another important result was that microstructures of casting solidified on shaped mold are more uniform. Anyalebechi [110] studied on the effects of different types of ungrooved mold surface topographies such as polished, spark roughened, shot peened and alligator on growth instability during solidification of Al alloy. The results showed that increasing in casting speed causes unstable growth for all mold surface topographies and start peened mold surface prevents the gap formation on the casting surface. The most uniform shell growth and subsurface microstructure were observed for peened mold. Some other experimental studies about the effects of the mold surface topography are reported in [111-115].

Hector et al. [116] worked theoretically about the effects of the mold surface topographies on uneven shell growth during solidification of pure metals. They developed two uncoupled models for solidification of a pure metal on a sinusoidal mold by using linear perturbation method. They neglected the effect of the thermal capacity of the solidified shell in both models. In the first model the heat flux at the shell/mold interface was assumed constant and in the second one the temperature of the mold surface was constant. They observed that air gaps nucleate at the troughs of the mold surface and it cause spatial variations at the thickness of the solidified shell.

Yigit and Hector [117] extended the heat prescribed uncoupled model in [116] by considering the effects of thermal capacity of the shell. The mold was assumed rigid and the effects of its properties were negligible. They found that when the thermal capacitance of the solidified shell is increased, the amplitude of the perturbation on contact pressure decreases and on the other hand increase in wavelength cause longer gap nucleation time.

Yigit [118] investigated the effects of thermal capacity of the mold material on the growth instability using the developed first uncoupled model in [116]. The results indicated that the perturbation in contact pressure tends to maximum value at larger time asymptotically for the lower values of the thermal capacities of the mold material. However the thermal capacity of the mold material has a stabilizing effect on the growth of the perturbation in shell thickness.

Hector et al. [119] studied on a coupled model for determining the formation time and location of the gaps at the shell/mold interface during solidification of pure metal on a

rigid sinusoidal mold. The results show that the contact pressure falls to zero at the troughs and air gaps form at these regions of the mold surface. An increasing in the wavelength of the mold surface causes longer gap nucleation times and thickness of the solidified shell increases accordingly.

Yigit and Hector [120,121] extended the previous coupled model for sinusoidal deformable mold of finite thickness. They investigated the effects of the mold surface topography on the formation of the air gap and growth of the solidified shell using different material combinations as shell-mold materials. The critical wavelength band was determined and the wavelengths of the mold surface lie in this band cause air gap nucleation at the troughs of the mold surface. Vice versa if air gaps form at the crest, the stability of the system increases and uniform shell growth is observed. In addition when the distortivity of the shell material is greatly exceeds the mold material, gap nucleation time reduces and the bandwidth becomes more sensitive to mold thickness. Increasing mold thickness leads to larger bandwidth.

Howarth and Hector [122] investigated the solidification of pure material with small Stefan number on a plane wall with single asperity of arbitrary geometries such as Gaussian, triangular and trapezoidal. The contact pressure associated with shell distortion due to asperity geometry was determined from stress field. They found that the contact pressure is a minimum at positions of maximum positive curvature but for early stages of solidification process this behavior of contact pressure becomes opposite.

Howarth and Hector [123] developed a model for obtaining a formula for contact pressure at shell/mold interface as the mold moves into the molten liquid. The results showed that the contact pressure perturbation increases with decreasing wavelength and gaps will nucleate for all sufficiently small wavelengths. The effect of mold movement at a constant velocity into molten liquid is that it diminishes the magnitude of the contact pressure at both trough and crest regions on the surfaces.

The effects of the mold properties such as wavelength of the mold surface and thickness on the growth of the shell during solidification of pure metal on deformable mold without interfacial coupling effects were investigated in Yigit et al. [124]. They neglected the thermal capacities of shell and mold materials. The results indicated that mold surface wavelength has a stabilizing effect but mean shell thickness decreases for any wavelength due to increase in heat flux. Other important results of this study were that the thermal properties of the mold play no role under these conditions and absence

of the interfacial coupling leads to eliminate the effects of the mold distortion on the shell/mold contact mechanics.

Yigit [125] studied on the combined effects of the interfacial coupling and the thermal capacity of solidified shell without mold deformation and effects of its properties using different materials as shell material. They found that the formation of the gaps for iron shell is faster than aluminum shell and critical wavelengths for the iron shell are larger than the aluminum shell.

Yigit [126] investigated the combined effects of another combination of system parameters, which are mold distortion and thermal capacity of shell material, on the growth instability during the solidification of the pure metal on a sinusoidal mold of finite thickness with interfacial coupling. The results showed that when the wavelength of the mold surface is decreased, the time of air gap formation on troughs becomes smaller. The optimum mold thickness was determined and the combined stability effects of mold distortivity and thermal capacity of shell material cause to longer gap nucleation time.

Yigit [127] studied on the uncoupled model for solidification of pure metal on a deformable mold for investigating the effects of the mold properties on gap nucleation time with thermal capacities of shell and mold materials were not negligible. He found that thermal capacity of the mold has stabilizing effect on the growth of shell but on the other hand thermal conductivity of the mold has destabilizing effect on the growth instability during the solidification. When contact pressure is increased, gap nucleation time becomes longer but critical wavelengths and optimum mean thickness of the mold decrease.

Samanta and Zabaras [128] presented a numerical study to determine the effects of uneven mold surfaces on fluid flow, macro segregation and inverse segregation in solidified aluminum alloys shell. The results showed that macro segregation affects the process highly when the mold surface unevenness is increased. Additionally, an increase in surface unevenness causes to increase in heat transfer and phase change rates. The degree of segregation decreases with increasing surface unevenness.

All developed models in above studies are valid before the air formation at shell/mold interface. After the formation of air gaps, the dynamics of the solidification problem changes. Lewis and Rensing [129] developed a model for predicting the air gap thickness at the shell/mold interface. They determined interfacial heat transfer coefficient and it is decreased inversely with the thickness of the air gap.



Tan and Zabaras [130] modeled the influences of the topography on the mold surface on the uneven growth of the shell during solidification of aluminum. The time of air gap formation at shell/mold interface, thermal stress development and pattern of growth solidified shell after air-gap nucleation were determined for different mold topographies. They found that time of the air gaps nucleation becomes smaller when the wavelength of the sinusoidal mold surface decreases. For the smooth mold, the unevenness in growth of shell increases.

Samanta and Zabaras [131] investigated the effects of the varying wavelengths and amplitudes of uneven surface at moving boundary on heat transfer, fluid flow, phase change, macro segregation and inverse segregation processes during solidification of Al alloys. The results showed that heat transfer at the shell/mold interface is affected by variation of surface of shell and fluid flow is significantly affected near the sinusoids. But the effect of the heat transfer changes on the phase change process is greater than the effect of fluid flow.

Tan and Zabaras [132] analyzed the early stages of solidification of Al alloys to determine the effects of mold surface topographies on the growth of the shell on a deformable mold. They modelled air-gap formation at shell/mold interface and determined thermal boundary condition at this interface dynamically using contact pressure/air-gap relations. They indicated that smooth mold surface and high pressure are preferred at early stages of solidification for better heat transfer profile. A larger thermal conductivity material for mold increases the effect of the mold topographies.

Samanta and Zabaras [133] extended previous work by adding inverse segregation effect due to shrinkage driven fluid flow in solidified alloy. They determined the effects of mold and melt properties on the stress field, air gap nucleation and growth instability and compared the results with similar cases in previous study for specify the effect of segregation clearly. They found that air-gap sizes and actual stress field are changed under segregation effect. The inverse segregation has a destabilizing effect on growth of solidified shell and gives additional degree to unevenness at moving interface.

#### **1.2.4 Mold Coating**

The uneven shell growth due to the non-uniform heat extraction at the shell/mold interface causes severe defects in final casting. Mold coating is one of the most important factors controlling the heat transfer rate and hence, it has very important role

on the solidification rate and development of microstructure. Other purposes of the using coating layer on the mold in manufacturing processes are protecting mold surface and improving the surface quality of the mold. The mold is a main part in the overall economics of a casting process. There are lots of innovative studies to increase its working life or to satisfy the new demands to be met by the mold liners. A protective layer is required because molten metal behaves like a solvent and can damage mold material and reduce quality of its surface. Mold coating acts like a barrier between the shell and mold and promotes thermal properties. On the other hand mold coating is used for get over the various operating needs such as low wettability, high hardness, good wear resistance and low cost. Another advantage of using mold coating is that it assists with casting release from the mold. [134]

In the literature there were some studies about mold coating in casting process as follows. These works were generally experimentally and investigated the effects of the coating properties such as thickness and material on the solidification process and quality of the final cast.

Chen et al. [135] investigated the Cu mold casting technique of rapid solidification. They proposed to reduce and eliminate the negative effect of solidification concentration on the cooling rate. Mold was coated with a thin liquid alloy coating for increasing cooling rate. The results show that Ga-In-Sn liquid alloy coating is effective for increasing cooling rate of cu mold casting by reducing the interfacial thermal resistance. On the other hand, the liquid alloy causes homogeneous nucleation in the final cast.

Jafari et al. [136] determined the effects of mold coating and sand grain size on the properties of thin-wall ductile iron experimentally. The results show that using fine sand grain size associated with graphite-based zircon coating causes to reduce in average nodularity but increase in diameter of graphite in microstructure of casting. They indicated that mold coating has a more significant effect on the mechanical and metallurgical properties of casting than san grain size.

Chen et al. [137] studied on the effects of the cavity surface coating on mold temperature variation and quality of casting during injection molding casting process. The low thermal conductivity materials or the thermal insulated materials such as TiN and Teflon with different thicknesses were selected as a coating material for reducing

mold temperature variation. The results show that Teflon improves part surface smoothness and shows more tensile strength for weld line than TiN.

Salas et al. [138] proposed to design a coating for Al die casting for increasing mold surface tribological behavior and mold life by comparing several coating materials. The wear resistance and the adhesion performance of the coating were analyzed and were grouped based on the morphology observation of the track. They found that hardness and coefficient of friction cannot be used as single guides for either wear or adhesion performance. TiAlN, TiN/TiCN, CrN coatings performed well in wear and adhesion.

Karimian et al. [139] investigated the effects of thickness of pattern coating on imperfection and porosity percentage of lost foam Al-Si-Cu alloy casting experimentally. They found that increasing coating thickness associated with increase in slurry viscosity or dipping time has a great effect on the casting microstructure and thinner coatings cause refined microstructure and increase the quality of casting with less porosity.

Acimovic and Pavlovic et al. [140] studied on the effects of the TALC –based coating on the quality of casting during solidification of Al-Si alloy. The result shows that coating layer has positive effects such as provides uniform solidification of entire casting volume and eliminates pattern decomposition rapidly.

Hamasaiid et al. [141] investigated the effects of mold coating thickness and material and alloy composition on the extraction of heat at shell/mold interface during permanent mold casting of aluminum alloys. Graphite and TiO<sub>2</sub> based were used for solidification of two different aluminum alloys. They found that heat transfer coefficient (HTC) decreases when the thickness of coating increases and HTC of graphite coating is higher than ceramic coating of similar thickness. The effect of coating material diminishes after air gap nucleation at shell/mold interface.

The low fluidity the material causes severe defects during the casting process. Mold coating has significant effects on the fluidity of casting. Lu et al. [142] determined the effects of the ceramic coatings on fluidity during the solidification of magnesium alloys on plain mold. They wanted to increase fluidity because mold filling may not be accomplished due to fast solidification rate of magnesium alloys. TiAlN, CrN, CrC and AlCrN coating materials performances were compared and the results show that all of the surfaces coating materials increase fluidity performance since reducing heat loss and

providing insulation. The ranking of the fluidity enhancement is: TiAlN, CrC, AlCrN and CrN. Borouni et al. [143] reported the influence of three different types of coating and the section thickness of the part on the fluidity of aluminum alloy casting. They indicated that nano-ceramic mold coatings increase the fluidity length and quality of casting because melt fills the mold easily.

Wei et al. [144] proposed to control and adjust the heat transfer at shell/mold interface by using C/BN, Zn and organic coatings during AISI304 stainless steel solidification on the copper mold. They found that C/BN coating improves the uniformity of heat flux and the surface of casting is coarse. Zn coating increases the heat flux and solidification rate and causes the fine solidified shell occurs in wide range. They observed that remelted layers in shell surface for organic coating due to decreasing in heat transfer.

Lee et al. [145] studied the effects of the pressure and coat permeability on casting characteristics such as molten metal flow, casting failures and casting microstructure and surfaces during evaporative pattern casting of magnesium alloys. The results show that a complete mold filling was observed by using high permeability coating. When coating of high permeability material was used, the effect of the casting thickness in the stairway type pattern on the microstructure was not significant and decrease in the pressure cause to reduce in the average grain size of the magnesium alloy.

Srivastava et al. [146] developed a new method for fatigue resistance that uses three layer coating to reduce the heat transfer and chemical diffusion. They used rare-earth oxide material in outer layer of coating for providing thermal barrier and TiAlN material in the middle layer for diffusion barrier and a thin Ti in inner layer. The results show that outer layer of the coating causes to reduce the number and depth of cracks and new coating increases the thermal fatigue resistance of the substrate.

Shivpuri et al. [147] investigated the effects of the metallic coating of W, Mo and Pt materials on erosive wear on die surface under production conditions. The result show that the W coating showed improvement in the erosive wear resistance of steel substrate due to its high hardness, high yield strength and high toughness. But Pt and Mo coatings did not protect the substrate as well as the W coating.

Sulaiman et al. [148] studied on the influence of pattern coating thickness on porosity, mechanical properties and microstructure of casting of Al-Si alloy with lost foam casting experimentally. The foam pattern was coated up to fifth layer. The results show

that porosity distribution on Al-Si alloy casting increases when the thickness of pattern is increased but increase in thickness cause to decrease in tensile strength of casting. Finally they indicated that mechanical strength has inverse relationship with porosity.

Sands and Shivkumar [149] investigated the mold filling characteristics of aluminum alloy 319 experimentally for different coating thickness and sand fineness under various flow velocities. The permeability of the mold was changed depending on the coating thickness and particle size distribution in the sand. They found that thicker coating layer and finer sand leads to higher fill time.

Nwaogu and Tiedje [150] wrote a peer review paper about foundry coating technology. They explain the description, component, characteristic and mechanism of coating with some examples. New area of innovation for further development and improvement of foundry coating technology was also introduced.

In the literature there are lots of experimental studies about effects of coating layer on solidification process. But there are not enough theoretical studies about the casting process with mold coating layer. Dynamical effects of the coating layer on the occurred thermal and mechanical behaviors during the solidification of metals and alloys and interaction of the properties of coating layer and the other system parameters are not investigated in detail in the literature.

Turgut et al. [151] considered the conduction problem during solidification of pure metals on a coated planar mold of finite thickness. They investigated the influences of thickness of coating layer, thermal conductivity ratio between solidified shell, coating and mold material on the growth of solidified shell. The results show that thicker coating cause a slower growth of perturbation in solidification front but thinner coating and thinner mold cause rapid growth due to high cooling rate.

### **1.3 Industrial Application Areas**

Casting enables to produce different type parts such as complex shapes, parts having hollows, parts that contain curved surfaces, very large and heavy parts and the metal parts which have low machinability. Therefore, casting has very large usage area in manufacturing processes and the casting parts are used in different industries such as automobiles, aerospace, railways, motors, generators, pumps and many more. Due to the widely usage of casting parts, the quality of these parts becomes very important. The

defects that occur in part during casting process reduce its quality and usability. These imperfect castings do not satisfy the necessity of the manufacturer and they are stood out to recycling or need to extra operation for using. The studies about the analysis of the stability analysis during the casting process in the previous section aim to understand the growth instability mechanism and reduce the defects in the final cast associated with this unstable growth. Some patents are discussed below consist invention of the methods to improve the quality of the parts of some industrial products which producing by casting. For this purpose inventors used the results of developed theoretical studies about growth instability during the casting process.

Hanna et al. [152] developed equipment and a method which provides a brake rotor assembly. The brake rotor assembly consist an annular rotor, rotor flange and hub section. The rotor is produced by casting of steel or iron and the annular hub section of rotor is preferably produced by casting of a material such as aluminum or magnesium which lighter by volume than material of rotor. The quality of these parts of brake rotor is important. Hanna et al. [153] developed a damped product with a layer which includes a material for preventing vibrations and other oscillations in brake rotor system whose parts are manufactured by casting and are assembled. They used different type materials layer with different thickness in the layer which is located between a portion of substrate and the body of the brake rotor. Schroth [154] suggested a method for reducing the vehicle noise and produced a component by casting of steel for this reason. They used this part into powertrain housing components to provide noise damping layer within the components. Since the quality of the final cast affects the damping performance, minimizing the several defects due to uneven shell growth is very important in such cases. Hanna et al. [155] determined a method for manufacturing a friction damped bi-metal disk brake rotor in which an insert is cast into rotor in a sense to reducing noise without exposing the rotor corrosion. Their method involves two steps which are positioning an insert into a mold and casting a rotor cheek of disk brake rotor in the mold around the insert. They used theoretical and experimental studies in the literature to improve the cast quality. Agarwal et al. [156] enhanced a method for producing an insert to provide vibration damping which involves a body portion, a plurality tabs which are tapered. This insert with taps is produced by casting and production of this part without defects improves the vibration reduction performance. Golden et al. [157] developed a product which has a body with cavity from first end to

second end. The cavity in the product is filled a material and relative movement among other things between the body and filler may help dampen vibration and other oscillation in a body. The invented product with hollow is produced by casting process. They used this part in brake rotor to reduce the vibration of rotor. Hanna et al. [158] developed a production method of brake rotor with vents for cooling and with embedded annular inserts for noise damping. A pair of like or identical vented brake rotors are manufactured by a sand casting process. The annular insert has a coating which comprises particles or flakes or fibers and radially extending locating tabs. Hanna et al. [159] developed a method for producing a coulomb damped disk brake rotor by casting. The manufacturing process involves providing a mold having a shape of disc brake rotor, placing an annular insert with tabs for ensuring coulomb damping and pouring the casting material into the mold in order to wrap the insert with this casting material for formation a rotor cheek. Hanna et al. [160] developed a method which involves a positioning an insert in a vertical mold and including a metal round at least a portion of the insert for casting a material. The casting comprises pouring the material into one gate located in the bottom of the vertical mold wherein only one gate is positioned in between two adjacent tabs. They took advantages of the studies about thermoelastic instability during casting process to increase the cast quality.

#### **1.4 Thesis Overview**

The purpose of this study is to improve our knowledge about the growth instability during solidification of pure metals on a coated mold of finite thickness and determine the conditions for increasing the stability of the growth. This study extends the previous works by taking into account the properties of the deformable coating layer in the process. The effects of this coating layer on the uneven shell growth of the solidified shell during solidification are investigated theoretically. The thermal and mechanical problems are affected each other through contact pressure dependent thermal contact resistance. Mathematical model of the system are derived by using linear perturbation method which separates the two dimensional solidification problem into two one dimensional parts called as zeroth and first order problem. The zeroth order problem show the unperturbed nonlinear solution of the full problem and the first order problem represents the perturbed linear problem. Since the zeroth and first order problems involve fields varying in only one spatial dimension and time, they are considerably

easier to implement and more efficient computational effort than a full two-dimensional numerical solution of the solidification problem. The thermal diffusivities of the solidified shell, coating layer and mold materials are assumed infinitely large. The physical meaning of this assumption is that the thermal capacities of the materials are zero and the temperature fields change linearly in the solid layers. This assumption provides us to solve heat transfer problem analytically. Then the uniform stress fields in the solidified shell, coating layer and mold are derived depending on the temperature fields. At the end of the solution of both thermal and mechanical problems, we obtain two second order ordinary differential equations which involve the unknown function of magnitude of the perturbation in the solidified shell thickness and residual stress in the solidified shell. These coupled differential equations are solved simultaneously by using variable step variable order predictor and corrector algorithm after they are converted the state space form. Numerical solutions are compared with the results in Yigit [107] under same conditions to verify the accuracy of our mathematical model.

The results show that the effect of the thickness of the coating on the growth instability changes depending on the thermal and mechanical problems coupling between the solidified shell and coating or coating layer and mold. It has destabilizing effect under weak coupling but when at least one of the coupling rates at shell/coating and coating/mold interfaces are increased, this destabilizing effect turns opposite. Also, the material of the coating layer changes the effect of the coating thickness. The effect of thickness on growth instability increases when the material of high thermal conductivity is used as a coating material. It is also shown that the perturbation grows rapidly at the moving interface when the sensitivity of the thermal contact resistances at the interfaces between solid layers to contact pressure is increased. The combined effects of properties of the coating layer such as thickness and coating and interfacial coupling at shell/coating and coating/mold interfaces are investigated in detail.

Heat conduction problem with phase-change and thermal stresses problem are presented in Chapter 2 and Chapter 3, respectively. The temperature and stress fields are derived analytically. At the end of these chapters we have ordinary differential equations with variable coefficients. The dimensionless representation of the problem for generalizing the solution and simplifying the mathematical complexity of the problem and solution procedure for this stiff problem are given in Chapter 4. The comparison with the limiting problem and the effects of the properties of deformable coating layer and other



system parameters on the growth of the perturbation are presented in Chapter 5. Finally we summarize our study and give important obtained conclusion from this work in Chapter 6. Some research topics for future studies are also suggested in this chapter.

### **1.5 Contributions of the Thesis**

In this study the analysis of thermoelastic growth instability in the solidification of pure metals on a coated mold is presented. The difference between this study and the previous studies which are mentioned in the literature review section is that the effects of the properties of the coating layer on the stability of solidification process are investigated theoretically in this study. The key question is that how the properties of the coating layer are selected depending on the other process parameters such as the materials of the solidified shell and mold, thickness of the mold and coupling between the layers, for reducing the unevenness in the growth of the solidified shell. This question is answered by developing a theoretical basis. This theoretical study helps to manufacturer to determine the conditions which eliminates or minimizes growth instability of shell and increase the quality of the casting. The original contributions of this research can be summarized as follows:

1. The two dimensional solidification problem with mold coating layer is solved using linear perturbation method. An analytical solution for the both temperature and stress field is derived for the limiting case where the thermal capacity effects of the material are negligible and our developed model is valid for only early stages of the solidification.
2. The solutions of this works are used as initial conditions for fully coupled problem, in which the thermal diffusivities of materials of solidified shell, coating layer and mold are finite.
3. The effects of material and thickness of the coating layer on the development of sinusoidal perturbations during the unidirectional of pure metals are investigated in detail.
4. The system parameters such as material and thickness of the mold, material of the solidified shell, the wavelength of the perturbation on the heat flux and the newly added parameters to the system such as the coupling rates at shell/coating and coating/mold interface, thermal contact resistances at these interface, the thermal conductivity ratio between solidified shell and coating materials and

thermal conductivity ratio between coating and mold materials on the growth instability are investigated in detail.

5. The combined effects of the coating properties and interfacial couplings at shell/coating and coating/mold interfaces are studied and case studies are done for applying our model to real material solidification process by using different material combinations as shell, coating and mold materials. The conditions are determined for improving the quality of casting of pure metals.

## CHAPTER 2

---

### HEAT CONDUCTION PROBLEM

#### 2.1 Introduction

In this chapter the two dimensional heat conduction problem with phase-change for solidification of pure metals on a deformable planar coated mold of finite thickness is considered. The temperature fields in the solidified shell, coating layer and mold and location of the moving interface is derived. The solution of the phase change problems is very difficult since the location of the solidification is not in a priori must calculate as a part of the solution. Due to the nonlinearity of the governing equations, exact analytical solution is found for some limiting case only. In this limiting case some simplifying assumptions are made but the problem is not handed fully. Therefore, a substantial amount of work has been devoted toward the development of approximate analytical as well as numerical techniques. In the previous chapter some of these analytical, approximate analytical and numerical solutions are reported. The thermal diffusivities of the materials are assumed to be infinitely large and the physical meaning of this assumption is that the thermal capacities of the materials of solidified shell, coating layer and mold are zero. This assumption allows us to solve this heat conduction problem analytically. The heat conduction equations are solved for obtaining temperature fields in the solidified shell, coating layer and mold by using thermal boundary conditions at the moving interface, shell/coating and coating/mold interfaces and at the bottom of the mold. For simplifying the complex solution of the two dimensional heat transfer problem, linear perturbation method is used to reduce the dimensionality of the problem and to provide less computational effort. All obtained results are corrected by comparing the results in Yigit [107] for limiting case. The results show good agreement with each other.

## 2.2 Formulation of the Problem

We consider a two dimensional phase-change heat transfer problem for solidification of metals on a coated deformable planar mold of finite thickness. The physical model of the solidification process, as depicted in Figure 2.1, consists of liquid and solid phases of solidified material, coating layer and mold. The temperature in the liquid region is assumed to be spatially uniform and constant in time. It is equal to the melting temperature  $T_m$  and therefore the thermal effect of molten metal on the uneven shell growth is negligible. This assumption provides us that the temperature at moving interface between the solid and liquid phases is always equal to melting temperature of molten metal.

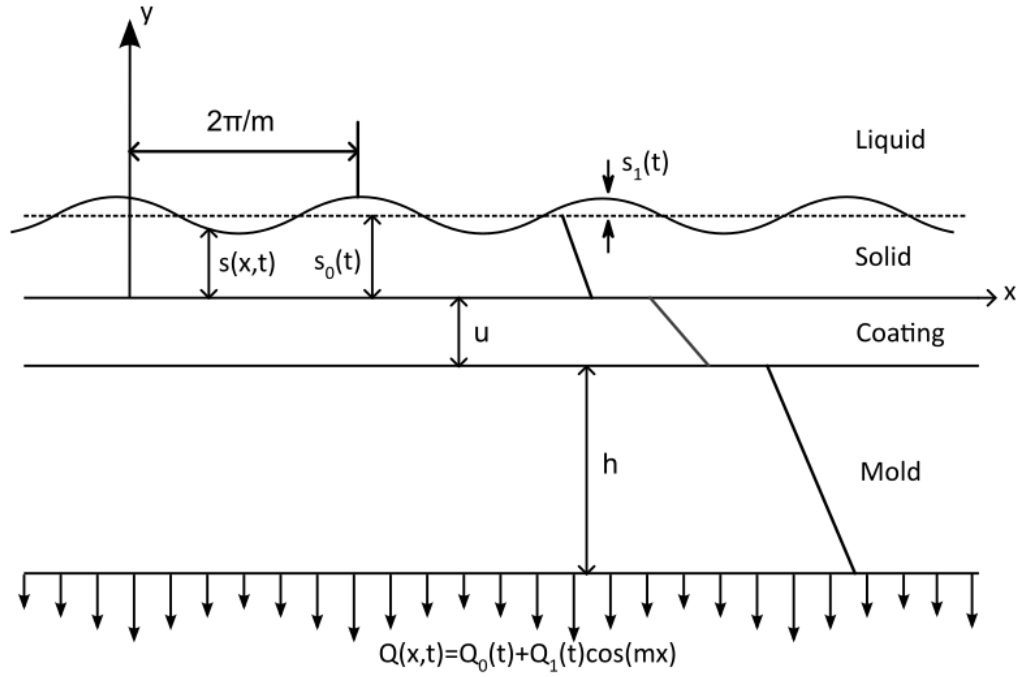


Figure 2.1 Geometry of the system

As shown in the figure, no heat flux is transferred from the surfaces other than the bottom of the mold and  $Q(x,t)$  denotes extracting heat flux there from. As already mentioned, experimental studies show that the extraction of heat flux from the process is non-uniform and small perturbation is added on the uniform heat flux to simulate this behavior. Solidification takes place at a distinct temperature, and the solid and liquid phases are separated by a sharp moving interface since the present analysis is valid only for the solidification of pure materials. The properties of the materials of the solidified shell, coating layer and the mold are independent of temperature and time.  $u$  and  $h$  symbolize the thicknesses of coating layer and deformable mold, respectively. It is

assumed that the upper surface of the coating layer which is in contact with the solidified shell along the  $y = 0$  and lower surface which is in contact with mold at  $y = -u$ . The upper surface of the mold is at  $y = -u$  and its lower surface at  $y = -h - u$ . After a time, the liquid forms a solid shell of thickness  $s(x, t)$ .  $s(x, t)$  defines instantaneous position of the freezing front and it consists of two parts such as  $s_0(t)$  and  $s_1(t)$ .  $s_0(t)$  indicates the mean shell thickness and  $s_1(t)$  denotes the amplitude of the developing periodic variation at moving interface due to non-uniform heat extraction. Thermal and mechanical problems are coupled through the contact pressure dependent thermal contact resistances at the shell/coating and coating/mold interfaces.  $T^c(x, y, t)$ ,  $T^b(x, y, t)$  and  $T^d(x, y, t)$  show the temperature fields in the solidified shell, coating layer and mold, respectively. These temperatures must satisfy the heat conduction differential equation;

$$\nabla^2 T^i(x, y, t) = \frac{1}{\alpha^i} \frac{\partial T^i}{\partial t}(x, y, t), \quad i = (b, c, d) \quad (2.1)$$

where  $\alpha^c$ ,  $\alpha^b$ ,  $\alpha^d$  denote the thermal diffusivities of the materials of solidified shell, coating layer and mold, respectively. The heat conduction parabolic equations are subject to the following boundary conditions:

$$T^c(x, s, t) = T_m \quad (2.2)$$

$$K^c \frac{\partial T^c}{\partial y}(x, s, t) = L_c \rho_c \frac{ds}{dt}(x, t) \quad (2.3)$$

$$K^c \frac{\partial T^c}{\partial y}(x, 0, t) = K^b \frac{\partial T^b}{\partial y}(x, 0, t) \quad (2.4)$$

$$K^b \frac{\partial T^b}{\partial y}(x, -u, t) = K^d \frac{\partial T^d}{\partial y}(x, -u, t) \quad (2.5)$$

$$T^d(x, -u - h, t) = 0 \quad (2.6)$$

$$K^d \frac{\partial T^d}{\partial y}(x, -u - h, t) = Q(t) \quad (2.7)$$

where  $L^c$ ,  $\rho^c$ ,  $K^c$ ,  $K^b$  and  $K^d$  define the latent heat, density of the solidified material and thermal conductivities of the solidified shell, coating layer and mold materials,

respectively. Eq. (2.2) shows that the temperature at the moving interface between the solid and liquid phases is always at melting temperature  $T_m$ . Eq. (2.3) defines an energy balance between heat conducted away from the freezing front into the solidified shell and the latent heat released during solidification. Eq.(2.4) and Eq. (2.5) state that the heat flux from the casting to coating layer and from coating layer to mold must be continuous. Eq. (2.6) defines the temperature at the bottom of the mold. The heat flux drawn from the bottom of the mold is given in Eq. (2.7).

If a heat flux is imposed across the junction, the uniform flow of heat is generally restricted to conduction through the contact spots. The limited number and size of the contact spots results in an actual contact area which is significantly smaller than the apparent contact area. This limited contact area causes a thermal resistance and this thermal contact resistance at the interface between the two metallic solid surfaces prevents the heat flux and cause mutual temperature differences at the opposite sides of this interface. The magnitude of the contact conductance is a function of a number of parameters including the thermophysical and mechanical properties of the materials in contact, the characteristics of the contacting surfaces, the presence of gaseous or nongaseous interstitial media, the apparent contact pressure, the mean junction temperature, and the conditions surrounding the junction [161]. Some additional factors which may affect the contact resistance are the direction of the heat flux, surface scratches or cracks, nonuniform loading which causes uneven contact pressure, relative motion or slipping between the surfaces, and the presence of oxides or contaminants on the contacting surfaces. In our model there will generally be some thermal contact resistance at the shell/coating and coating/mold interface due to the effects of surface roughness and contaminants films. Eq. (2.8) defines this relation between heat flux and thermal contact resistance.

$$Q(x, t) = \frac{T^c(x, 0, t) - T^b(x, 0, t)}{R} = \frac{T^b(x, -u, t) - T^d(x, -u, t)}{R_m} \quad (2.8)$$

where  $R$  is the thermal contact resistance at the shell/coating interface and  $R_m$  is contact resistance at coating/mold interface. The thermal contact resistance is very sensitive to changes in the local contact pressure. If the local pressure increases, the actual contact area at the interface increase and heat transfer rate at this region becomes higher since decrease in the contact resistance. For solidification process increasing heat transfer at

the interfaces between the solid layers cause the liquid metal solidify faster above the region where the thermal contact resistance decreases, than the other region. Inversely, decreasing in the contact pressure leads to decrease the actual contact area and accordingly leads to increase in the thermal contact resistance locally at this interface. The molten liquid above these local regions solidifies slower than the other region. Periodic variations at the moving interface occur as a result of these changes in the thermal contact resistance. Therefore, thermal and mechanical problems are analyzed together with the assumption is that thermal contact resistances  $R$  and  $R_m$  assumed to be continuous and differentiable function of contact pressure  $P(x, t)$ . Experiments about the pressure dependence of thermal contact resistance show that like in Figure 2.2.

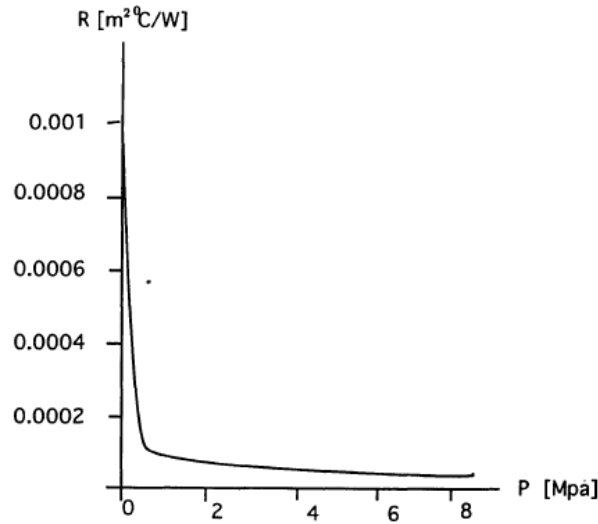


Figure 2.2 Typical experimental results for the variation of thermal contact resistance with contact pressure

### 2.3 The Perturbation Analysis

The rate of solidification of metals and the resulting properties of the cast product are controlled by the conditions at the shell/coating and coating/mold interfaces. If the mold is at uniform temperature, there is clearly a one-dimensional solution to the problem described above, in which the solidification front at any given time is defined by the straight line  $y = s_0(t)$  and all physical quantities are functions of  $y$ ,  $t$ , but are independent of  $x$ . If an  $x$ -dependent perturbation is to grow on this unperturbed or ‘zeroth order’ process, its development will be influenced by the instantaneous zeroth order quantities. As long as the perturbation is small compared with the zeroth order values, the perturbation will be linear, and permits us to use Fourier transformation in  $x$ .

This leads to reducing the dimensionality of the problem. Since the zeroth and first order problems involve fields varying in only one spatial dimension and time, they are considerably easier to implement and more efficient computationally than a full two dimensional numerical solution of the solidification problem.

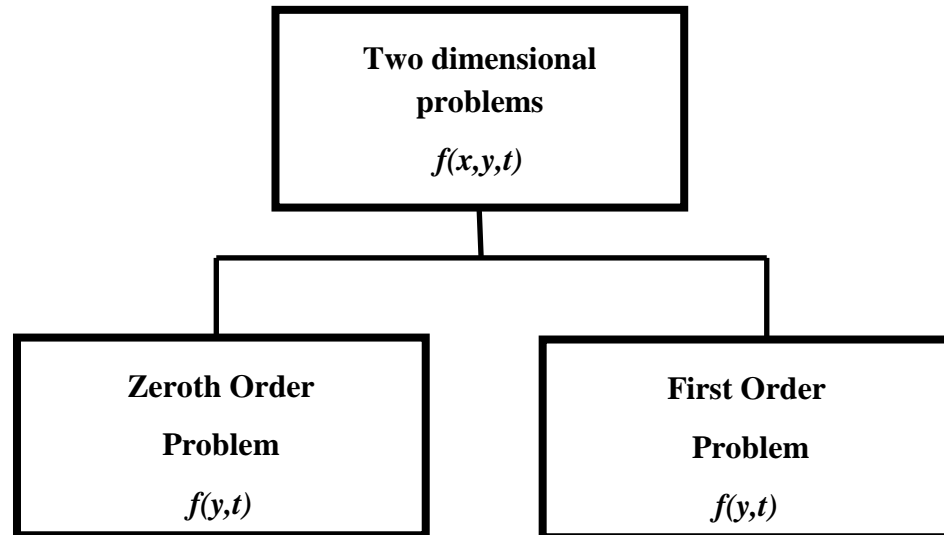


Figure 2.3 Reducing order of the problem by using linear perturbation method

When the thermal stresses are combined into the heat conduction problem as introduced above, we have to solve a nonlinear problem in  $y, t$  to determine the zeroth order solution, then the perturbation problem will be defined by differential equations with variable coefficients and first order quantities are derived by using zeroth order solutions. Since the nonlinearity of the problem is confined to the zeroth order process, which therefore generally requires a numerical solution, no extra difficulty will be introduced by using a fully nonlinear constitutive law for the material deformation. The rate of solidification of metals and the resulting properties of the cast product are largely controlled by the physics of the mold–shell interface. In particular, the interfacial heat flux is strongly moderated by contraction of the casting at the mold– shell interface which leads to local air gaps. Consequently, the local heat flux across the gaps becomes distorted since significant heat flow occurs through the solid–solid contacts in comparison to that across the gaps. Additionally, the mold surface might be imperfectly wetted because of surface tension in the molten metal, and therefore solid skin nucleation begins at asperity peaks with micro-air gaps between peaks. This action prevents heat from being extracted uniformly. Experimental observations indicate that the development of solidification front exhibits sinusoidal perturbations. It is anticipated



that this nonuniform shell growth could be a response to a pre-existing nonuniformity in the heat flux drawn from the mold surface. The suitable form of the heat flux with adding these sinusoidal non-uniformities is shown in Eq. (2.9).

$$Q(x, t) = Q_0(t) + Q_1(t) \cos(mx) \quad Q_0(t) \gg Q_1(t) \quad (2.9)$$

Where  $Q_0(t)$  and  $Q_1(t)$  are the time-dependent variables and define the uniform heat flux and magnitude of the adding perturbation into heat flux, respectively. The constant  $m$  is the wave number that describes the wavelength  $\lambda$  of the perturbation through Eq. (2.10).

$$\lambda = \frac{2\pi}{m} \quad (2.10)$$

Subscript 0 and 1 define the x-independent zeroth order process and the amplitude of the sinusoidal perturbation on the field quantities or first order process, respectively. Since the perturbation is sufficiently small compared with the unperturbed process and the other field quantities such as temperature fields and solidification front are defined in the form of similar inequalities in Eq. (2.11) and Eq. (2.12).

$$T(x, y, t) = T_0(y, t) + T_1(y, t) \cos(mx) \quad T_0(y, t) \gg T_1(y, t) \quad (2.11)$$

$$s(x, t) = s_0(t) + s_1(t) \cos(mx) \quad s_0(t) \gg s_1(t) \quad (2.12)$$

We assumed that the amplitude of this perturbation is small in comparison with its wavelength (i.e.  $ms_1 \ll 1$ ), in which the slope of the moving front,  $\partial s / \partial x$ , is very much less than unity. Therefore, the heat flux in the x-direction is negligible to the first order.

The thermal diffusivities of the mold, coating and solidified shell materials are assumed infinitely large. The physical meaning of this assumption is that the thermal capacities of the materials of the mold, coating and shell are zero. This assumption is correct at the beginning of the solidification since the materials properties have no significant effects on the process. This assumption allows us to solve the heat conduction problem analytically because the temperature distributions in the each layer changes linearly in space coordinate. This assumption converts the heat conduction equations in Eq. (2.1) to Laplace form like as follows

$$\nabla^2 T^c = 0 \quad \nabla^2 T^b = 0 \quad \nabla^2 T^d = 0 \quad (2.13)$$

The perturbation added form of temperature field in Eq. (2.11) substitutes into Eq. (2.13) then the periodic and uniform term are separated for obtaining the zeroth and first order heat conduction equations;

$$\frac{\partial^2 T_0^c}{\partial y^2}(y, t) = 0 \quad \frac{\partial^2 T_0^b}{\partial y^2}(y, t) = 0 \quad \frac{\partial^2 T_0^d}{\partial y^2}(y, t) = 0 \quad (2.14)$$

$$\begin{aligned} \frac{\partial^2 T_1^c}{\partial y^2}(y, t) - m^2 T_1^c(y, t) &= 0 \\ \frac{\partial^2 T_1^b}{\partial y^2}(y, t) - m^2 T_1^b(y, t) &= 0 \\ \frac{\partial^2 T_1^d}{\partial y^2}(y, t) - m^2 T_1^d(y, t) &= 0 \end{aligned} \quad (2.15)$$

The temperature fields are expanded in the vicinity of the mean shell thickness  $y = s_0(t)$ , in the form of Taylor series since perturbation on the shell thickness  $s_1(t)$  is very small compared with the  $s_0(t)$ . Then the boundary conditions can then be written by separating periodic and uniform terms and dropping the second and higher order and product terms in the small quantities. This procedure is applied to the boundary condition in Eq. (2.2) and it can be written as

$$\begin{aligned} T_0^c(s_0, t) + \frac{\partial T_0^c(s_0, t)}{\partial y} s_1(t) \cos(mx) + \frac{\partial^2 T_0^c(s_0, t)}{\partial y^2} \frac{s_1(t)^2 \cos^2(mx)}{2!} \\ + \left[ T_1^c(s_0, t) + \frac{\partial T_1^c(s_0, t)}{\partial y} s_1(t) \cos(mx) + \dots \right] \cos(mx) = T_m \end{aligned} \quad (2.16)$$

Then neglecting the third and fourth terms in left side of Eq. (2.16) and separating the periodic and uniform terms, we obtain the two first order equations;

$$T_0^c(s_0, t) = T_m \quad (2.17)$$

$$s_1(t) \frac{\partial T_0^c}{\partial y}(s_0, t) + T_1^c(s_0, t) = 0 \quad (2.18)$$

Similar procedure is applied to other thermal boundary conditions in Eq. (2.3) – Eq. (2.7). The obtained zeroth order boundary conditions are shown in Eq. (2.19) - Eq. (2.23) and the first order boundary conditions are given in Eq. (2.24) - Eq. (2.28).

The zeroth order thermal boundary conditions are

$$K^c \frac{\partial T_0^c}{\partial y}(s_0, t) = L_c \rho_c \frac{ds_0}{dt}(x, t) \quad (2.19)$$

$$K^c \frac{\partial T_0^c}{\partial y}(0, t) = K^b \frac{\partial T_0^b}{\partial y}(0, t) \quad (2.20)$$

$$K^b \frac{\partial T_0^b}{\partial y}(-u, t) = K^d \frac{\partial T_0^d}{\partial y}(-u, t) \quad (2.21)$$

$$T_0^d(-u - h, t) = 0 \quad (2.22)$$

$$K^d \frac{\partial T_0^d}{\partial y}(-u - h, t) = Q_0(t) \quad (2.23)$$

The first order thermal boundary conditions are

$$K^c \left[ \frac{\partial T_1^c}{\partial y}(s_0, t) + s_1(t) \frac{\partial^2 T_0^c}{\partial y^2}(s_0, t) \right] = L_c \rho_c \frac{ds_1}{dt}(x, t) \quad (2.24)$$

$$K^c \frac{\partial T_1^c}{\partial y}(0, t) = K^b \frac{\partial T_1^b}{\partial y}(0, t) \quad (2.25)$$

$$K^b \frac{\partial T_1^b}{\partial y}(-u, t) = K^d \frac{\partial T_1^d}{\partial y}(-u, t) \quad (2.26)$$

$$T_1^d(-u - h, t) = 0 \quad (2.27)$$

$$K^d \frac{\partial T_1^d}{\partial y}(-u - h, t) = Q_1(t) \quad (2.28)$$

Now we can rewrite the thermal contact resistances and heat flux relation at the shell/coating and coating/mold interfaces for unperturbed and perturbed processes. For zeroth order process contact pressure is constant and therefore it is not affected the thermal distortions in the solid layers. Therefore, zeroth order thermal contact resistance at shell/coating interface,  $R$ , and resistance at coating/mold interface,  $R_m$ , don't change during the process.

The zeroth order relations are

$$Q_0 = \frac{T_0^c(0, t) - T_0^b(0, t)}{R_0} = \frac{T_0^b(-u, t) - T_0^d(-u, t)}{R_m^0} \quad (2.29)$$

In order to obtain first order relations between the thermal contact resistances and the first order heat flux, we use following equations which are obtained by using developed procedure in [162,163].

$$\begin{aligned} \Delta Q &= Q_1(t) \cos(mx) \\ \Delta T^i &= T_1^i(t) \cos(mx) \quad (i = c, b, d) \\ \Delta P &= P_1(t) \cos(mx) \end{aligned} \quad (2.30)$$

Then differentiating Eq. (2.8) we obtain

$$\frac{\Delta Q}{Q_0} = \frac{\Delta T^c - \Delta T^b}{T_0^c - T_0^b} - \frac{R'(P_0) \Delta P}{R_0} \quad \text{at} \quad y = 0 \quad (2.31)$$

$$\frac{\Delta Q}{Q_0} = \frac{\Delta T^b - \Delta T^d}{T_0^b - T_0^d} - \frac{R'_m(P_0) \Delta P}{R_m^0} \quad \text{at} \quad y = -u \quad (2.32)$$

where  $R' = dR/dP$  and  $R'_m = dR_m/dP$  define the changes of the thermal contact resistances along the surfaces at  $y = 0$  and  $y = -u$  depending on the small variations in contact pressure at these interfaces. Each of the perturbed quantities changes with  $x$  only through the multiplier  $\cos(mx)$  and hence Eq. (2.31) and Eq. (2.32) are formed as

$$\frac{Q_1}{Q_0} = \frac{T_1^c - T_1^b}{T_0^c - T_0^b} - \frac{R'(P_0) P_1}{R_0} \text{ at } y = 0 \quad (2.33)$$

$$\frac{Q_1}{Q_0} = \frac{T_1^b - T_1^d}{T_0^b - T_0^d} - \frac{R'_m(P_0) P_1}{R_m^0} \text{ at } y = -u \quad (2.34)$$

As seen in the equations, first order problems includes terms of zeroth order solution such as  $s_0(t)$ ,  $T_0^c(y, t)$ ,  $T_0^b(y, t)$ ,  $T_0^d(y, t)$  and  $Q_0(t)$ . Therefore, firstly zeroth order problem is solved analytically then the solutions for added small perturbations in the field quantities are derived using these time dependent unperturbed solutions.

## 2.4 Solution of the Heat Conduction Problem

### 2.4.1 Solution for Zeroth-Order Thermal Problem

Due to the neglecting the effect of the thermal capacities of the solidified shell, coating layer and mold by assuming the thermal diffusivities are infinitely large, the heat conduction problem is solved analytically. Zeroth order heat conduction equations in Eq. (2.14) are solved using thermal boundary conditions in Eq. (2.17) and Eq. (2.20) - (2.23). The temperature fields in the solidified shell, coating layer and mold are

$$T_0^c(y, t) = T_m + \frac{Q_0(t)}{K^c} [y - s_0(t)] \quad (2.35)$$

$$T_0^b(y, t) = T_m + Q_0(t) \left[ \frac{y}{K^b} - \frac{s_0(t)}{K^c} - R_0 \right] \quad (2.36)$$

$$T_0^d(y, t) = \frac{Q_0(t)}{K^d} [y + u + h] \quad (2.37)$$

The unperturbed heat flux is obtained by substituting Eq. (2.36) and Eq. (2.37) into the right part of Eq. (2.29) with the result

$$Q_0(t) = \frac{T_m K^c K^b K^d}{(R_0 + R_m^0) K^c K^b K^d + u K^c K^d + s_0(t) K^b K^d + h K^c K^b} \quad (2.39)$$

Finally we calculate the unperturbed location of the moving interface by substituting Eq. (2.35) into Eq. (2.19), we obtain a first order ordinary differential equation as shown in Eq. (2.40).

$$\frac{ds_0(t)}{dt} = \frac{T_m K^c K^b K^d}{L^c \rho^c [(R_0 + R_m^0) K^c K^b K^d + u K^c K^d + s_0(t) K^b K^d + h K^c K^b]} \quad (2.40)$$

We solve this equation for determining mean shell thickness by using the initial condition  $s_0(0) = 0$ , we obtain

$$s_0(t) = \frac{-L^c \rho^c K^c [u K^d + K^b (h + (R_0 + R_m^0) K^d)]}{L^c \rho^c K^b K^d} + \frac{\sqrt{L^c \rho^c K^c \{L^c \rho^c K^c [u K^d + K^b (h + (R_0 + R_m^0) K^d)]^2 + 2t K^b K^d T_m\}}}{L^c \rho^c K^b K^d} \quad (2.41)$$

### 2.4.2 Solution for First-Order Thermal Problem

Subject to the governing equations for the first order heat conduction differential equations in Eq. (2.15), we assume general solutions for first order temperature field in the solidified shell, coating layer and mold as follows

$$T_1^c(y, t) = c_1(t) \sinh(my) + c_2(t) \cosh(my) \quad (2.42)$$

$$T_1^b(y, t) = c_3(t) \sinh(my) + c_4(t) \cosh(my) \quad (2.43)$$

$$T_1^d(y, t) = c_5(t) \sinh(my) + c_6(t) \cosh(my) \quad (2.44)$$

These equations put into the first order boundary conditions in Eq. (1.18) and Eq. (2.25) – Eq. (2.28) and we obtain the time-dependent coefficients as

$$c_1(t) = \frac{c_3(t)K^b}{K^c} \quad (2.45)$$

$$c_2(t) = -[s_1(t) \frac{Q_0(t)}{K^c \cosh(ms_0)} + c_1(t) \tanh(ms_0)] \quad (2.46)$$

$$c_3(t) = \frac{Q_1(t)}{mK^b} (\cosh(mu + mh) \cosh^2(mu) - \sinh(mu + mh) \sinh(mu) \cosh(mu))$$

$$+ \left( \frac{Q_1(t)}{Q_0(t)} + \frac{R'_m P_1(t)}{R_m} \right) \left( T_m + Q_0(t) \left( -\frac{u}{K^b} - \frac{s_0(t)}{K^c} - R_0 - \frac{h}{K^d} \right) \right) \sinh(mu) \quad (2.47)$$

$$+ \frac{Q_1(t)}{mK^d} (-\cosh(mu + mh) \sinh^2(mu) + \sinh(mu + mh) \cosh(mu) \sinh(mu))$$

$$c_4(t) = \left( \frac{Q_1(t)}{Q_0(t)} + \frac{R'_m P_1(t)}{R_m} \right) \left( T_m + Q_0(t) \left( -\frac{u}{K^b} - \frac{s_0(t)}{K^c} - R_0 - \frac{h}{K^d} \right) \right) \cosh(mu) \quad (2.48)$$

$$+ \frac{Q_1(t)}{mK^d} (-\cosh(mu + mh) \cosh(mu) \sinh(mu) + \sinh(mu + mh) \cosh^2(mu))$$

$$\frac{Q_1(t)}{mK^b} (\cosh(mu + mh) \cosh(mu) \sinh(mu) - \sinh(mu + mh) \sinh^2(mu))$$

$$c_5(t) = \frac{Q_1(t)}{mK^d} \cosh(mu + mh) \quad (2.49)$$

$$c_6(t) = \frac{Q_1(t)}{mK^d} \sinh(mu + mh) \quad (2.50)$$

For determining the magnitude of the perturbation on the heat flux at the bottom of the mold, we substitute Eq. (2.36), Eq. (2.37), Eq. (2.39), Eq. (2.42) and Eq.(2.43) into Eq. (2.34) and we obtain

$$Q_1(t) = \frac{d_1}{d_2} \quad (2.51)$$

where

$$d_1 = L^c \rho^c \frac{ds_1(t)}{dt} + ms_1(t)Q_0(t) \tanh(ms_0(t)) - \frac{R'_m(P_o)P_1(t)mK^b B \sinh(mu)}{\cosh(ms_0(t)) R_m^0} \quad (2.52)$$

$$d_2 = \frac{\cosh(mu + mh) \cosh^2(mu) - \sinh(mu + mh) \sinh(mu) \cosh(mu)}{\cosh(ms_0(t))} + \frac{B \sinh(mu) mK^b}{\cosh(ms_0(t)) Q_0(t)} + \frac{K^b}{K^d} \left( \frac{-\cosh(mu + mh) \sinh^2(mu) + \sinh(mu + mh) \cosh(mu) \sinh(mu)}{\cosh(ms_0(t))} \right) \quad (2.53)$$

$$B = T_m + Q_o(t) \left( -\frac{u}{K^b} - \frac{s_0(t)}{K^c} - R_0 - \frac{h}{K^d} \right) \quad (2.54)$$

Finally the magnitude of the perturbation on the mean shell thickness is not found directly because thermal contact resistance is a function of the contact pressure and first order contact pressure changes depending on the thermal distortions. Hence, we find the one of the coupled differential equations which contains thermal and mechanical terms by using Eq. (2.33). Eqs. (2.39), (2.51), (2.35), (2.36), (2.42) and (2.43) are substituted into Eq. (2.33) and rearranging the terms, we obtain

$$d_3 \frac{ds_1(t)}{dt} + d_4 s_1(t) + d_5 = 0 \quad (2.55)$$

where

$$\begin{aligned}
d_3 = & (L^c \rho^c (\cosh(mh) \cosh(ms_0(t)) \sinh(mu) K^c K^d) \\
& + \sinh(mu) \sinh(ms_0(t)) K^{b^2} (\sinh(mh) + mK^d R_m^0) \\
& + K^b (\cosh(mh) \cosh(mu) \sinh(ms_0(t)) K^d \\
& + \cosh(ms_0(t)) K^c (\cosh(mu) (\sinh(mh) + mK^d R_m^0) + mK^d R_0))) (uK^c K^d \quad (2.56) \\
& + K^b (K^c (h + K^d (R_0 + R_m^0)) + K^d s_0(t))))
\end{aligned}$$

$$\begin{aligned}
& / (mT_m K^{b^2} K^{c^2} K^d (\cosh(mh) \cosh(mu) K^d \\
& + \sinh(mu) K^b (\sinh(mh) + mK^d R_m^0)) R_0) \\
d_4 = & (mT_m \cosh(ms_0(t)) \sinh(mh) \sinh(mu) K^{b^3} K^c K^d \\
& + mT_m \cosh(mu) \sinh(mh) \sinh(ms_0(t)) K^{b^2} K^{c^2} K^d \\
& + mT_m \cosh(mh) \cosh(mu) \cosh(ms_0(t)) K^{b^2} K^c K^{d^2} \\
& + mT_m \cosh(mh) \sinh(mu) \sinh(ms_0(t)) K^b K^{c^2} K^{d^2} \\
& + m^2 T_m \cosh(ms_0(t)) \sinh(mu) K^{b^3} K^c K^{d^2} R_m^0 \quad (2.57) \\
& + m^2 T_m \cosh(mu) \sinh(ms_0(t)) K^{b^2} K^{c^2} K^{d^2} R_m^0 \\
& + m^2 T_m \sinh(ms_0(t)) K^{b^2} K^{c^2} K^{d^2} R_0)
\end{aligned}$$

$$\begin{aligned}
& / (mT_m K^{b^2} K^{c^2} K^d (\cosh(mh) \cosh(mu) K^d \\
& + \sinh(mu) K^b (\sinh(mh) + mK^d R_m^0)) R_0)
\end{aligned}$$

$$\begin{aligned}
d_5 = & (mT_m \cosh(mh) K^{b^2} K^{c^2} K^{d^2} P_1(t) R'_m \\
& - m^2 T_m \sinh(mu) K^{b^3} K^{c^2} K^{d^2} P_1(t) R'_m R_0 \\
& + mT_m \sinh(mh) \sinh(mu) K^{b^3} K^{c^2} K^d P_1(t) R' \quad (2.58) \\
& + mT_m \cosh(mh) \cosh(mu) K^{b^2} K^{c^2} K^{d^2} P_1(t) R' \\
& + m^2 T_m \sinh(mu) K^{b^3} K^{c^2} K^{d^2} P_1(t) R_m^0 R') \\
& / (mT_m K^{b^2} K^{c^2} K^d (\cosh(mh) \cosh(mu) K^d
\end{aligned}$$



$$+ \sinh(mu) K^b (\sinh(mh) + mK^d R_m^0) R_0)$$

Notice that  $d_5$  term involves the term of perturbation in contact pressure  $P_1(t)$  and it is obtained from the thermal stress problem which is discussed in the following section. Eventually first order thermal problem is coupled with the first order mechanical problem.

## CHAPTER 3

---

### DETERMINATION OF STRESS FIELDS

#### 3.1 Introduction

In the previous chapter, we determine the temperature fields in the solidified shell, coating layer and the mold. If the thermal behavior of the system is known, the stress field can be determined. Thermal stresses are one of the major factors responsible for generation of defects during the solidification process. Owing to the non-uniform thermal distortion in the solidified layer and mold due to the temperature variation, undesirable thermal stresses are developed in the solidification ingot. If these developed stresses reach the sufficient magnitude, they cause to failure such as formation of cracks in the final cast. Thermoelastic stresses in the solid layers are dependent of the thermal and mechanical behavior of the system during the solidification process. In this chapter, we determine the stress fields depending on the temperature fields. Developed solution procedure in [100] for obtaining the thermoelastic stress solution of solidification process is presented in Section 3.2. The unperturbed stress field depending on the mean contact pressure is given Section 3.3. In Section 3.4 the perturbed solution of the stress field which is corresponding to first order thermal and mechanical conditions, are obtained.

#### 3.2 Solution Procedure

Obtaining stress fields in the solidified shell, coating layer and mold necessitate complex calculations since the material is continually being solidified while the solid is in a deformed state. Residual stress is occurred in the final cast product, even after the temperature of the casting has been reduced at steady state value. We use linear

constitutive model for simplifying the modeling complexity. This model is much idealized condition because when the temperature of a material comes closer to its melting temperature, the yield strength of the material decreases. The solidified material is assumed to behave elastically during solidification in this model. Furthermore, there is no discontinuous change in the stress state of a particle as it passes from liquid to solid state and no significant shear stress will be occurred near the moving interface. Also no inelastic strains can occur at any point in the cast after it has solidified. The properties of the materials do not change with the temperature and density change effect between the solid and liquid phases is negligible.

Thermo-elastic stresses in the solidified shell, coating layer and mold corresponding to non-uniform temperature fields during the solidification are represented in the form

$$\sigma = \sigma^p + \sigma^h \quad (3.1)$$

$\sigma^p$  is a particular thermo-elastic solution and symbolizes the determining solution depending on the temperature distribution and it does not satisfy the mechanical boundary conditions.  $\sigma^h$  is the solution of homogeneous problem without any thermal strains. Homogeneous solution allows us to satisfy the mechanical boundary conditions by providing additional degree of freedom. A particular solution is determined based on the thermo-elastic displacement potential ( $\phi$ ) where

$$\nabla^2 \phi = \frac{E\alpha}{1-\nu} T \quad (3.2)$$

where  $T$  describes the temperature field and  $E$ ,  $\alpha$  and  $\nu$  are the Young's modulus, coefficient of thermal expansion and Poisson's ratio of the material, respectively. As mentioned before all properties of material do not vary with temperature. The stress and displacement components can then be expressed in terms of  $\phi$  using the following relations in Eqs. (3.3)

$$\begin{aligned} \sigma_{xx}^p &= -\frac{\partial^2 \phi}{\partial y^2} - \frac{\partial^2 \phi}{\partial z^2} \\ \sigma_{xy}^p &= \frac{\partial^2 \phi}{\partial x \partial y} \\ \sigma_{yy}^p &= -\frac{\partial^2 \phi}{\partial x^2} - \frac{\partial^2 \phi}{\partial z^2} \end{aligned} \quad (3.3)$$

$$\frac{E}{1+\nu} u_y^p = \frac{\partial \phi}{\partial y}$$

The homogenous solution can be obtained by using Airy stress function ( $\Phi$ ) where

$$\sigma_{xx}^h = \frac{\partial^2 \Phi}{\partial y^2} \quad \sigma_{xy}^h = \frac{\partial^2 \Phi}{\partial x \partial y} \quad \sigma_{yy}^h = \frac{\partial^2 \Phi}{\partial x^2} \quad (3.4)$$

These equations provide that the equilibrium conditions are satisfied by the obtained thermal stress field. The displacement potential function is obtained as a function of temperature field but however, Airy stress function is determined depending on the mechanical behavior of the system. During the solidification process, liquid material is continually solidified while the solid material is in a deformed state and all material is liquid phase at the beginning of the solidification. According to this, there is no appropriate initial condition for determining the displacement field. Because of this reason, the strains do not need to satisfy the compatibility equation and Airy stress function does not have to be biharmonic. The incompatible strains don't change as a function of time because we assumed that there is no inelastic strains can occur at any point of the solid after it has solidified. Therefore, Airy stress function is having the following form

$$\frac{\partial}{\partial t} \nabla^4 \Phi = 0 \quad (3.5)$$

The general solution of Eq. (3.5) can be written into two parts,

$$\Phi = \Phi_1 + \Phi_2 \quad (3.6)$$

$$\frac{\partial \Phi_1}{\partial t} = 0; \quad \nabla^4 \Phi_2 = 0 \quad (3.7)$$

where  $\Phi_1$  and  $\Phi_2$  denote the residual stress and instantaneous suitable response of the solid to the varying temperature field, respectively. Residual stress is the remaining stress when the casting has been cooled to uniform temperature after end of the solidification. Residual stress is independent of time but it is not necessarily biharmonic and hence, it has traction-free boundaries.

The mechanical boundary conditions in the present problem can be written as follows:

$$\sigma_{xx}^c = -p \quad \sigma_{yy}^c = -p \quad \sigma_{xy}^c = 0 \quad y = s(t) \quad \forall t \quad (3.8)$$

$$\sigma_{xy}^c = 0 \quad \sigma_{yy}^c = \sigma_{yy}^b \quad \sigma_{xy}^b = 0 \quad \dot{u}_y^c = \dot{u}_y^b \quad y = 0 \quad \forall t \quad (3.9)$$

$$\sigma_{xy}^b = 0 \quad \sigma_{yy}^b = \sigma_{yy}^d \quad \sigma_{xy}^d = 0 \quad \dot{u}_y^b = \dot{u}_y^d \quad y = -u \quad \forall t \quad (3.10)$$

$$\sigma_{xy}^b = 0 \quad \dot{u}_y^d = 0 \quad y = -u - h \quad \forall t \quad (3.11)$$

where  $p$  is the constant hydrostatic pressure in the molten metal. The boundary conditions associated with the displacements are written in terms of a time derivative because there is no reference state for determining displacements. Eqs. (3.8a) and (3.8b) define that the material is initially solidified under constant hydrostatic pressure.  $\sigma_{xy}^i = 0, (i = c, b, d)$ , denotes the frictionless contact at the solidified shell-coating and coating-mold interfaces. Eq. (3.11b) indicates that mold stands on the rigid surface and there is no displacement changes are occurred at the bottom of the mold. Due to the sinusoidal form of the temperature fields and heat flux with added perturbation on them, the thermal stress fields in the solidified shell, coating layer and mold, and contact pressure at the shell/coating and coating/mold interfaces may be written in following forms

$$\sigma(x, y, t) = \sigma_0(y, t) + \sigma_1(x, y, t) \quad \sigma_0(y, t) \gg \sigma_1(x, y, t) \quad (3.12)$$

The magnitude of the perturbation,  $\sigma_1(y, t)$ , is very small compared with the zeroth order stress  $\sigma_0(y, t)$ . The contact pressure at the solidified shell/coating interface can also be written as

$$P(x, t) = P_0(t) + P_1(t)\cos(mx) \quad P_0(t) \gg P_1(t) \quad (3.13)$$

In the solidified shell the magnitude and direction of the contact pressure at the solid/coating layer interface are same with the y-directional stress field but it has negative sense which is defined by

$$P(x, t) = -\sigma_{yy}^c(x, 0, t) \quad (3.14)$$

$$P_0(t) = -\sigma_{yy0}^c(0, t), \quad P_1(t) = -\sigma_{yy1}^c(0, t)$$

### 3.3 Determination of Zeroth Order Stress Field

#### 3.3.1 Particular Solution $((\sigma_0^i)^p)$

Firstly we consider the particular solution of the unperturbed stress field by choosing an appropriate displacement potential. The displacement potential function must satisfy the Eq. (3.2) corresponding to the temperature field  $T_0(y, t)$ . The temperature fields in the solidified shell, coating and mold are functions of only one spatial coordinate and time. Therefore Eq. (3.2) will take the form

$$\frac{\partial^2 \phi_0}{\partial y^2} = \frac{E\alpha}{1-\nu} T_0(y, t) \quad (3.15)$$

Also the first equation in Eq. (3.3) becomes

$$\sigma_{xx0}^p = -\frac{\partial^2 \phi_0}{\partial y^2} \quad (3.16)$$

where

$$\nabla^2 \phi_0 = \frac{E\alpha}{1-\nu} T_0(y, t) \quad (3.17)$$

Substituting the Eq. (3.16) into the Eq. (3.2), particular solution of the zeroth order stress field is determine in the form

$$(\sigma_{xx0}^p)^i = -\frac{E^i \alpha^i}{1-\nu^i} T_0^i(y, t) \quad (i = c, b, d) \quad (3.18)$$

The temperature fields in the solidified shell, coating layer and mold are determined in the previous section. We substitute the temperature fields in Eqs. (2.35), (2.36) and (2.37) into the Eq. (3.18) and then the particular solutions for x-directional zeroth order stress fields in the solidified shell, coating layer and mold are determined as follows

$$(\sigma_{xx0}^c)^p = -\frac{E^c \alpha^c}{1-\nu^c} \left\{ T_m + \frac{Q_0(t)}{K^c} [y - s_0(t)] \right\} \quad (3.19)$$

$$(\sigma_{xx0}^b)^p = -\frac{E^b \alpha^b}{1-\nu^b} \left\{ T_m + Q_0(t) \left[ \frac{y}{K^b} - \frac{s_0(t)}{K^c} - R_0 \right] \right\} \quad (3.20)$$

$$(\sigma_{xx0}^d)^p = -\frac{E^d \alpha^d}{1 - \nu^d} \left\{ \frac{Q_0(t)}{K^d} [y + u + h] \right\} \quad (3.21)$$

Since displacement potential  $\Phi_0$  is a function only of  $y$  and  $t$ , the other components of the zeroth order particular stress equations in Eq. (3.18) are equal to zero.

$$\begin{aligned} (\sigma_{xy0}^c)^p &= 0 & (\sigma_{yy0}^c)^p &= 0 & (\sigma_{xy0}^b)^p &= 0 & (\sigma_{yy0}^b)^p &= 0 \\ (\sigma_{xy0}^d)^p &= 0 & (\sigma_{yy0}^d)^p &= 0 \end{aligned} \quad (3.22)$$

The superscript  $c$ ,  $b$  and  $d$  symbolize the solidified shell, coating layer and mold, respectively.

### 3.3.2 Homogeneous Solution $((\sigma_0^i)^h)$

The homogeneous solution is determined by using uniform biaxial stress field and it always satisfy the mechanical boundary conditions in Eqs. (3.8) – (3.11)

$$(\sigma_{xx0}^c)^h = \frac{E^c \alpha^c}{1 - \nu^c} T_m - p \quad (\sigma_{xy0}^c)^h = 0 \quad (\sigma_{yy0}^c)^h = -p \quad (3.23)$$

$$\begin{aligned} (\sigma_{xx0}^b)^h &= \left( E^c (1 - (\nu^b)^2) \right)^{-1} \left( E^b (1 - (\nu^c)^2) \right) p \\ &\quad + \frac{E^b E^c Q_0(t) s_0(t)}{K^c} (\alpha^c (1 + \nu^c) - \alpha^b (1 + \nu^b)) \end{aligned} \quad (3.24)$$

$$+ E^b \nu^c (1 + \nu^c) p - E^c \nu^b (1 + \nu^b) p + E^c E^b (1 + \nu^b) \alpha^b (T_m - Q_0(t) R_0)$$

$$(\sigma_{xy0}^b)^h = 0 \quad (\sigma_{yy0}^b)^h = -p$$

$$(\sigma_{xx0}^d)^h = -\frac{p \nu^d}{1 - \nu^d} T_m - p \quad (\sigma_{xy0}^d)^h = 0 \quad (\sigma_{yy0}^d)^h = -p \quad (3.25)$$

### 3.3.3 Complete Solution $(\sigma_0^i)$

We superpose zeroth order particular and homogeneous stress field to get the complete zeroth order thermal stress field as follows;

$$\sigma_{xx0}^c = \frac{E^c \alpha^c}{1 - \nu^c} \frac{Q_0(t)}{K^c} [y - s_0(t)] - p \quad \sigma_{xy0}^c = 0 \quad \sigma_{yy0}^c = -p \quad (3.26)$$

$$\begin{aligned}\sigma_{xx0}^c = & \left(E^c(1 - (\nu^b)^2)\right)^{-1} \left(E^b(1 - (\nu^c)^2)\right) p + \frac{E^b E^c Q_0(t) s_0(t)}{K^c} (\alpha^c(1 + \nu^c) \\ & - \alpha^b(1 + \nu^b)) + E^b \nu^c(1 + \nu^c) p - E^c \nu^b(1 + \nu^b) p \\ & + E^c E^b(1 + \nu^b) \alpha^b (T_m - Q_0(t) R_0) \\ & - \frac{E^b \alpha^b}{1 - \nu^b} \left\{ T_m + Q_0(t) \left[ \frac{y}{K^b} - \frac{s_0(t)}{K^c} - R_0 \right] \right\}\end{aligned}\quad (3.27)$$

$$\sigma_{xy0}^b = 0 \quad \sigma_{yy0}^b = -p$$

$$\sigma_{xx0}^d = \frac{E^d \alpha^d}{1 - \nu^d} \left\{ \frac{Q_0(t)}{K^c} [y + u + h] \right\} - \frac{p \nu^d}{1 - \nu^d} \quad \sigma_{xy0}^d = 0 \quad \sigma_{yy0}^d = -p \quad (3.28)$$

$p$  is the constant hydrostatic pressure in the liquid. According to Eq. (3.14b) and Eq. (3.23c), unperturbed contact pressure  $P_0(t)$  at the solidified shell/coating interface and coating/mold interface is equal to this constant pressure as follows

$$P_0(t) = p \quad (3.29)$$

### 3.4 Determination of first order stress field

#### 3.4.1 Particular Solution $((\sigma_1^l)^p)$

The particular solution of the first order stress field is changed depending on the first order temperature fields,  $T_1^c(y, t) \cos(mx)$ ,  $T_1^b(y, t) \cos(mx)$  and  $T_1^d(y, t) \cos(mx)$ . The suitable particular solutions can be obtained by assuming the potentials in the forms of  $\phi_1^c = f^c(y, t) \cos(mx)$ ,  $\phi_1^b = f^b(y, t) \cos(mx)$  and  $\phi_1^d = f^d(y, t) \cos(mx)$  and we put them in the Eq. (3.2) to determine the functions  $f^c(y, t)$ ,  $f^b(y, t)$  and  $f^d(y, t)$

$$\frac{\partial^2 f^c(y, t)}{\partial y^2} - m^2 f^c(y, t) = \frac{E^c \alpha^c}{1 - \nu^c} T_1^c(y, t) \quad (3.30)$$

$$\frac{\partial^2 f^b(y, t)}{\partial y^2} - m^2 f^b(y, t) = \frac{E^b \alpha^b}{1 - \nu^b} T_1^b(y, t) \quad (3.31)$$

$$\frac{\partial^2 f^d(y, t)}{\partial y^2} - m^2 f^d(y, t) = \frac{E^d \alpha^d}{1 - \nu^d} T_1^d(y, t) \quad (3.32)$$



Notice that these equations must be satisfied for all  $t$  and hence it is an ordinary differential equation for  $f$  in which  $t$  appears only as a parameter. The displacement potential functions can be found as

$$\phi_1^c = \frac{E^c \alpha^c}{2m(1 - \nu^c)} [c_2(t) y \sinh(my) + c_1(t) y \cosh(my)] \cos(mx) \quad (3.33)$$

$$\phi_1^b = \frac{E^b \alpha^b}{2m(1 - \nu^b)} [c_4(t) y \sinh(my) + c_3(t) y \cosh(my)] \cos(mx) \quad (3.34)$$

$$\phi_1^d = \frac{E^d \alpha^d}{2m(1 - \nu^d)} [c_6(t) y \sinh(my) + c_5(t) y \cosh(my)] \cos(mx) \quad (3.35)$$

We can write the particular solution for the first-order stress fields in the solidified shell, coating layer and mold by substituting the Eqs. (3.33) - (3.35) into Eq. (3.3) as follows

$$\begin{aligned} \sigma_{xx1}^c &= -f^{c''}(y, t) \cos(mx) & \sigma_{xy1}^c &= -m f^{c'}(y, t) \cos(mx) \\ \sigma_{xx1}^c &= m^2 f^c(y, t) \cos(mx) \end{aligned} \quad (3.36)$$

$$\begin{aligned} \sigma_{xx1}^b &= -f^{b''}(y, t) \cos(mx) & \sigma_{xy1}^b &= -m f^{b'}(y, t) \cos(mx) \\ \sigma_{xx1}^b &= m^2 f^b(y, t) \cos(mx) \end{aligned} \quad (3.37)$$

$$\begin{aligned} \sigma_{xx1}^d &= -f^{d''}(y, t) \cos(mx) & \sigma_{xy1}^d &= -m f^{d'}(y, t) \cos(mx) \\ \sigma_{xx1}^d &= m^2 f^d(y, t) \cos(mx) \end{aligned} \quad (3.38)$$

where (') denotes differentiation with respect to  $y$ .

The particular first order stress fields in the solidified shell, coating layer and mold are

$$\begin{aligned} (\sigma_{xx1}^c)^p &= -\frac{E^c \alpha^c}{1 - \nu^c} \left\{ \left[ c_1(t) + \frac{m c_2(t)}{2} y \right] \sinh(my) \right. \\ &\quad \left. + \left[ c_2(t) + \frac{m c_1(t)}{2} y \right] \cosh(my) \right\} \cos(mx) \end{aligned} \quad (3.39)$$

$$\begin{aligned} (\sigma_{xy1}^c)^p &= -\frac{E^c \alpha^c}{2(1 - \nu^c)} \{ [c_2(t) + c_1(t) m y] \sinh(my) \\ &\quad + [c_1(t) + c_2(t) m y] \cosh(my) \} \cos(mx) \end{aligned} \quad (3.40)$$

$$(\sigma_{xy1}^c)^p = \frac{mE^c\alpha^c}{2(1-\nu^c)}\{c_2(t)y \sinh(my) + c_1(t)y \cosh(my)\}\cos(mx) \quad (3.41)$$

$$(\sigma_{xx1}^b)^p = -\frac{E^b\alpha^b}{1-\nu^b}\left\{\left[c_3(t) + \frac{mc_4(t)}{2}y\right]\sinh(my) + \left[c_4(t) + \frac{mc_3(t)}{2}y\right]\cosh(my)\right\}\cos(mx) \quad (3.42)$$

$$(\sigma_{xy1}^b)^p = -\frac{E^b\alpha^b}{2(1-\nu^b)}\{[c_4(t) + c_3(t)my]\sinh(my) + [c_3(t) + c_4(t)my]\cosh(my)\}\cos(mx) \quad (3.43)$$

$$(\sigma_{xy1}^b)^p = \frac{mE^b\alpha^b}{2(1-\nu^b)}\{c_4(t)y \sinh(my) + c_3(t)y \cosh(my)\}\cos(mx) \quad (3.44)$$

$$(\sigma_{xx1}^d)^p = -\frac{E^d\alpha^d}{1-\nu^d}\left\{\left[c_5(t) + \frac{mc_6(t)}{2}y\right]\sinh(my) + \left[c_6(t) + \frac{mc_5(t)}{2}y\right]\cosh(my)\right\}\cos(mx) \quad (3.45)$$

$$(\sigma_{xy1}^d)^p = -\frac{E^d\alpha^d}{2(1-\nu^d)}\{[c_6(t) + c_5(t)my]\sinh(my) + [c_5(t) + c_6(t)my]\cosh(my)\}\cos(mx) \quad (3.46)$$

$$(\sigma_{xy1}^d)^p = \frac{mE^d\alpha^d}{2(1-\nu^d)}\{c_6(t)y \sinh(my) + c_5(t)y \cosh(my)\}\cos(mx) \quad (3.47)$$

### 3.4.2 Homogeneous Solution $((\sigma_1^i)^h)$

The homogeneous solution can be determined by using Airy stress function and must satisfy the mechanical boundary conditions. The first order mechanical boundary conditions are obtained from boundary conditions in Eqs. (3.8) - (3.11) by using Taylor series expansion in the vicinity of mean shell thickness since amplitude of added perturbation is very small in comparison with the zeroth order quantities. The first boundary condition in Eq. (3.8) can be written, dropping second, higher and product terms in small quantities,  $\sigma_1$ ,  $s_1$ , as follows

$$\sigma_{xx0}^c(s_0, t) + \frac{\partial \sigma_{xx0}^c(s_0, t)}{\partial y} s_1(t) \cos(mx) + \sigma_{xx1}^c(s_0, t) = -p \quad (3.48)$$

Separating periodic and uniform terms and using Eq. (3.26a), we obtain the boundary condition for  $\sigma_{xx1}^c$  at  $y = s_0(t)$ , that is

$$\sigma_{xx1}^c(x, s_0, t) = \frac{E^c \alpha^c}{1 - \nu^c} T_0^{c'}(y, t) s_1(t) \cos(mx) \quad (3.49)$$

The derivative of the temperature field in the solidified shell with respect to  $y$  is calculated by using Eq. (2.35), with the result

$$T_0^{c'} = \frac{Q_0(t)}{K^c} \quad (3.50)$$

Applying the same procedure to the remaining boundary conditions in Eq. (3.8), we obtain

$$\sigma_{xy1}^c(x, s_0, t) = 0 \quad \sigma_{yy1}^c(x, s_0, t) = 0 \quad (3.51)$$

Similar procedure is applied to boundary conditions in Eqs. (3.9), (3.10) and (3.11), we have

$$\sigma_{xy1}^c(x, 0, t) = 0 \quad \sigma_{yy1}^c(x, 0, t) = \sigma_{yy1}^b(x, 0, t) \quad (3.52)$$

$$\sigma_{xy1}^b(x, 0, t) = 0 \quad \dot{u}_{y1}^c(x, 0, t) = \dot{u}_{y1}^b(x, 0, t) \quad (3.53)$$

$$\sigma_{xy1}^b(x, -u, t) = 0 \quad \sigma_{yy1}^b(x, -u, t) = \sigma_{yy1}^d(x, -u, t) \quad (3.54)$$

$$\sigma_{xy1}^d(x, -u, t) = 0 \quad \dot{u}_{y1}^b(x, 0, t) = \dot{u}_{y1}^d(x, 0, t) \quad (3.55)$$

$$\sigma_{xy1}^d(x, -u - h, t) = 0 \quad \dot{u}_{y1}^d(x, -u - h, t) = 0 \quad (3.56)$$

After determining the first order mechanical boundary conditions we can obtain the Airy stress functions  $\Phi^c$ ,  $\Phi^b$  and  $\Phi^d$  for each solid layers in the process. As we mentioned before the Airy stress function  $\Phi$  decompose two parts such as one can interpret time-independent residual stress and other one represent instantaneous compatible response of the solid to the changing temperature field. The time derivative of functions  $\Phi^c$ ,  $\Phi^b$  and  $\Phi^d$  must be biharmonic. Appropriate form of the Airy stress function is

$$\Phi^c = \{[a_1(t) + a_2(t)y] \cosh(my) + [a_3(t) + a_4(t)y] \sinh(my) + g(y)\} \cos(mx) \quad (3.57)$$

$$\Phi^b = \{[A_1(t) + A_2(t)y] \cosh(my) + [A_3(t) + A_4(t)y] \sinh(my)\} \cos(mx) \quad (3.58)$$

$$\Phi^d = \{[B_1(t) + B_2(t)y] \cosh(my) + [B_3(t) + B_4(t)y] \sinh(my)\} \cos(mx) \quad (3.59)$$

where  $a_1(t) - a_4(t)$ ,  $A_1(t) - A_4(t)$  and  $B_1(t) - B_4(t)$  are time-dependent coefficients and  $g(y)$  is the time-independent residual stress function. The homogeneous stress fields in the solidified shell, coating layer and mold are found by using Eq. (3.4), with the results

$$(\sigma_{xx1}^c)^h = \left\{ \left[ a_1(t) + a_2(t)y + \frac{2a_4(t)}{m} \right] \cosh(my) + \left[ a_3(t) + a_4(t)y + \frac{2a_2(t)}{m} \right] \sinh(my) + \frac{g''(y)}{m^2} \right\} m^2 \cos(mx) \quad (3.60)$$

$$(\sigma_{xy1}^c)^h = \left\{ \left[ a_1(t) + a_2(t)y + \frac{a_4(t)}{m} \right] \sinh(my) + \left[ a_3(t) + a_4(t)y + \frac{a_2(t)}{m} \right] \cosh(my) + \frac{g'(y)}{m} \right\} m^2 \sin(mx) \quad (3.61)$$

$$(\sigma_{yy1}^c)^h = -\{[a_1(t) + a_2(t)y] \cosh(my) + [a_3(t) + a_4(t)y] \cosh(my) + g(y)\} m^2 \cos(mx) \quad (3.62)$$

$$(\sigma_{xx1}^b)^h = \left\{ \left[ A_1(t) + A_2(t)y + \frac{2A_4(t)}{m} \right] \cosh(my) + \left[ A_3(t) + A_4(t)y + \frac{2A_2(t)}{m} \right] \sinh(my) \right\} m^2 \cos(mx) \quad (3.63)$$

$$(\sigma_{xy1}^b)^h = \left\{ \left[ A_1(t) + A_2(t)y + \frac{A_4(t)}{m} \right] \sinh(my) + \left[ A_3(t) + A_4(t)y + \frac{A_2(t)}{m} \right] \cosh(my) \right\} m^2 \sin(mx) \quad (3.64)$$

$$(\sigma_{yy1}^b)^h = -\{[A_1(t) + A_2(t)y] \cosh(my) + [A_3(t) + A_4(t)y] \cosh(my)(y)\} m^2 \cos(mx) \quad (3.65)$$

$$(\sigma_{xx1}^d)^h = \left\{ \left[ B_1(t) + B_2(t)y + \frac{2B_4(t)}{m} \right] \cosh(my) + \left[ B_3(t) + B_4(t)y + \frac{2B_2(t)}{m} \right] \sinh(my) \right\} m^2 \cos(mx) \quad (3.66)$$

$$(\sigma_{xy1}^d)^h = \left\{ \left[ B_1(t) + B_2(t)y + \frac{B_4(t)}{m} \right] \sinh(my) + \left[ B_3(t) + B_4(t)y + \frac{B_2(t)}{m} \right] \cosh(my) \right\} m^2 \sin(mx) \quad (3.67)$$

$$(\sigma_{yy1}^d)^h = -\{ [B_1(t) + B_2(t)y] \cosh(my) + [B_3(t) + B_4(t)y] \sinh(my) \} m^2 \cos(mx) \quad (3.68)$$

### 3.4.3 Complete Solution ( $\sigma_1^i$ )

We superpose first order particular and homogeneous stress field for determining the complete first order thermal stress field

$$\sigma_{xx1}^c(x, y, t) = \left\{ \left[ a_1(t) + a_2(t)y + \frac{2a_4(t)}{m} - \frac{r_1 c_2(t)}{m^2} - \frac{r_1 c_1(t)}{2m} y \right] \cosh(my) + \left[ a_3(t) + a_4(t)y + \frac{2a_2(t)}{m} - \frac{r_1 c_1(t)}{m^2} - \frac{r_1 c_2(t)}{2m} y \right] \sinh(my) + \frac{g''(y)}{m^2} \right\} m^2 \cos(mx) \quad (3.69)$$

$$\sigma_{xy1}^c(x, y, t) = \left\{ \left[ a_1(t) + a_2(t)y + \frac{a_4(t)}{m} - \frac{r_1 c_2(t)}{2m^2} - \frac{r_1 c_1(t)}{2m} y \right] \sinh(my) + \left[ a_3(t) + a_4(t)y + \frac{a_2(t)}{m} - \frac{r_1 c_1(t)}{2m^2} - \frac{r_1 c_2(t)}{2m} y \right] \cosh(my) + \frac{g'(y)}{m} \right\} m^2 \sin(mx) \quad (3.70)$$

$$\sigma_{yy1}^c(x, y, t) = \left\{ \left[ -a_1(t) - a_2(t)y + \frac{r_1 c_1(t)}{2m} y \right] \cosh(my) + \left[ -a_3(t) - a_4(t)y + \frac{r_1 c_2(t)}{2m} y \right] \sinh(my) - g(y) \right\} m^2 \cos(mx) \quad (3.71)$$

$$\begin{aligned}\sigma_{xx1}^b(x, y, t) = & \left\{ \left[ A_1(t) + A_2(t)y + \frac{2A_4(t)}{m} - \frac{r_2c_4(t)}{m^2} - \frac{r_2c_3(t)}{2m} y \right] \cosh(my) \right. \\ & + \left[ A_3(t) + A_4(t)y + \frac{2A_2(t)}{m} - \frac{r_2c_3(t)}{m^2} \right. \\ & \left. \left. - \frac{r_2c_4(t)}{2m} y \right] \sinh(my) \right\} m^2 \cos(mx)\end{aligned}\quad (3.72)$$

$$\begin{aligned}\sigma_{xy1}^b(x, y, t) = & \left\{ \left[ A_1(t) + A_2(t)y + \frac{A_4(t)}{m} - \frac{r_2c_4(t)}{2m^2} - \frac{r_2c_3(t)}{2m} y \right] \sinh(my) \right. \\ & + \left[ A_3(t) + A_4(t)y + \frac{A_2(t)}{m} - \frac{r_2c_3(t)}{2m^2} \right. \\ & \left. \left. - \frac{r_2c_4(t)}{2m} y \right] \cosh(my) \right\} m^2 \sin(mx)\end{aligned}\quad (3.73)$$

$$\begin{aligned}\sigma_{yy1}^b(x, y, t) = & \left\{ \left[ -A_1(t) - A_2(t)y + \frac{r_2c_3(t)}{2m} y \right] \cosh(my) \right. \\ & + \left[ -A_3(t) - A_4(t)y + \frac{r_2c_4(t)}{2m} y \right] \sinh(my) \left. \right\} m^2 \cos(mx)\end{aligned}\quad (3.74)$$

$$\begin{aligned}\sigma_{xx1}^d(x, y, t) = & \left\{ \left[ B_1(t) + B_2(t)y + \frac{2B_4(t)}{m} - \frac{r_3c_6(t)}{m^2} - \frac{r_3c_5(t)}{2m} y \right] \cosh(my) \right. \\ & + \left[ B_3(t) + B_4(t)y + \frac{2B_2(t)}{m} - \frac{r_3c_5(t)}{m^2} \right. \\ & \left. \left. - \frac{r_3c_6(t)}{2m} y \right] \sinh(my) \right\} m^2 \cos(mx)\end{aligned}\quad (3.75)$$

$$\begin{aligned}\sigma_{xy1}^d(x, y, t) = & \left\{ \left[ B_1(t) + B_2(t)y + \frac{B_4(t)}{m} - \frac{r_3c_6(t)}{2m^2} - \frac{r_3c_5(t)}{2m} y \right] \sinh(my) \right. \\ & + \left[ B_3(t) + B_4(t)y + \frac{B_2(t)}{m} - \frac{r_3c_5(t)}{2m^2} \right. \\ & \left. \left. - \frac{r_3c_6(t)}{2m} y \right] \cosh(my) \right\} m^2 \sin(mx)\end{aligned}\quad (3.76)$$

$$\begin{aligned}\sigma_{yy1}^d(x, y, t) = & \left\{ \left[ -B_1(t) - B_2(t)y + \frac{r_3c_5(t)}{2m} y \right] \cosh(my) \right. \\ & + \left[ -B_3(t) - B_4(t)y + \frac{r_3c_6(t)}{2m} y \right] \sinh(my) \left. \right\} m^2 \cos(mx)\end{aligned}\quad (3.77)$$

where

$$r_1 = \frac{E^c \alpha^c}{1 - \nu^c} \quad r_2 = \frac{E^b \alpha^b}{1 - \nu^b} \quad r_3 = \frac{E^d \alpha^d}{1 - \nu^d} \quad (3.78)$$

$c_1(t)$ ,  $c_2(t)$ ,  $c_3(t)$ ,  $c_4(t)$ ,  $c_5(t)$  and  $c_6(t)$  are the coefficients of first order temperature fields in the solidified shell, coating layer and mold which are determined during the solution of the thermal problem as in Eqs. (2.46)–(2-50). Elastic constitutive relations are used for the plane strain conditions to determine derivatives of displacements with the results

$$\begin{aligned} \dot{u}_{y1}^c(x, y, t) = & -\frac{1 + \nu^c}{E^c} \left\{ \left[ \dot{a}_1(t) + \dot{a}_2(t)y - \frac{1 - 2\nu^c}{m} \dot{a}_4(t) - \frac{r_1 \dot{c}_2(t)}{2m^2} \right. \right. \\ & \left. \left. - \frac{r_1 \dot{c}_1(t)}{2m} y \right] \sinh(my) \right. \\ & + \left[ \dot{a}_3(t) + \dot{a}_4(t)y - \frac{1 - 2\nu^c}{m} \dot{a}_2(t) - \frac{r_1 \dot{c}_1(t)}{2m^2} \right. \\ & \left. \left. - \frac{r_1 \dot{c}_2(t)}{2m} y \right] \cosh(my) \right\} m \cos(mx) \end{aligned} \quad (3.79)$$

$$\begin{aligned} \dot{u}_{y1}^b(x, y, t) = & -\frac{1 + \nu^b}{E^b} \left\{ \left[ \dot{A}_1(t) + \dot{A}_2(t)y - \frac{1 - 2\nu^b}{m} \dot{A}_4(t) - \frac{r_2 \dot{c}_4(t)}{2m^2} \right. \right. \\ & \left. \left. - \frac{r_2 \dot{c}_3(t)}{2m} y \right] \sinh(my) \right. \\ & + \left[ \dot{A}_3(t) + \dot{A}_4(t)y - \frac{1 - 2\nu^b}{m} \dot{A}_2(t) - \frac{r_2 \dot{c}_3(t)}{2m^2} \right. \\ & \left. \left. - \frac{r_2 \dot{c}_4(t)}{2m} y \right] \cosh(my) \right\} m \cos(mx) \end{aligned} \quad (3.80)$$

$$\begin{aligned} \dot{u}_{y1}^d(x, y, t) = & -\frac{1 + \nu^d}{E^d} \left\{ \left[ \dot{B}_1(t) + \dot{B}_2(t)y - \frac{1 - 2\nu^b}{m} \dot{B}_4(t) - \frac{r_3 \dot{c}_6(t)}{2m^2} \right. \right. \\ & \left. \left. - \frac{r_3 \dot{c}_5(t)}{2m} y \right] \sinh(my) \right. \\ & + \left[ \dot{B}_3(t) + \dot{B}_4(t)y - \frac{1 - 2\nu^b}{m} \dot{B}_2(t) - \frac{r_3 \dot{c}_5(t)}{2m^2} \right. \\ & \left. \left. - \frac{r_3 \dot{c}_6(t)}{2m} y \right] \cosh(my) \right\} m \cos(mx) \end{aligned} \quad (3.81)$$

The unknown time dependent coefficients  $a_1(t) - a_4(t)$ ,  $A_1(t) - A_4(t)$  and  $B_1(t) - B_4(t)$  are determined using first order mechanical boundary conditions in Eq. (3.49) – Eq. (3.56). We can use the first order stress field complete solutions in first order mechanical boundary conditions. The resulting calculations give 12 coupled algebraic equations which can be solved by using Cramer's rule to determine unknown coefficients in Airy stress functions.

$$\begin{aligned}
& z_1 a_1(t) + [s_0(t)z_1 + 2z_2/m]a_2(t) + z_2 a_3(t) + [s_0(t)z_2 + 2z_1/m]a_4(t) \\
& \quad + g''(s_0(t))/m^2 \\
& \quad = r_1 Q_0 s_1(t) / m^2 K^c + r_1 [c_2(t)/m^2 + c_1(t)s_0(t)/2m]z_1 \\
& \quad + r_1 [c_1(t)/m^2 + c_2(t)s_0(t)/2m]z_2
\end{aligned} \tag{3.82}$$

$$\begin{aligned}
& z_1 a_1(t) + s_0(t)z_1 a_2(t) + z_2 a_3(t) + s_0(t)z_2 a_4(t) + g(s_0(t)) \\
& \quad = r_1 c_1(t)s_0(t)z_1/2m + r_1 c_2(t)s_0(t)z_2/2m
\end{aligned} \tag{3.83}$$

$$\begin{aligned}
& z_2 a_1(t) + [s_0(t)z_2 + z_1/m]a_2(t) + z_1 a_3(t) + [s_0(t)z_1 + z_2/m]a_4(t) \\
& \quad + g'(s_0(t))/m \\
& \quad = r_1 [c_2(t)/2m^2 + c_1(t)s_0(t)/2m]z_2 \\
& \quad + r_1 [c_1(t)/2m^2 + c_2(t)s_0(t)/2m]z_1
\end{aligned} \tag{3.84}$$

$$a_3(t) + a_2(t)/m = r_1 c_1(t)/2m^2 \tag{3.85}$$

$$A_3(t) + A_2(t)/m = r_2 c_3(t)/2m^2 \tag{3.86}$$

$$a_1(t) = A_1(t) \tag{3.87}$$

$$\begin{aligned}
& \frac{1 + \nu^c}{E^c} \left[ a_3(t) - \frac{1 - 2\nu^c}{m} a_2(t) - \frac{r_1 c_1(t)}{2m^2} \right] \\
& \quad = \frac{1 + \nu^b}{E^b} \left[ A_3(t) - \frac{1 - 2\nu^b}{m} A_2(t) - \frac{r_2 c_3(t)}{2m^2} \right]
\end{aligned} \tag{3.88}$$

$$\begin{aligned}
& -z_4 A_1(t) + [uz_4 + z_3/m]A_2(t) + z_3 A_3(t) + [-uz_3 - z_4/m]A_4(t) \\
& \quad = r_2 [c_3(t)u/2m - c_4(t)/2m^2]z_4 \\
& \quad + r_2 [c_3(t)/2m^2 - c_4(t)u/2m]z_3
\end{aligned} \tag{3.89}$$



$$\begin{aligned}
& -z_4 B_1(t) + [uz_4 + z_3/m]B_2(t) + z_3 B_3(t) + [-uz_3 - z_4/m]B_4(t) \\
& = r_3[c_5(t)u/2m - c_6(t)/2m^2]z_4 \\
& + r_3[c_5(t)/2m^2 - c_6(t)u/2m]z_3
\end{aligned} \tag{3.90}$$

$$\begin{aligned}
& -z_3 A_1(t) + uz_3 A_2(t) + z_4 A_3(t) - uz_4 A_4(t) + z_3 B_1(t) - uz_3 B_2(t) \\
& - z_4 B_3(t) + uz_4 B_4(t) \\
& = r_2[c_3(t)uz_3/2m - c_4(t)uz_4/2m] \\
& + r_3[-c_5(t)uz_3/2m - c_6(t)uz_4/2m]
\end{aligned} \tag{3.91}$$

$$\begin{aligned}
& \frac{1 + v^b}{E^b} \left\{ -z_4 A_1(t) + \left[ uz_4 - \frac{1 - 2v^c}{m} z_3 \right] A_2(t) + z_3 A_3(t) \right. \\
& + \left[ -uz_3 + \frac{1 - 2v^b}{m} z_4 \right] A_4(t) \\
& + r_2 \left[ \frac{c_4(t)z_4}{2m^2} - \frac{c_3(t)uz_4}{2m} - \frac{c_3(t)z_3}{2m^2} + \frac{c_4(t)uz_3}{2m} \right] \Big\} \\
& = \frac{1 + v^d}{E^d} \left\{ -z_4 B_1(t) + \left[ uz_4 - \frac{1 - 2v^d}{m} z_3 \right] B_2(t) + z_3 B_3(t) \right. \\
& + \left[ -uz_3 + \frac{1 - 2v^d}{m} z_4 \right] B_4(t) \\
& + r_3 \left[ \frac{c_6(t)z_4}{2m^2} - \frac{c_5(t)uz_4}{2m} - \frac{c_5(t)z_3}{2m^2} + \frac{c_6(t)uz_3}{2m} \right] \Big\}
\end{aligned} \tag{3.92}$$

$$\begin{aligned}
& -z_6 B_1(t) + \left[ (u + h)z_6 - \frac{1 - 2v^d}{m} z_5 \right] B_2(t) + z_5 B_3(t) \\
& + \left[ -(u + h)z_5 + \frac{1 - 2v^d}{m} z_6 \right] B_4(t) \\
& = r_3[-c_6(t)/2m^2 + c_5(t)(u + h)/2m]z_6 \\
& + r_3[c_5(t)/2m^2 - c_6(t)(u + h)/2m]z_5
\end{aligned} \tag{3.93}$$

$$\begin{aligned}
& -z_6 B_1(t) + [(u + h)z_6 + z_5/m]B_2(t) + z_5 B_3(t) \\
& + [-(u + h)z_5 + z_6/m]B_4(t) \\
& = r_3[-c_6(t)/2m^2 + c_5(t)(u + h)/2m]z_6 \\
& + r_3[c_5(t)/2m^2 - c_6(t)(u + h)/2m]z_5
\end{aligned} \tag{3.94}$$

where (‘) denotes differentiation with respect to y.  $\mathbf{z_1}$  to  $\mathbf{z_6}$  coefficients are defined as follows

$$\begin{aligned} z_1 &= \cosh(ms_0(t)) & z_2 &= \sinh(ms_0(t)) & z_3 &= \cosh(mu) \\ z_4 &= \sinh(mu) & z_5 &= \cosh(mh) & z_6 &= \sinh(mh) \end{aligned} \quad (3.95)$$

After determining the time-dependent coefficients, all coefficients substitute into Eq. (3.94) and we can obtain the following differential equation

$$\alpha_6 \frac{ds_1(t)}{dt} + \alpha_7 s_1(t) + \alpha_8 g''(s_0(t)) + \alpha_9 g'(s_0(t)) + \alpha_{10} g(s_0(t)) = 0 \quad (3.96)$$

Then, we calculated the first order contact pressure using Eq. (4.14c) and Eq. (3.71) with the result

$$\begin{aligned} P_1(t) &= m^2 a_1(t) \\ a_1(t) &= \alpha_1 \frac{ds_1(t)}{dt} + \alpha_2 s_1(t) + \alpha_3 g''(s_0(t)) + \alpha_4 g'(s_0(t)) + \alpha_5 g(s_0(t)) \end{aligned} \quad (3.97)$$

Eq. (3.97) is substituted into Eq. (2.55) then we obtained the second differential equation in the following form

$$\alpha_{11} \frac{ds_1(t)}{dt} + \alpha_{12} s_1(t) + \alpha_{13} g''(s_0(t)) + \alpha_{14} g'(s_0(t)) + \alpha_{15} g(s_0(t)) = 0 \quad (3.98)$$

Eqs. (3.96) and (3.98) serve to determine residual stress function and position of the moving boundary as a function of time. These coupled equations need to be solved simultaneously and the solution method is discussed in the following section.

## CHAPTER 4

### NUMERICAL SOLUTION

#### 4.1 Dimensionless Presentation

Before proceeding to the solution, it is convenient to introduce the following dimensionless variables for generalization of the problem and simplifying the mathematical complexity.

$$Y = my \quad S(\beta) = ms(t) \quad H = mh \quad U = mu \quad (4.1)$$

$$\beta = m^2 \frac{K^c T_m}{\rho^c L^c} t \quad \bar{T}(Y, \beta) = \frac{T(y, t)}{T_m} \quad \bar{Q} = \frac{Q}{mK^c T_m} \quad (4.2)$$

$$\bar{P}(\beta) = \frac{1 - v^c}{E^c \alpha^c T_m} P(t) \quad G(Y) = \frac{m^2 (1 - v^c)}{E^c \alpha^c T_m} g(y) \quad R = mK^c R_0 \quad (4.3)$$

$$R_m = mK^c R_m^0 \quad \bar{R}' = \frac{E^c \alpha^c T_m mK^c}{1 - v^c} R'(P_0) \quad \bar{R}'_m = \frac{E^c \alpha^c T_m mK^c}{1 - v^c} R'_m(P_0) \quad (4.4)$$

$$\zeta_1 = \frac{K^c}{K^b} \quad \zeta_2 = \frac{K^b}{K^d} \quad \zeta_3 = \frac{K^c}{K^d} \quad \lambda_1 = \frac{1 - v^c}{1 - v^b} \quad \lambda_2 = \frac{1 - v^b}{1 - v^d} \quad (4.5)$$

$$\omega_1 = \frac{E^b \alpha^b}{E^c \alpha^c} \quad \omega_2 = \frac{E^d \alpha^d}{E^b \alpha^b} \quad \eta_1 = \omega_1 \lambda_1 \quad \eta_2 = \omega_2 \lambda_2 \quad (4.6)$$

$$\gamma_1 = \frac{E^b}{E^c} \frac{1 + v^c}{1 + v^b} \quad \gamma_2 = \frac{E^d}{E^b} \frac{1 + v^b}{1 + v^d} \quad (4.7)$$

Using these dimensionless parameters we can rewrite the thermal and mechanical equations. The dimensionless solutions of the zeroth order heat conduction problem are

$$\bar{T}_0^c(Y, \beta) = \frac{(R + R_m) + Y + U\zeta_1 + H\zeta_1\zeta_2}{(R + R_m) + S_0(\beta) + U\zeta_1 + H\zeta_1\zeta_2} \quad (4.8)$$

$$\bar{T}_0^b(Y, \beta) = \frac{R_m + Y\zeta_1 + U\zeta_1 + H\zeta_1\zeta_2}{(R + R_m) + S_0(\beta) + U\zeta_1 + H\zeta_1\zeta_2} \quad (4.9)$$

$$\bar{T}_0^d(Y, \beta) = \frac{\zeta_1\zeta_2(Y + U + H)}{(R + R_m) + S_0(\beta) + U\zeta_1 + H\zeta_1\zeta_2} \quad (4.10)$$

Then we convert the mean shell thickness in Eq. (2.41) and mean heat flux at the bottom of the mold in Eq. (2.39) to dimensionless forms, with the results

$$S_0(\beta) = -(\zeta_1 U + \zeta_1 \zeta_2 H + \bar{R}^T) + \sqrt{(U\zeta_1)^2 + (H\zeta_1\zeta_2)^2 + (\bar{R}^T)^2 + 2UH\zeta_1^2\zeta_2 + 2\bar{R}^T H\zeta_1\zeta_2 + 2U\bar{R}^T\zeta_1 + 2\beta} \quad (4.11)$$

$$\bar{Q}_0(\beta) = \frac{1}{\bar{R}^T + S_0(\beta) + U\zeta_1 + H\zeta_1\zeta_2} \quad (4.12)$$

where

$$\bar{R}^T = R + R_m \quad (4.13)$$

The first order temperature fields in Eqs. (2.42) – (2.44) can be written as

$$\bar{T}_1^c(Y, \beta) = C_1(\beta)\sinh(Y) + C_2(\beta)\cosh(Y) \quad (4.14)$$

$$\bar{T}_1^b(Y, \beta) = C_3(\beta)\sinh(Y) + C_4(\beta)\cosh(Y) \quad (4.15)$$

$$\bar{T}_1^d(Y, \beta) = C_5(\beta)\sinh(Y) + C_6(\beta)\cosh(Y) \quad (4.16)$$

where  $C_{1.....6}(\beta)$  are the time dependent dimensionless coefficients and dimensionless form of these coefficients are shown below.

$$C_1(\beta) = \frac{C_3(\beta)}{\zeta_1} \quad (4.17)$$

$$C_2(\beta) = -\left(\frac{Q_0(\beta)}{\cosh(S_0(\beta))} S_1(\beta) + C_1(\beta)\tanh(S_0(\beta))\right) \quad (4.18)$$

$$C_3(\beta) = \zeta_1 \bar{Q}_1(\beta)(\cosh(U + H)\cosh^2(U) - \sinh(U + H)\sinh(U)\cosh(U)) \quad (4.19)$$

$$\begin{aligned}
& + \left( \frac{\bar{Q}_1(\beta)}{\bar{Q}_0(\beta)} + \frac{\bar{R}'_m}{R_m} \right) (\sinh(U) - \sinh(U) \bar{Q}_0(\beta) (\zeta_1 U + S_0(\beta) + R + \zeta_1 \zeta_2 H)) \\
& + \zeta_1 \zeta_2 \bar{Q}_1(\beta) (-\cosh(U + H) \sinh^2(U) + \sinh(U + H) \cosh(U) \sinh(U)) \\
C_4(\beta) = & \left( \frac{\bar{Q}_1(\beta)}{\bar{Q}_0(\beta)} + \frac{\bar{R}'_m}{R_m} \right) (\cosh(U) - \cosh(U) \bar{Q}_0(\beta) (\zeta_1 U + S_0(\beta) + R \\
& + \zeta_1 \zeta_2 H)) \\
& + \zeta_1 \zeta_2 \bar{Q}_1(\beta) (-\cosh(U + H) \cosh(U) \sinh(U) + \sinh(U + H) \cosh^2(U)) \\
& + \zeta_1 \bar{Q}_1(\beta) (\cosh(U + H) \sinh(U) \cosh(U) - \sinh(U + H) \sinh^2(U))
\end{aligned} \tag{4.20}$$

$$C_5(\beta) = \zeta_1 \zeta_2 \bar{Q}_1(\beta) \cosh(U + H) \tag{4.21}$$

$$C_6(\beta) = \zeta_1 \zeta_2 \bar{Q}_1(\beta) \sinh(U + H) \tag{4.22}$$

where dimensionless form of the perturbed heat flux  $\bar{Q}_1(\beta)$  is obtained by using Eq. (2.51) in Chapter 2. It can be written as

$$\bar{Q}_1(\beta) = \frac{d_6}{d_7} \tag{4.23}$$

where

$$\begin{aligned}
d_6 = & \frac{dS_1(\beta)}{d\beta} + \bar{Q}_0(\beta) S_1(\beta) \tanh(S_0(\beta)) \\
& - \frac{\bar{R}'_m \bar{P}_1 (1 + Q_0(\beta) (-\zeta_1 U - S_0(\beta) - R - \zeta_1 \zeta_2 H)) \sinh(U)}{\zeta_1 \cosh(S_0(\beta)) \bar{R}'_m}
\end{aligned} \tag{4.24}$$

$$\begin{aligned}
d_7 = & \frac{\cosh(U + H) \cosh^2(U) - \sinh(U + H) \sinh(U) \cosh(U)}{\cosh(S_0(\beta))} \\
& + \frac{\sinh(U) (1 + Q_0(\beta) (-\zeta_1 U - S_0(\beta) - R - \zeta_1 \zeta_2 H))}{\zeta_1 \cosh(S_0(\beta)) \bar{Q}_0(\beta)} \\
& + \zeta_2 \left( \frac{-\cosh(U + H) \sinh^2(U) + \sinh(U + H) \cosh(U) \sinh(U)}{\cosh(S_0(\beta))} \right)
\end{aligned} \tag{4.25}$$

The first governing differential equation in Eq. (2.55), can be written dimensionless form as

$$d_8 \frac{dS_1(\beta)}{d\beta} + d_9 S_1(\beta) + d_{10} = 0 \quad (4.26)$$

where

$$d_8 = (\cosh(H)\cosh(S_0(\beta))\sinh(U)\frac{\zeta_1}{\zeta_2} + \sinh(U)\sinh(S_0(\beta))(\sinh(H) + \frac{R_m}{\zeta_1\zeta_2})) \quad (4.27)$$

$$+ \cosh(H)\cosh(U)\sinh(S_0(\beta))\frac{1}{\zeta_2} + \cosh(H)\zeta_1(\cosh(U)\sinh(H) + \cosh(U)\bar{R}^T\frac{1}{\zeta_1\zeta_2}))(u\zeta_1\zeta_2 + \zeta_1\zeta_2^2H + \zeta_2\bar{R}^T + \zeta_2S_0(\beta))$$

$$d_9 = \cosh(S_0(\beta))\sinh(H)\sinh(U)\zeta_2 + \cosh(U)\sinh(H)\sinh(S_0(\beta))\zeta_1\zeta_2 + \cosh(H)\cosh(U)\cosh(S_0(\beta)) + \cosh(H)\sinh(U)\sinh(S_0(\beta))\zeta_1 \quad (4.28)$$

$$+ \cosh(S_0(\beta))\sinh(U)\frac{R_m}{\zeta_1} + \cosh(U)\sinh(S_0(\beta))R_m + \sinh(S_0(\beta))R$$

$$d_{10} = \bar{P}_1(\cosh(H)\bar{R}'_m - \frac{\sinh(U)\bar{R}'_m R}{\zeta_1} + \sinh(H)\sinh(U)\zeta_2\bar{R}') + \cosh(H)\cosh(U)\bar{R}' + \frac{\sinh(U)\bar{R}'R_m}{\zeta_1} \quad (4.29)$$

The dimensionless form of the first order contact pressure is located in Eq. (4.28). The first order contact pressure is found in the solution of the mechanical problems and it is determined as in Eq. (3.96) and Eq. (3.97). These equations can be written in the dimensionless form as follows

$$\bar{P}_1(\beta) = \bar{a}_1(\beta) \quad (4.30)$$

$$\bar{a}_1(\beta) = \bar{\alpha}_1 \frac{dS_1(\beta)}{d\beta} + \bar{\alpha}_2 S_1(\beta) + \bar{\alpha}_3 G''(S_0(\beta)) + \bar{\alpha}_4 G'(S_0(\beta)) + \bar{\alpha}_5 G(S_0(\beta)) \quad (4.31)$$

We substitute the Eq. (4.30) and Eq. (4.31) into the Eq. (4.26) for writing first differential equation as a function of  $S_1(\beta)$  and  $G(S_0(\beta))$ , with the result

$$\bar{\alpha}_6 \frac{dS_1(\beta)}{d\beta} + \bar{\alpha}_7 S_1(\beta) + \bar{\alpha}_8 G''(S_0(\beta)) + \bar{\alpha}_9 G'(S_0(\beta)) + \bar{\alpha}_{10} G(S_0(\beta)) = 0 \quad (4.32)$$

Finally the governing second ordinary differential equation in Eq. (3.98) can be written dimensionless form as

$$\bar{\alpha}_{11} \frac{dS_1(\beta)}{d\beta} + \bar{\alpha}_{12} S_1(\beta) + \bar{\alpha}_{13} G''(S_0(\beta)) + \bar{\alpha}_{14} G'(S_0(\beta)) + \bar{\alpha}_{15} G(S_0(\beta)) = 0 \quad (4.33)$$

where  $(\bar{\phantom{x}})$  denotes the dimensionless form of the corresponding parameters. The dimensionless coefficients  $\bar{\alpha}_j$  ( $j = 1, \dots, 15$ ) are functions of  $S_0(\beta)$  and the other dimensionless constants and their terms are given in Appendix.

The differential equations in (4.32) and (4.33) constitute a pair of coupled ordinary differential equations to determine the unknown quantities  $G(Y)$  and  $S_1(\beta)$  by using given suitable initial condition at  $Y = 0$ . These coupled equations are solved simultaneously and the method of solution of this stiff problem is discussed in the following part.

## 4.2 Solution Method

The second order differential equations with variable coefficients Eq. (4.32) and Eq. (4.33) are solved by using similar approach in Yigit [107]. Firstly these coupled equations can be written in the state-space form with three state variables and solve them simultaneously. Before starting the solution we should write the equations as a function of only one variable as  $S_0(\beta)$  for this purpose. As seen in the equations there is a only one term is not a function of  $S_0(\beta)$  which is  $dS_1(\beta)/d\beta$ . We use chain rule for obtaining derivation of the  $S_1(\beta)$  with respect to  $S_0(\beta)$  instead of the derivation of  $S_1(\beta)$  with respect to  $\beta$  and we obtained

$$\frac{dS_1(\beta)}{dS_0(\beta)} = (\bar{R}^T + S_0(\beta) + U\zeta_1 + H\zeta_1\zeta_2) \frac{dS_1(\beta)}{d\beta} \quad (4.34)$$

Substituting the Eq. (4.34) into Eq. (4.32) and Eq. (4.33), the coupled differential equations are in the form of

$$\bar{\alpha}_{16} \frac{dS_1(\beta)}{dS_0(\beta)} + \bar{\alpha}_7 S_1(\beta) + \bar{\alpha}_8 G''(S_0(\beta)) + \bar{\alpha}_9 G'(S_0(\beta)) + \bar{\alpha}_{10} G(S_0(\beta)) = 0 \quad (4.35)$$

$$\bar{\alpha}_{17} \frac{dS_1(\beta)}{dS_0(\beta)} + \bar{\alpha}_{12}S_1(\beta) + \bar{\alpha}_{13}G''(S_0(\beta)) + \bar{\alpha}_{14}G'(S_0(\beta)) + \bar{\alpha}_{15}G(S_0(\beta)) = 0 \quad (4.36)$$

where  $\bar{\alpha}_{16}$  and  $\bar{\alpha}_{17}$  are the dimensionless coefficients as a function of  $S_0(\beta)$  and other system parameter and they are given in Appendix.

The state variables are defined as

$$x_1 = S_1(\beta) \quad x_2 = G(S_0(\beta)) \quad x_3 = G'(S_0(\beta)) \quad (4.37)$$

After that, the Eq. (4.35) and Eq. (4.36) are written in the form

$$x_1' = f_1x_1 + f_2x_2 + f_3x_3 + f_4 \quad (4.38)$$

$$x_2' = x_3 \quad (4.39)$$

$$x_3' = f_4x_1 + f_5x_2 + f_6x_3 + f_8 \quad (4.40)$$

where (') shows the differentiation with respect to  $S_0$  and the coefficients  $f_i$  ( $i = 1 \dots 8$ ) are the function of  $S_0$  and the other time-independent coefficient.  $f_i$  coefficients are given in Appendix.

In order to compare the results of this study with the limiting case in Yigit [107], the same initial conditions are used for solution. The initial conditions are defined in Eq. (4.41) when  $S_0$  is very small but finite.

$$x_1' = 0.1 \quad x_1 = 0 \quad x_3 = 0 \quad (4.41)$$

The initial condition given to  $x_1'$  is not a state but used for  $x_2$  and initial value of  $x_2$  state is determined with this artificial condition. Hence the first order problem is linear in contrast to the nonlinear zeroth order process and all the perturbed quantities are proportional to this initial value.

The solution is obtained by integrating Eq. (4.38), Eq. (4.39) and Eq. (4.40) with given initial conditions. The solution of this stiff problem is obtained by using a variable step variable-order predictor-corrector algorithm is presented in Bryne and Hindmarsh [164]. The constant process parameters are chosen to be  $\eta_1 = 1.3756$ ,  $\eta_2 = 1.5$ ,  $v_c = 0.37$ ,  $v_b = 0.32$ ,  $v_d = 0.28$ ,  $\gamma_1 = 3.4785$ ,  $\gamma_2 = 3$ .



### STABILITY ANALYSIS OF THERMOELASTIC CONTACT

#### 5.1 Introduction

In previous chapters we discussed the modelling of heat transfer and thermal stress problem and new dimensionless parameters are defined to extend the analysis. After that, we obtained two coupled second order ordinary differential equations with variable coefficients. Numerical solution of these coupled equations is determined by using variable step variable order corrector and predictor algorithm after converting the equations in state space form. In this chapter we investigate the effects of system parameters such as thickness of coating and mold, the thermal conductivity ratios between solidified shell, coating layer and mold materials, the thermal contact resistances at shell/coating and coating/mold interfaces, wavelength of the extracting heat at the bottom of the mold and coupling rates of the thermal and mechanical problems at the shell/coating and coating/mold interfaces, on the growth instability during solidification process. The results of these analyses are discussed in Section 5.2. A case study is done for applying the developed theoretical model to solidification of real pure metals in Section 5.3. For this purpose we examine the changes of the growth perturbation at solidification front between solid and liquid phases for specific material combinations and process parameter.

#### 5.2 Effects of the System Parameters

Before investigating the effects of system parameters on the growth of the perturbation in solidified shell thickness, we will compare the results of this study to the previously obtained solution due to Yigit [107], in which the pure metal solidifies on a deformable planar mold without a coating layer. The present theoretical model approaches the

Yigit's model in [107] when  $H = 5$ ,  $\bar{R}' = -1$ ,  $R = 0.3$ ,  $\eta_1 = 1.3756$ ,  $\nu_c = 0.37$ ,  $\nu_d = 0.28$  and  $\gamma_1 = 3.4785$  while  $U \ll 1$ ,  $R_m \ll 1$ ,  $\bar{R}'_m = 0$ ,  $\eta_2 = 1$ ,  $\gamma_2 = 1$  and  $\nu_b = 0.28$ . The coating thickness is not equal to zero because numerical algorithm doesn't allow us due to dividing zero. Figure 5.1 compares the perturbed solidification front obtained from the present model with the previous solution due to Yigit [107] when coupling rates between the solidified shell and mold are equal to -1 and -100, respectively. The results show excellent agreement signifying the performance of the numerical algorithm used in the solution of the present model. The particular interest will be given to the effect of coating properties on the growth instability in the present work. Therefore, thickness of the deformable mold is assumed to be constant as  $H = 4$  for all of the following simulations. Other process parameters are chosen to be  $R = 0.5$ ,  $R_m = 0.5$ ,  $\eta_1 = 1.3756$ ,  $\eta_2 = 1.5$ ,  $\nu_c = 0.37$ ,  $\nu_b = 0.32$ ,  $\nu_d = 0.28$ ,  $\gamma_1 = 3.4785$ ,  $\gamma_2 = 3$ .

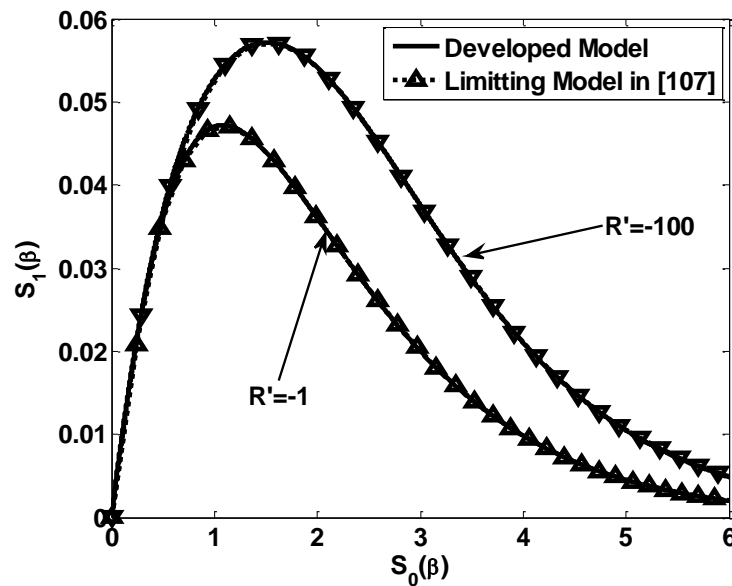


Figure 5.1 Comparison of the developed model with the limiting case in Yigit [107]

### 5.2.1 Effects of thermal conductivity of coating material

The effects of the thermal conductivity of coating material on the growth of the perturbation in solidified shell thickness for two different coating thickness ( $U = 0.1$  and  $U = 1$ ) and thermal conductivity ratio between shell and mold materials ( $\zeta_3 = 0.5$  and  $\zeta_3 = 2$ ) in four different coupling rate at the shell/coating and coating/mold interface cases in the following figures. Before determining the effects of thermal

conductivity of coating material on the growth instability, we must dwell on important parameter which is called thermal distortivity. Thermal distortivity of a material is a constant parameter which identifies the formed curvature in a body due to flowing heat through it [165]. It depends on the properties of the material of body and thermal distortivity of a material is formulated as

$$\delta = \alpha(1 + \nu)/K \quad (5.1)$$

where  $\alpha$ ,  $\nu$  and  $K$  are linear thermal expansion coefficient, Poisson's ratio and the thermal conductivity of the material, respectively. If two elastic bodies at different temperatures are placed in contact, there will be generally some contact resistance due to surface roughness and other contaminant films. Thermal contact resistance is a function of the local contact pressure and pressure distribution in contact area is very sensitive to small changes in surface profile. Thermoelastic distortions due to temperature fields in the bodies cause comparatively small surface variations and the total contact area at this interface changes. When heat flows through the interface between two different materials, then the ratio of the distortivities of these two materials comprising the interface deform relative to one another under the imposed thermal load.

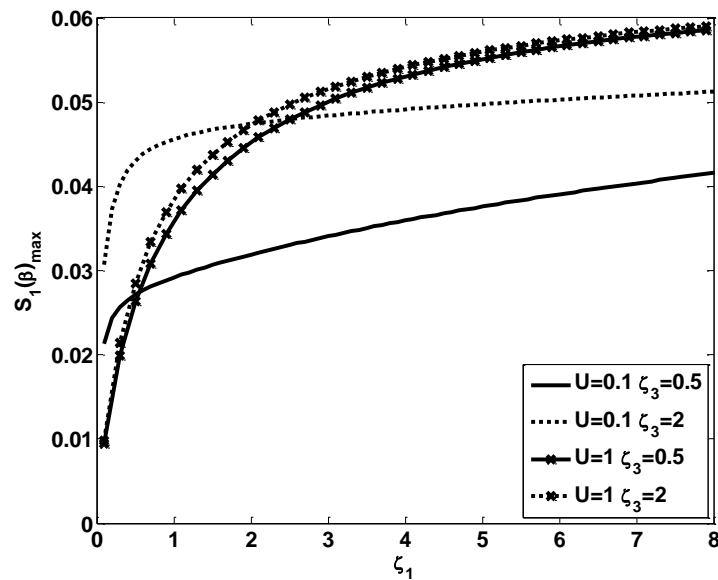


Figure 5.2 Maximum amplitude of perturbation in solidification front as a function of  $\zeta_1$  for selected values of coating thickness and  $\zeta_3$  when  $\bar{R}' = -1$ ,  $\bar{R}'_m = -1$

Figure 5.2 indicates the variations of maximum values of perturbed solidification front,  $S_1(\beta)_{max}$  with the thermal conductivity ratio between solidified shell and coating layer

materials,  $\zeta_1$  when the thermal and mechanical problems are weakly coupled at both lower and upper surfaces of the coating between the solidified shell and mold. The results show that increase in  $\zeta_1$  has the destabilizing effect on the growth of the solidifying shell for all combinations of  $\zeta_3$  (thermal conductivity ratio between the shell and mold materials) and mold thickness,  $U$  considered. In this way, an increase in thermal conductivity of the coating material leads to more non-uniform growth of the perturbation at moving interface regardless of its thickness and materials of the shell and mold. This suggests that selecting coating layer less distortive than the solidified shell and mold improves the quality of the final cast product. Thicker coating leads to more uniform growth for a coating layer with higher thermal conductivity. On the other hand, thinner coating layer improves the growth stability when the thermal conductivity of the coating material is decreased. It is also noteworthy that an increase in  $\zeta_3$  leads to increase in  $S_1(\beta)_{max}$  for fixed values of  $\zeta_1$ . In other words, decrease in thermal conductivity of the mold deteriorates growth stability of the solidified shell. This effect however diminishes as the coating layer thickness increases.

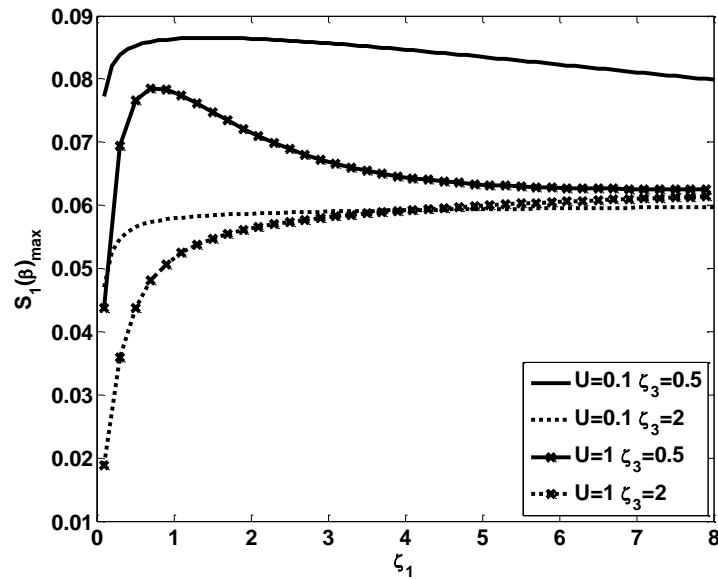


Figure 5.3 Maximum amplitude of perturbation in solidification front as a function of  $\zeta_1$  for selected values of coating thickness and  $\zeta_3$  when  $\bar{R}' = -100$ ,  $\bar{R}'_m = -1$

In order to investigate the effect of coupling rate at the shell/coating interface on the growth instability, we increased the value of  $\bar{R}'$  in Figure 5.3. When  $\zeta_3 < 1$ , increase in  $\zeta_1$  leads to two contrary effects on the growth of perturbation in solidified shell. There is a critical  $\zeta_1$  value for leading most non-uniform growth. This critical value is equal to 1

for both coating thicknesses considered. This means that when the thermal conductivity of coating material is selected close to the thermal conductivity of shell material, amplitude of the growth perturbation reaches its maximum value. This suggests that the thermal conductivity of coating material should be selected much greater or smaller than the thermal conductivity of shell material to minimize the growth instability. On the other hand, when the mold is more distortive than the solidified shell, ( $\zeta_3 > 1$ ),  $\zeta_1$  shows destabilizing effect on the growth of the perturbation for considered all coating thicknesses. Physically, decrease in thermal conductivity of the coating material leads to more non-uniform growth in the solidified shell. So, the thermal conductivity of the coating material should be selected much greater than the thermal conductivity of shell material to improve the cast quality.

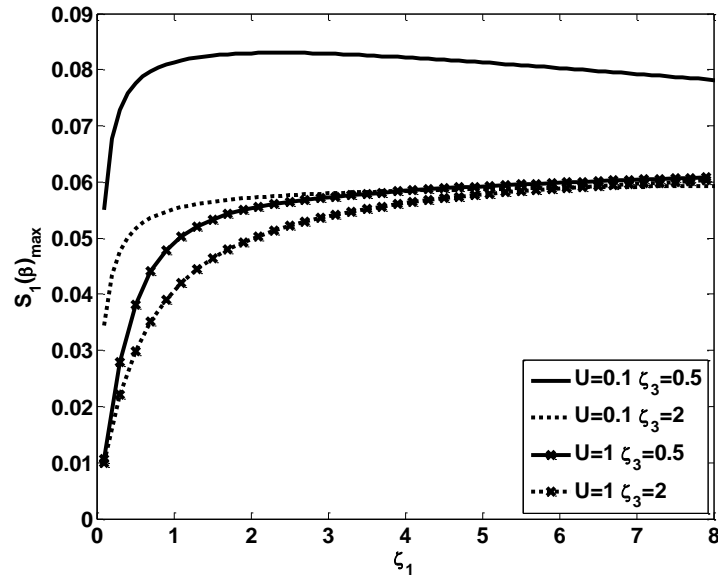


Figure 5.4 Maximum amplitude of perturbation in solidification front as a function of  $\zeta_1$  for selected values of coating thickness and  $\zeta_3$  when  $\bar{R}' = -1$ ,  $\bar{R}'_m = -100$

Figure 5.4 shows the variation of maximum amplitude of growth perturbation as a function of  $\zeta_1$  when the coupling rate is increased only at lower surface of the coating layer. We observed that an increase in  $\zeta_1$  changes the characteristic of the variation of  $S_1(\beta)_{max}$  only when  $U < 1$  and  $\zeta_3 < 1$ . The critical value of  $\zeta_1$  for leading the highest amplitude of growth perturbation is approximately equal to 2. Accordingly, thermal conductivity of the coating layer should not be selected close to the half of the value of thermal conductivity of shell material for a thin coating layer to decrease the instability when the solidified shell is more distortive than the mold. However, if the shell is more

rigid than mold, thermal conductivity of the coating material shows stabilizing effect on the growth instability regardless of coating thickness. Therefore, thermal conductivity of the coating material must be chosen much greater than shell material to obtain more uniform growth and a better quality final cast. Similarly,  $\zeta_1$  has destabilizing effect for thicker coating when shell is more distortive than the mold.

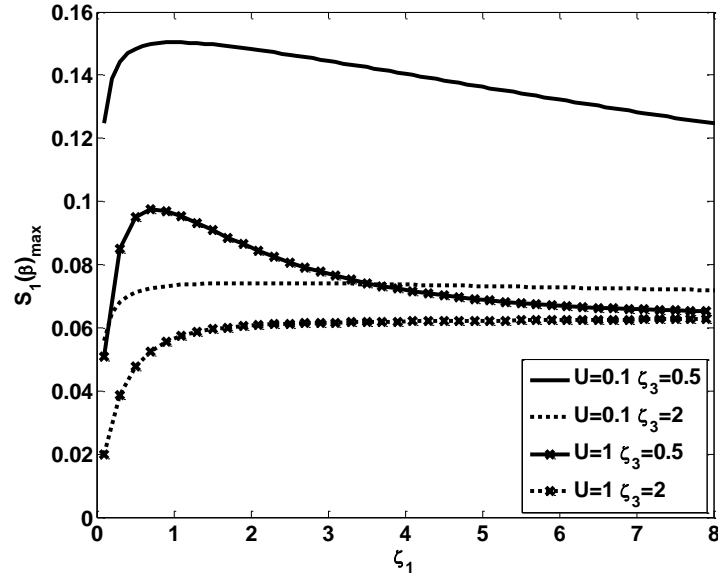


Figure 5.5 Maximum amplitude of perturbation in solidification front as a function of  $\zeta_1$  for selected values of coating thickness and  $\zeta_3$  when  $\bar{R}' = -100$ ,  $\bar{R}'_m = -100$

When thermal and mechanical problems are strongly coupled at the surfaces between shell/coating and coating/mold, the variation of  $S_1(\beta)_{max}$  is illustrated in Figure 5.5. The results show similar characteristics with the results in Figure 5.3. It can be seen that when  $\zeta_3 < 1$ , there are critical ratios, which are equal to 1 for both coating thicknesses considered. Similar to Figure 5.3, most non-uniform growth is observed when the thermal conductivities of shell and coating materials are selected close to the each other regardless of the coating thickness. On the other hand,  $\zeta_1$  has destabilizing effect on the growth of the solidifying shell when  $\zeta_3 > 1$ . In other words, thermal conductivity of coating material should be selected much less than thermal conductivity of solidified shell material to enhances the quality of final cast when mold is more distortive than shell. In addition, the coating thickness decreases the growth instability due to the less cooling rate. An increase in coating thickness also leads to increase the sensitivity of growth perturbation to thermal conductivity of coating material. It is also noteworthy that an increase in  $\zeta_3$  leads to decrease in growth instability for strong coupling rates at

both surfaces of coating layer. Additionally, it can be seen from the results in previous figures that  $\zeta_1$  dependence of the variation of magnitude of the growth perturbation at moving interface decreases for larger values of  $\zeta_1$ .

The variations of  $S_1(\beta)_{max}$  as a function of  $\zeta_1$  for  $\bar{R}'$ ,  $\bar{R}'_m$ ,  $U$  and  $\zeta_2$  are shown in the following figures. The physical meaning of increasing  $\zeta_1$  while  $\zeta_2$  is kept constant is that the thermal conductivity of solidified shell increases when thermal conductivity ratio between the coating and mold materials is not changed.

Figure 5.6 shows the variations of maximum values of perturbed solidification front,  $S_1(\beta)_{max}$  with the thermal conductivity ratio between solidified shell and coating layer materials,  $\zeta_1$  when the thermal and mechanical problems are weakly coupled at both lower and upper surfaces of the coating between the solidified shell and mold. The results show that increase in  $\zeta_1$  has the destabilizing effect on the growth of the solidifying shell for all combinations of  $\zeta_2$  (thermal conductivity ratio between the coating and mold materials) and mold thickness,  $U$  considered.

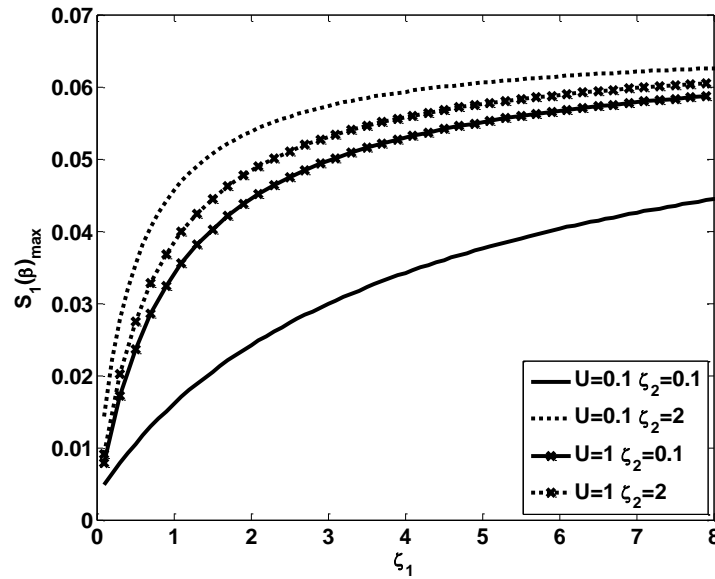


Figure 5.6 Maximum amplitude of perturbation in solidification front as a function of  $\zeta_1$  for selected values of coating thickness and  $\zeta_2$  when  $\bar{R}' = -1$ ,  $\bar{R}'_m = -1$

In physical meaning, thermal conductivity of solidified shell leads to increase in the magnitude of the growth perturbation in solidified shell regardless of the coating thickness and materials of the mold and coating. Therefore, the thermal conductivity of shell should be selected much less than thermal conductivity of the coating material for better quality. On the other hand, an increase in  $\zeta_2$  leads to more unstable growth of

perturbation in solidification front for fixed values of  $\zeta_1$ . This means that decrease in thermal conductivity of the mold material has destabilizing effect on the growth instability. However, this destabilizing effect diminishes when the coating thickness is increased. It should be also noted that coating thickness has destabilizing effect on the growth instability for weak coupling rates and an increase in  $\zeta_2$  leads to decrease in the sensitivity of the process to the coating thickness.

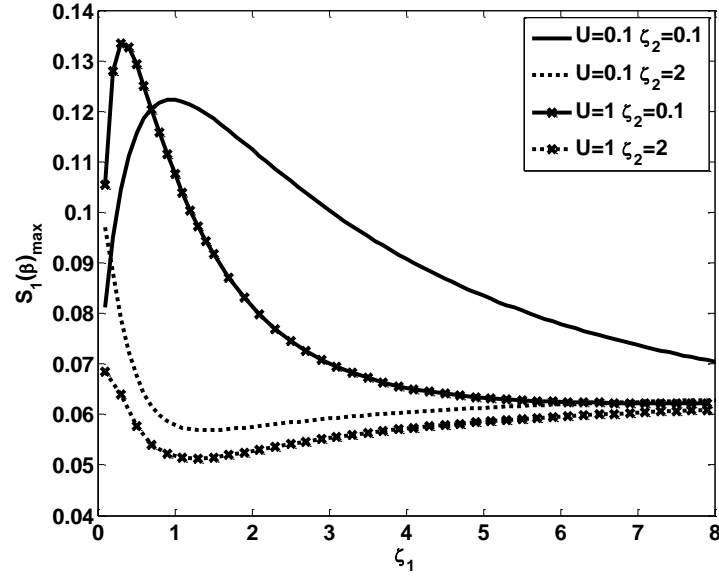


Figure 5.7 Maximum amplitude of perturbation in solidification front as a function of  $\zeta_1$  for selected values of coating thickness and  $\zeta_2$  when  $\bar{R}' = -100$ ,  $\bar{R}'_m = -1$

In order to investigate effects of coupling rates at the shell/coating and coating/mold interfaces  $\bar{R}'$  and  $\bar{R}'_m$  are increased individually in Figure 5.7 and Figure 5.8, respectively. It can be seen in Figure 5.7 that the characteristics of the curves are changed depending on the values of  $\zeta_2$ . When  $\zeta_2 < 1$ , there are critical  $\zeta_1$  values for leading most unstable growth in the solidified shell. These values are approximately equal to 1 and 0.4 for  $U = 0.1$  and  $U = 1$ , respectively. This suggests that thermal conductivity of solidified shell material must be chosen far enough away from thermal conductivity of coating material to minimize the unevenness in the solidified shell when the mold is coated with more distortive layer than itself. On the other hand, when  $\zeta_2 > 1$ , the characteristics of the curves are changed to be opposite for both coating thicknesses. The critical  $\zeta_1$  values for leading most stable growth at moving interface are equal to 1. Therefore, when the mold is coated with more rigid layer than itself, the thermal conductivity of solidified shell material should be selected close to thermal



conductivity of the coating layer regardless of the coating thickness. Additionally, the thickness of coating has stabilizing effect on the growth instability but an increase in  $\zeta_2$  leads to decrease in this effect.

The results in Figure 5.8 depict similar characteristics with the results in Figure 5.7 when the mold is more rigid than coating layer. The critical  $\zeta_1$  values are approximately equal to 1 and 0.6 for  $U = 0.1$  and  $U = 1$ , respectively. Similarly, selecting thermal conductivities of the shell and coating materials close to each other leads to the most non-uniform growth of the perturbation in solidified shell. When  $\zeta_2 > 1$ ,  $\zeta_1$  has stabilizing effect on the growth instability for relatively thin coating layer (i.e.,  $U = 0.1$ ) until it is approximately equal to 1. However, when  $\zeta_1$  exceeds this critical value, its stabilizing effect turns to destabilizing. It can be seen that most stable growth is observed when thermal conductivity of shell material should be selected close to thermal conductivity of the coating material for relatively thin coating layer (i.e.,  $U = 0.1$ ). Unlike that of Figure 5.7, an increase in  $\zeta_1$  leads to increase in the maximum of the growth perturbation in solidified shell thickness for relatively thicker coating layer ((i.e.,  $U = 1$ )) when  $\zeta_2 > 1$ .

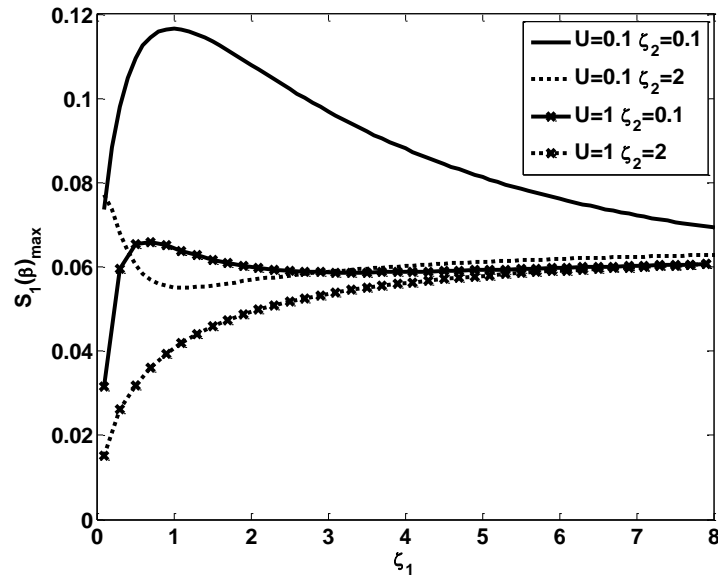


Figure 5.8 Maximum amplitude of perturbation in solidification front as a function of  $\zeta_1$  for selected values of coating thickness and  $\zeta_2$  when  $\bar{R}' = -1$ ,  $\bar{R}'_m = -100$

Combined effects of coupling rates at the shell/coating and coating/mold interfaces on the variation of  $S_1(\beta)_{max}$  are illustrated in Figure 5.9. It can be seen that the results for each combination show similar characteristics with Figure 5.7. Similar to Figure 5.7, the

results suggest that the thermal conductivity of the solidified shell material must be chosen much less or greater than the thermal conductivity of the coating material for both coating thicknesses considered when the mold is more rigid than the coating layer. On the other hand, when  $\zeta_2 > 1$ , the most stable growth is observed when thermal conductivities of the shell and coating materials are selected close to each other. In addition, an increase in coupling rates at both interfaces of coating layer leads to increase in the maximum of the growth perturbation at the moving interface.

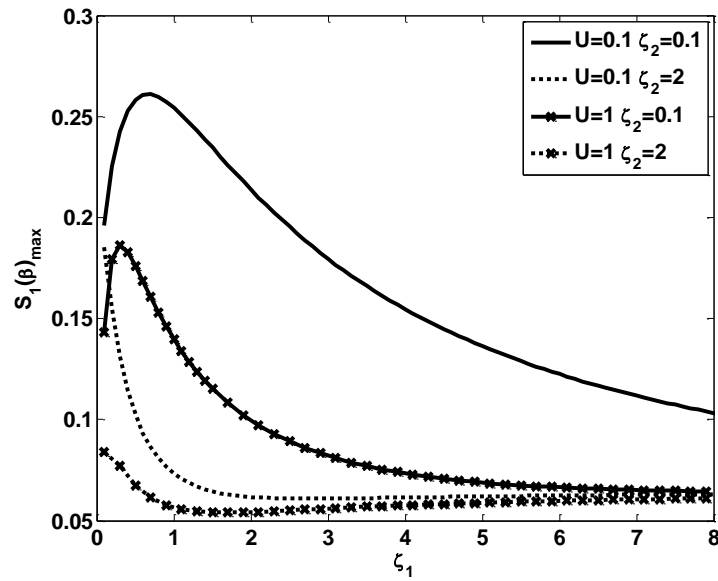


Figure 5.9 Maximum amplitude of perturbation in solidification front as a function of  $\zeta_1$  for selected values of coating thickness and  $\zeta_2$  when  $\bar{R}' = -100$ ,  $\bar{R}'_m = -100$

### 5.2.2 Effect of thickness of the mold coating layer, ( $U$ )

Thickness of the coating is an important parameter for the solidification process due to its thermal and mechanical effects on the thermoelastic instability during the solidification process. The thickness affects the mechanical stiffness of a layer and the temperature distribution in this layer significantly. An increase in the thickness of a layer leads to increase in the stiffness and decrease in the slope of temperature distribution in the layer. These two contrary effects of thickness have an important role on the growth instability when the material of the layer is selected highly distortive. The effects of the coating layer are investigated for different combinations of the thermal conductivity ratios of solidified shell, coating and mold materials and coupling rates at shell/coating and coating/mold interfaces. The dimensionless mold thickness is equal to

4 and the zeroth order thermal resistances at the shell/coating and coating/mold interfaces equals to 0.5 for all following simulations.

Figure 5.10 shows the variation of the growth perturbation in solidified shell as a function of the mean shell thickness for selected values of coating thickness when the thermal and mechanical problems are weakly coupled at upper and lower surfaces of coating layer. The thermal conductivity ratios are equal to 0.1 in this case. It means that the thermal conductivities of the materials are ranked as  $K^d > K^b > K^c$ . Therefore, solidified shell is most distortive and the mold is least distortive layer in the process.

The results show that coating thickness has destabilizing effect on the growth instability. For small coating thickness, coating layer shows more compliant to occurred distortions in the solidified shell. Therefore, the stabilizing effect of the stress relaxation overcomes the destabilizing effect of high cooling rate. This result suggests that coating thickness should be selected thinner for the case in which the thermal conductivities of solidified shell, coating and mold materials are ranked like this.

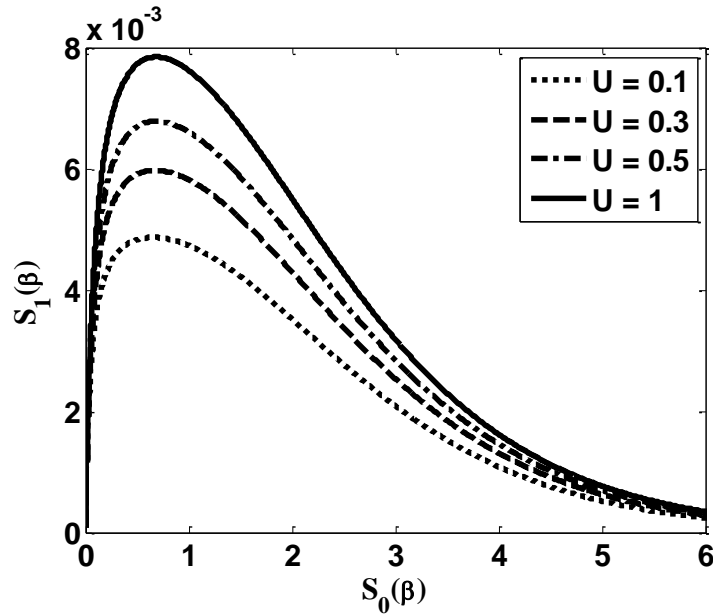


Figure 5.10 Perturbation in solidification front as a function of  $S_0(\beta)$  for selected values of  $U$  when  $\bar{R}' = -1$ ,  $\bar{R}'_m = -1$ ,  $\zeta_1 = 0.1$ ,  $\zeta_2 = 0.1$

On the other hand, it can be seen that the perturbation at the solidification front grows and reaches a maximum value for all cases. Then, the mean shell thickness becomes large enough, the conditions at the solidification front are less affected by the changes in the conditions at shell/coating and coating/mold interfaces. For this reason, the

amplitude of the perturbation starts to decrease and then completely diminishes at the end of the solidification process.

In order to investigate the effect of coating thickness when the thermal conductivity ranking of the materials is changed, Figure 5.11 is reproduced with the same parameters given in Figure 5.10 except the value of  $\zeta_1$ . We increased the value of  $\zeta_1$  from 0.1 to 2 and the thermal conductivities of the materials are ranked as  $K^d > K^c > K^b$ . The mold is still least distortive layer but differently from the previous figure, the coating layer is the most distortive material in this case. Similarly, increase in the coating layer leads to increase in amplitude of the perturbation in solidified shell when coupling rates are weak at both interfaces. Similar to previous case the stabilizing effect due to the high stress relaxation dominates the system behavior and overcomes to destabilizing effect of less cooling rate for thinner coating layer.

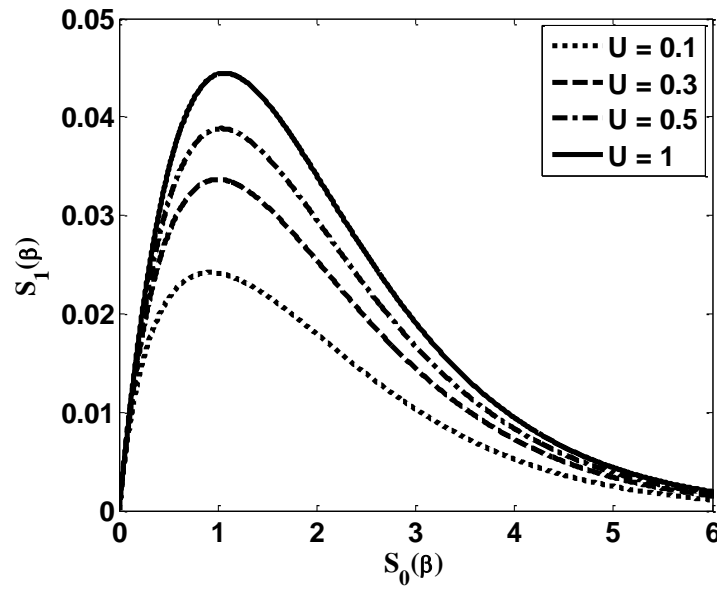


Figure 5.11 Perturbation in solidification front as a function of  $S_0(\beta)$  for selected values of  $U$  when  $\bar{R}' = -1$ ,  $\bar{R}'_m = -1$ ,  $\zeta_1 = 2$ ,  $\zeta_2 = 0.1$

It can be seen by comparing the previous figure that when the thermal conductivity of the coating material is selected less than the thermal conductivities of the solidified shell material, the amplitude of the perturbation at moving interface increases for all selected values of  $U$ . This result suggests that the coating material should be selected more rigid than the solidified shell regardless of the coating thickness to improve the quality of the casting. It is also noted that increase in  $\zeta_1$  leads to increase the coating thickness dependence of the growth instability when coupling rates are weak. On the other hand,

we can observed from the comparison this figure with the previous figure that the mean shell thickness when the perturbation reaches its maximum amplitude increases depending on an increase in  $\zeta_1$ .

Figure 5.12 shows the variation of the amplitude of the perturbation at moving interface as a function of mean shell thickness for ( $\zeta_1 = 0.1$ ,  $\zeta_2 = 2$ ) thermal conductivity ratio combination when coupling rates are weak. The thermal conductivities of the materials are ranked as  $K^b > K^d > K^c$ . As it is shown that the most rigid layer is coating and solidified shell is the most distortive layer in this case. It can be seen that the destabilizing effect of the coating thickness turns to opposite and increase in coating thickness leads to decrease in amplitude of the perturbation in solidified shell thickness. For highly rigid coating layer, stabilizing effect of less cooling rate overcomes the destabilizing effect of less stress relaxation.

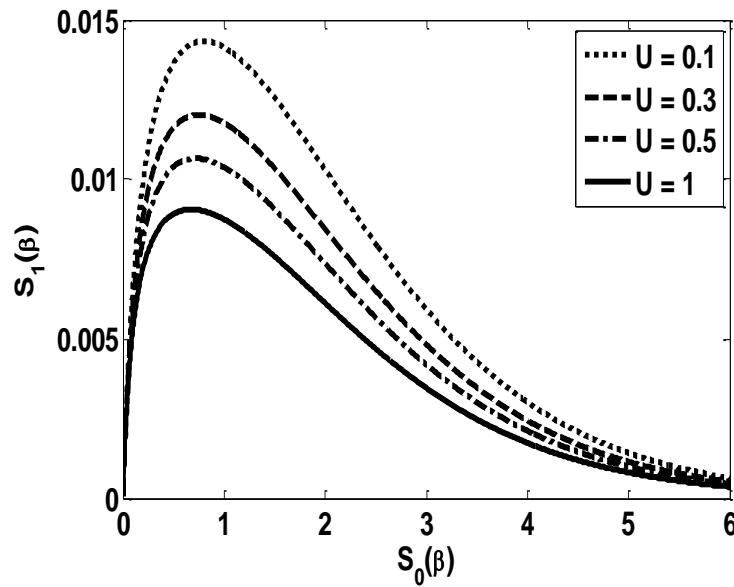


Figure 5.12 Perturbation in solidification front as a function of  $S_0(\beta)$  for selected values of  $U$  when  $\bar{R}' = -1$ ,  $\bar{R}'_m = -1$ ,  $\zeta_1 = 0.1$ ,  $\zeta_2 = 2$

This result suggests that when the mold is coated a layer which is more rigid than the mold, the thickness of highly rigid coating layer should be selected thicker for more uniform growth in the shell. On the other hand, when we compared the results in Figure 5.11 and Figure 5.12, we obtained that decrease in the thermal conductivity of coating material leads to decrease in the sensitivity of the growth perturbation to the coating thickness.

Figure 5.13 shows the effects of the coating thickness on growth instability when thermal conductivity ratios  $\zeta_1$  and  $\zeta_2$  are become greater than 1. The thermal conductivities of the materials are ranked as  $K^c > K^b > K^d$  for this case. The result shows that the thickness of coating layer has stabilizing effect on the growth of the perturbation in solidified shell but decrease in the maximum amplitude of the perturbation is less than the result in previous figure. Hence, an increase in  $\zeta_1$  decreases the stabilizing effect of the coating thickness on the growth instability. Physically, the sensitivity of the growth instability to coating thickness decreases when the mold and coating layer are more distortive than solidified shell. It can be seen by comparing the results in this figure and Figure 5.11 that increase in  $\zeta_2$  turns to effect of coating thickness from destabilizing to stabilizing. This means that increase in the thermal conductivity ratio between coating and mold materials leads to change the effect of the coating thickness on growth instability. However, coating thickness dependence of the process decreases when  $\zeta_1$  is increased while  $\zeta_2$  is equal to 2.

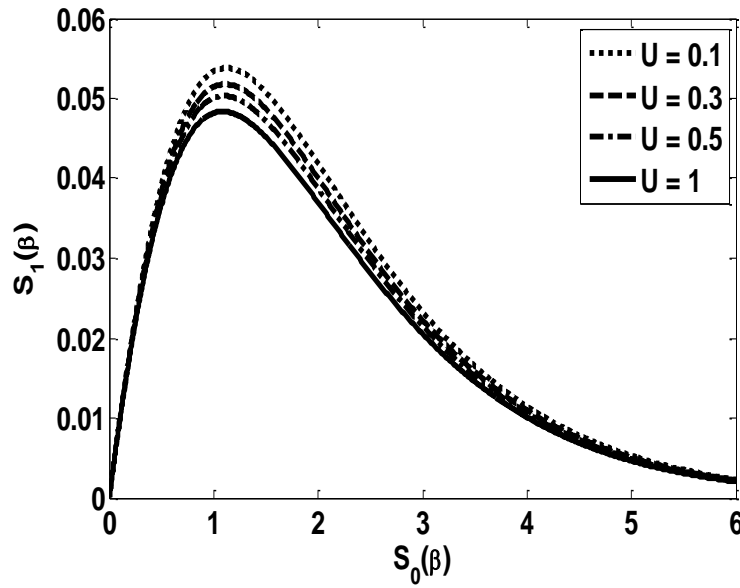


Figure 5.13 Perturbation in solidification front as a function of  $S_0(\beta)$  for selected values of  $U$  when  $\bar{R}' = -1$ ,  $\bar{R}'_m = -1$ ,  $\zeta_1 = 2$ ,  $\zeta_2 = 2$

In order to investigate the effect of the coupling effect at shell/coating interface on variation in the growth of the perturbation depending on the coating thickness, the value of the  $\bar{R}'$  is increased from -1 to -100 while the thermal and mechanical problems are coupled still weakly between coating layer and mold.

Figure 5.14 shows the variation of the growth perturbation in solidified shell for selected values of coating thickness when the both conductivity ratios between the solidified shell, coating layer and mold materials are less than one. Similar to Figure 5.10, coating thickness has destabilizing effect on the growth instability. The effect of the coupling at shell/coating interface does not change the destabilizing effect of the coating thickness but it leads to increase in amplitude of the perturbation for all coating thickness. In addition, the sensitivity of the uneven shell growth to coating thickness increases when the coupling rate at shell/coating interface is increased. On the other hand, the mean shell thickness when the perturbation reaches its maximum value becomes thicker for this combination of system parameters.

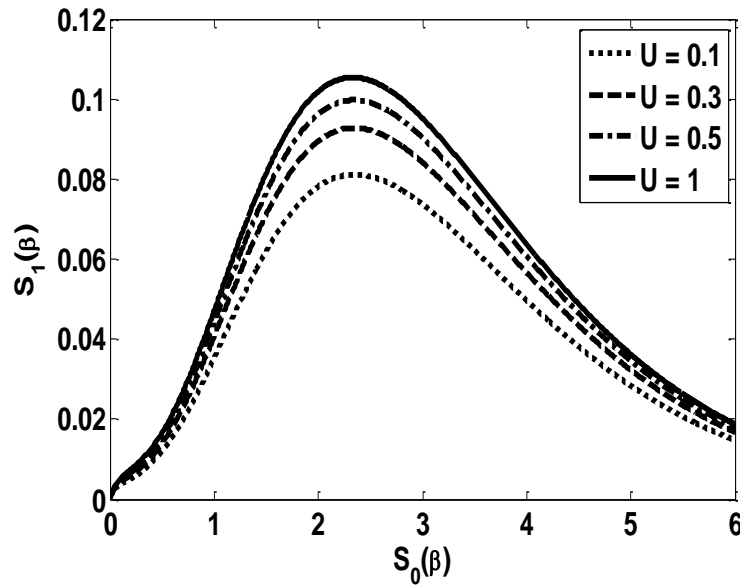


Figure 5.14 Perturbation in solidification front as a function of  $S_0(\beta)$  for selected values of  $U$  when  $\bar{R}' = -100$ ,  $\bar{R}'_m = -1$ ,  $\zeta_1 = 0.1$ ,  $\zeta_2 = 0.1$

Figure 5.15 indicates the effect of the coating thickness on the growth instability during solidification for same parameters given in previous figure except the value of  $\zeta_1$ . As mentioned before, the coating layer is more distortive than solidified shell but still mold is more rigid layer in this case. Differently from the results in Figure 5.11, increase in the thickness of coating layer leads to more uniform growth in the solidified shell when coupling rate at shell/coating interface is increased. As seen in the figure two different behaviors are shown depending on the increase in coating thickness during growth of the perturbation. Since  $U$  is large, its two contrary effects may be pronounced when the coating layer is highly distortive. First one is the stabilizing effect on the growth instability due to less cooling rate. However, the stiffness of the coating layer is high

due to large thickness and it necessitates higher stresses to straighten it out. This effect in turn will cause rapid growth of the perturbation. At the beginning of the process increasing coating thickness cause rapid growth for thicker coating since second destabilizing effect overcomes the first stabilizing effect. But these effects are not permanent and as the time progress the growing mean shell thickness gives positive contribution the stabilizing effect of the less cooling rate. Then, perturbation grows slowly for thicker coating layer and reaches smaller amplitude. When we compared this figure with the previous figure, the result show that increase in  $\zeta_1$  leads to change the effect of the coating thickness from destabilizing to stabilizing when coupling rate at shell/coating interface is strong while other one is weak. Additionally, the amplitude of the growth perturbation increases for all coating thickness when this coupling rate is increased. On the other hand, it can be seen by comparing the results in Figure 5.11 that coupling rate at the upper surface of coating changes the effect of the coating thickness on the process for same conditions.

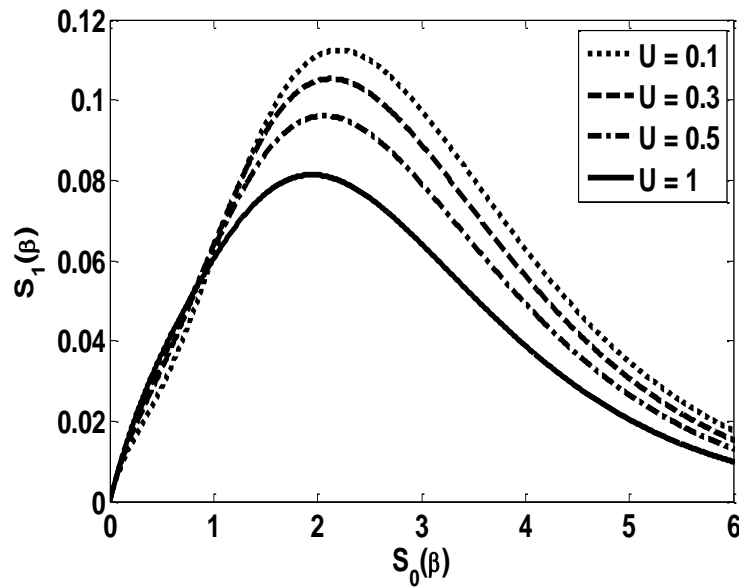


Figure 5.15 Perturbation in solidification front as a function of  $S_0(\beta)$  for selected values of  $U$  when  $\bar{R}' = -100$ ,  $\bar{R}'_m = -1$ ,  $\zeta_1 = 2$ ,  $\zeta_2 = 0.1$

Figure 5.16 depicts the effect of the coating thickness on the uneven shell growth during solidification under same coupling rates given in previous case when the thermal conductivity ratio between the coating and mold materials is increased to 2. The coating is most rigid layer in this case and increasing the coating thickness has a stabilizing effect on the growth instability. The stabilizing effect of less cooling rate overcomes the destabilizing effect of the less stress relaxation due to high rigidity of coating layer for



thicker coating layer. Since high rigidity of the coating layer, the destabilizing effect of coating stiffness has no significant effect for this case. It can be seen that the effect of the coating thickness on the growth instability does not change during the solidification like in the previous case. The perturbation grows slowly and reaches smaller amplitude for thicker coating. On the other hand, increase in coupling rate at shell/coating interface does not change the stabilizing effect of the coating thickness but it leads to increase in the mean shell thickness when the perturbation reaches its maximum amplitude. Additionally, this coupling rate increases the coating thickness sensitivity of the solidification process.

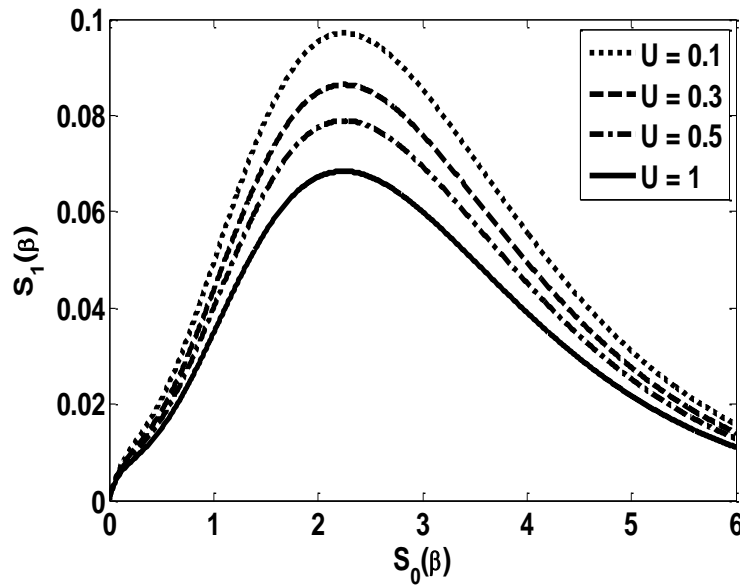


Figure 5.16 Perturbation in solidification front as a function of  $S_0(\beta)$  for selected values of  $U$  when  $\bar{R}' = -100$ ,  $\bar{R}'_m = -1$ ,  $\zeta_1 = 0.1$ ,  $\zeta_2 = 2$

Figure 5.17 shows the variation of the perturbation in solidified shell as a function of  $S_0(\beta)$  when  $\zeta_1$  and  $\zeta_2$  are greater than one. As described in Figure 5.13, highly rigid material solidifies on a more distortive mold and coating layer in this case. Similar to this figure, the destabilizing effect of stiffness of high distortive coating layer and stabilizing effect of less cooling rate suppress each other and coating thickness has minor stabilizing effect on the growth instability. It means that increase in coupling rate at shell/coating interface does not have significant effect on the effect of the coating thickness on the growth of the perturbation at moving interface. On the other hand, the sensitivity of the growth instability to coating thickness decreases when  $\zeta_1$  and  $\zeta_2$  is

greater than one. This means that when the solidified shell is selected more rigid than coating layer and mold, the effect of coating thickness reduces.

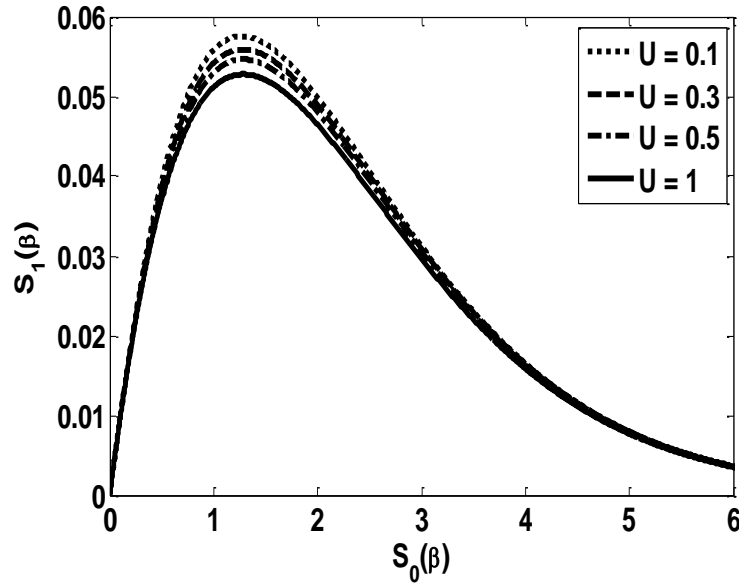


Figure 5.17 Perturbation in solidification front as a function of  $S_0(\beta)$  for selected values of  $U$  when  $\bar{R}' = -100$ ,  $\bar{R}'_m = -1$ ,  $\zeta_1 = 2$ ,  $\zeta_2 = 2$

In order to investigate the effect of the coating thickness on the growth of the perturbation in solidified shell when coupling between the coating and mold is strong only, we increased the value of  $\bar{R}'_m$  from -1 to -100 while  $\bar{R}'$  is still equal to -1. The influence of the coating thickness of the growth of the perturbation is shown in Figure 5.18 when the thermal conductivities of the materials are arranged as  $K^d > K^b > K^c$ .

The results show that thickness of the coating layer has stabilizing effect on the growth instability during the solidification process. The destabilizing effects of the coating thickness for same rank of thermal conductivity for different coupling rate combinations in Figure 5.10 and Figure 5.14 turns to stabilizing when the coupling rate at coating/mold interface is increased only. At the beginning of the process, destabilizing effect of less stress relaxation effect dominates the system but as the time is progressed stabilizing effect of the less cooling rate overcomes the destabilizing effects and growth of the perturbation slows down for thicker coating layer. This result suggest that increase in the coupling between the coating and the mold leads to more uniform growth in the solidified shell compared with increase in coupling between the solidified shell and the coating for thicker coating layer. On the other hand, dependence of the

growth instability on the coating thickness increases when the coupling at coating/mold interface is increased only.

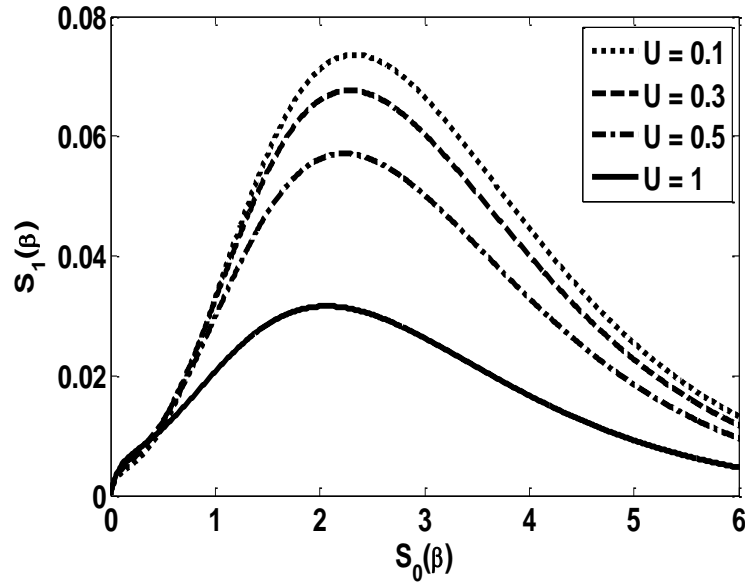


Figure 5.18 Perturbation in solidification front as a function of  $S_0(\beta)$  for selected values of  $U$  when  $\bar{R}' = -1$ ,  $\bar{R}'_m = -100$ ,  $\zeta_1 = 0.1$ ,  $\zeta_2 = 0.1$

Figure 5.19 shows the variation of the growth perturbation depending on the coating thickness for similar coupling rates with the previous case when the thermal conductivity ratios are arranged as  $\zeta_1 = 2$  and  $\zeta_2 = 0.1$ . When mean shell thickness is small, growth stability of the solidified shell is affected by the conditions at shell/coating and coating/mold interfaces very much. In this case, mold is more rigid than coating layer and destabilizing effect due to high stiffness of more distortive coating layer dominates the system behavior at the beginning of the process. Therefore, perturbation grows rapid for thicker coating layer at early stages of perturbation. But after a while, the stabilizing effect of less cooling rate overcomes this destabilizing effect and perturbation slows down. The thickness of the coating leads to decrease in the amplitude of the growth perturbation at freezing front. Due to high rigidity of the mold, its mechanical properties do not have significant effect on the process. When we compared the results in this figure and Figure 5.11, it is observed that increase in the coupling rate at coating/mold leads to change the effect of the coating thickness on growth stability from destabilizing to stabilizing. On the other hand, it can be seen by comparing the results in Figure 5.15 that the perturbation grows more uniform for all coating thickness when the coupling at coating/mold interface than when the coupling at

shell/coating interface. It is also noteworthy that the sensitivity of the growth instability to coating thickness when the coupling rate at coating/mold interface is increased is more than the sensitivity when coupling rate at shell/coating interface is increased only.

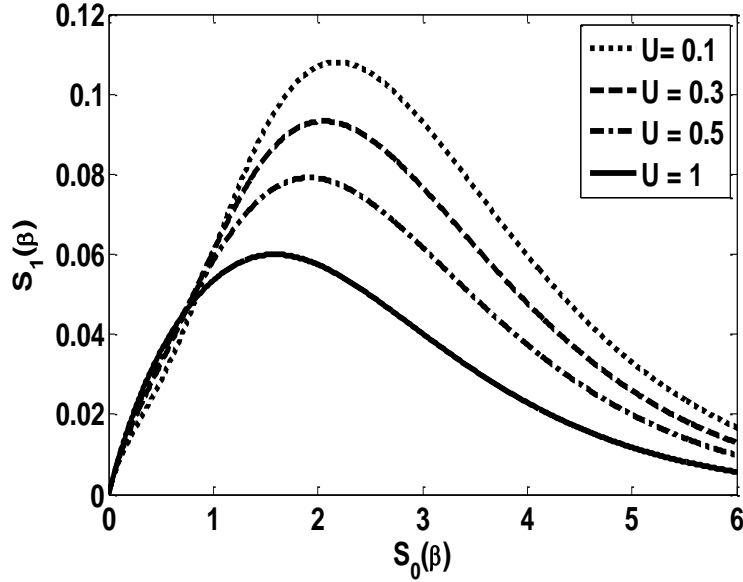


Figure 5.19 Perturbation in solidification front as a function of  $S_0(\beta)$  for selected values of  $U$  when  $\bar{R}' = -1$ ,  $\bar{R}'_m = -100$ ,  $\zeta_1 = 2$ ,  $\zeta_2 = 0.1$

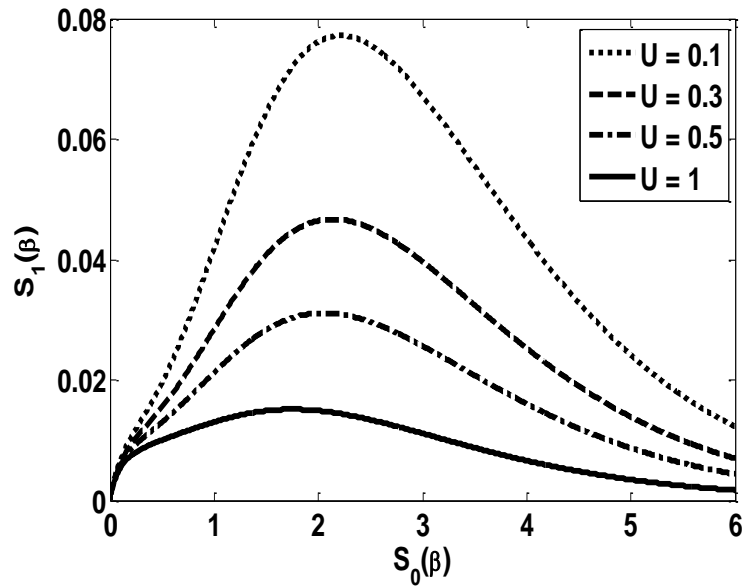


Figure 5.20 Perturbation in solidification front as a function of  $S_0(\beta)$  for selected values of  $U$  when  $\bar{R}' = -1$ ,  $\bar{R}'_m = -100$ ,  $\zeta_1 = 0.1$ ,  $\zeta_2 = 2$

Figure 5.20 shows that the effects of the coating thickness on the growth of the perturbation in the solidified shell when we use same parameters given in Figure 5.18 except the value of the  $\zeta_2$ .  $\zeta_2$  is increased from 0.1 to 2 and so that the mold is coated

more rigid coating layer than itself for this case. The result shows that thickness of the coating layer has stabilizing effect on the growth instability. Since the mold is more distortive than coating layer its mechanical stiffness becomes important. It causes destabilizing effect on the growth instability due to its stiffness. Stabilizing effect of less cooling rate overcomes the destabilizing effects of less stress relaxation due to high rigidity of coating layer for thicker coating layer. Thicker coating layer shows more uniform growth for all stages of solidification process. In comparison with the previous figure, increase in the rigidity of the coating layer leads to increase in sensitivity of the growth instability to coating thickness. It can be also seen by comparing this result with the result in Figure 5.16 that coupling rate at coating/mold interface leads to smaller amplitude of perturbation for all selected values of  $U$  than coupling rate at shell/coating when thermal conductivities of the materials are selected in this rank.

Similar to the results in Figure 5.13 and Figure 5.17, increases in the both thermal conductivity ratios between the solidified shell, coating layer and mold materials leads to decrease in the effect of the coating thickness on growth of the perturbation in solidified shell when the coupling at coating/mold interface is strong only. Similar characteristics are observed in this case with mentioned previous figures. It means that increases in the coupling rates at shell/coating and coating/mold interfaces individually do not have significant effect on the growth of the perturbation when  $\zeta_1$  and  $\zeta_2$  are greater than one. The effect of the coating thickness on the growth instability does not change when coupling rates are increased for this rank of thermal conductivities of materials.

When we examine the variation of growth of the perturbation depending on the coating thickness when the thermal and mechanical problems are strongly coupled at both shell/coating and coating mold interface, the results show that combined effects of coupling rates cause to increase in the amplitude of the perturbation for all cases except  $\zeta_1 = 2$  and  $\zeta_2 = 2$  case. Similar to the cases in which coupling rate at coating/mold is strong only, the thickness of coating layer has stabilizing effect on the growth instability during the solidification process for all combinations thermal conductivity ratios between the solidified shell, coating layer and mold materials. On the other hand, the sensitivity of the growth instability to the coating thickness increases for  $\zeta_1 = 0.1 - \zeta_2 = 0.1$ ,  $\zeta_1 = 2 - \zeta_2 = 0.1$  and  $\zeta_1 = 0.1 - \zeta_2 = 2$  conductivity ratios combinations when the coupling rates at the upper and lower surfaces of coating are become strong.

However, the thickness of coating has similar less stabilizing effect on the growth instability for the case in which  $\zeta_1$  and  $\zeta_2$  are greater than one. It means that when a less distortive material solidifies on a more distortive mold and coating layer, the process is less dependent on variations in the coating thickness and coupling rates at both interfaces.

### **5.2.3 Effect of zeroth order thermal contact resistances at shell/coating and coating/mold interfaces ( $R$ and $R_m$ )**

Since the effects of surface roughness and other contaminants films, there will be thermal contact resistances at the shell/coating and coating/mold interfaces. These thermal contact resistances have significant effect on the growth of instability because the thermal contact resistance between the two metallic solid surfaces prevents the heat flux and cause mutual temperature differences at the opposite sides of this interface. It is known that the extraction of heat by conduction across these interfaces increases in the regions where the thermal contact resistance is decreased and vice versa, it decreases in the regions where the thermal contact resistance is increased. These non-uniformities in the heat extraction cause undulatory structure at the moving interface between the liquid and solid interface and therefore, the quality of the cast reduces. As a result, contact resistances at the casting/coating and coating/mold interfaces play an important role in the solidification process and have to be taken into account in the stability analysis of the solidification of casting.

The effects of the zeroth order thermal contact resistances at shell/coating and coating/mold interfaces, which are constant associated with the constant unperturbed contact pressure  $P_0$ , on the growth instability are investigated in the following considered cases for the combinations of thermal conductivity ratios between solidified shell, coating and mold materials and coupling rates at the upper and lower surfaces of coating layer. In these cases, the dimensionless thicknesses of the coating and mold are equal to 0.5 and 4, respectively.

Figure 5.21 shows the variation of growth perturbation at moving interface as a function of mean shell thickness for selected values of the zeroth order thermal contact resistance at shell/coating interface while  $R_m$  is equal to 0.01. The thermal and mechanical problems are weakly coupled at both shell/coating and coating/mold interfaces and the thermal conductivity ratios between materials of solidified shell, coating and mold are

equal to 0.1 in this case. It can be seen that  $R$  has a destabilizing effect on the growth of the perturbation in solidified shell for weak coupling rates when the thermal conductivity of the materials are ranked as  $K^d > K^b > K^c$ . It means that when the solidified shell material is more distortive than the coating layer and mold, increase in the zeroth order thermal contact resistance at shell/coating interface leads to more rapid growth of the perturbation in solidified shell. This result suggests that the value of  $R$  should be selected very small for improving the quality of the final cast.

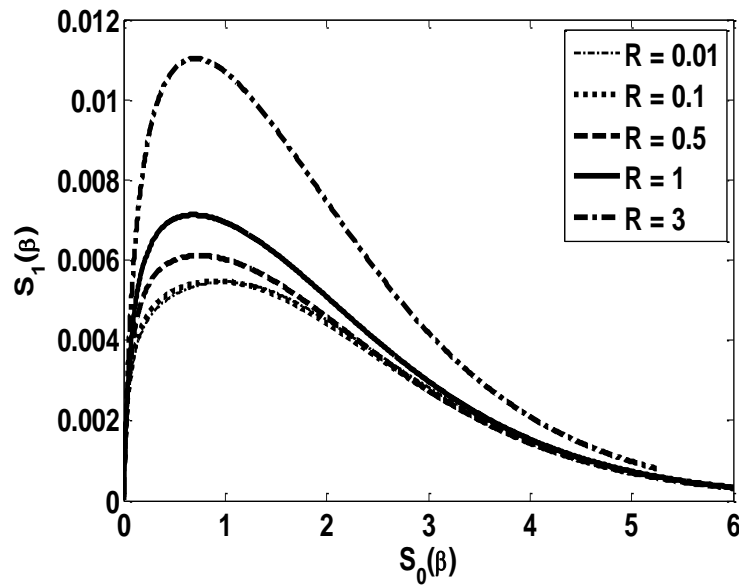


Figure 5.21 Perturbation in solidification front as a function of  $S_0(\beta)$  for selected values of  $R$  when  $H = 4$ ,  $U = 0.5$ ,  $\bar{R}' = -1$ ,  $\bar{R}'_m = -1$ ,  $\zeta_1 = 0.1$ ,  $\zeta_2 = 0.1$  and  $R_m = 0.01$

Figure 5.22 is reproduced with the same parameters given in Figure 5.21 except the value of  $\zeta_1$ .  $\zeta_1$  is increased from 0.1 to 2 and the coating layer is become more distortive than the solidified shell. The result shows that when the highly rigid mold is coating a material whose thermal conductivity is greater than its and casting material's thermal conductivities, thermal resistance at shell/coating interface does not have any significant effect on the growth of the perturbation in solidified shell during the solidification process. In other words, increase in  $\zeta_1$  leads to decrease in the sensitivity of the process to the thermal contact resistance at shell/coating interface. It means that the effect of the  $R$  on the growth instability is eliminated for weak coupling rates at the upper and lower surfaces of the coating layer when ranking of the thermal conductivities of the materials are selected as  $K^d > K^c > K^b$ .

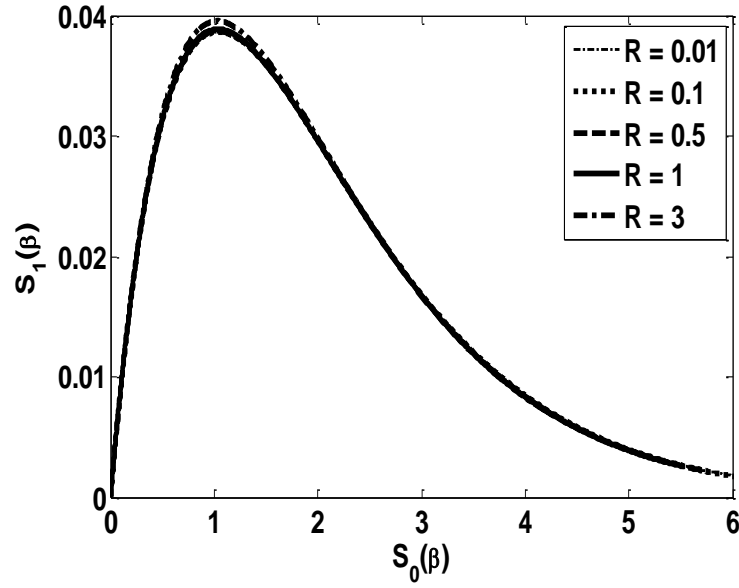


Figure 5.22 Perturbation in solidification front as a function of  $S_0(\beta)$  for selected values of  $R$  when  $H = 4$ ,  $U = 0.5$ ,  $\bar{R}' = -1$ ,  $\bar{R}'_m = -1$ ,  $\zeta_1 = 2$ ,  $\zeta_2 = 0.1$  and  $R_m = 0.01$

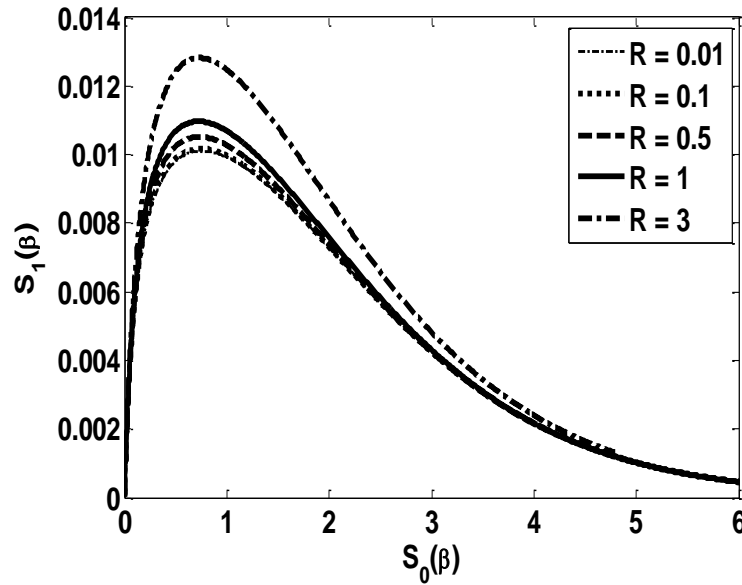


Figure 5.23 Perturbation in solidification front as a function of  $S_0(\beta)$  for selected values of  $R$  when  $H = 4$ ,  $U = 0.5$ ,  $\bar{R}' = -1$ ,  $\bar{R}'_m = -1$ ,  $\zeta_1 = 0.1$ ,  $\zeta_2 = 2$  and  $R_m = 0.01$

Figure 5.23 shows the effect of the thermal contact resistance at shell/coating interface on the growth of the perturbation in solidified shell when the thermal conductivity ratios combination is arranged as  $\zeta_1 = 0.1$  and  $\zeta_2 = 2$ . Now, the thermal conductivities of the material are ranked as  $K^b > K^d > K^c$  and it is seen that the coating layer is become the most rigid layer in the process.  $R$  has destabilizing effect on the growth instability similar to the results in Figure 5.21 but however, we observed that the dependence of



the shell growth on the thermal contact resistance at shell/coating interface reduces for this case. On the other hand, the thermal conductivity ratios between the mold and casting materials,  $\zeta_3$ , are same with the previous case. It can be seen that increase in the thermal conductivity of coating layer material leads to increase in the sensitivity of the growth instability to thermal contact resistance at shell/coating interface. It is also noteworthy that the amplitude of the perturbation at moving interface decreases for all selected values of  $R$  when the coating layer is selected more rigid than solidified shell and mold.

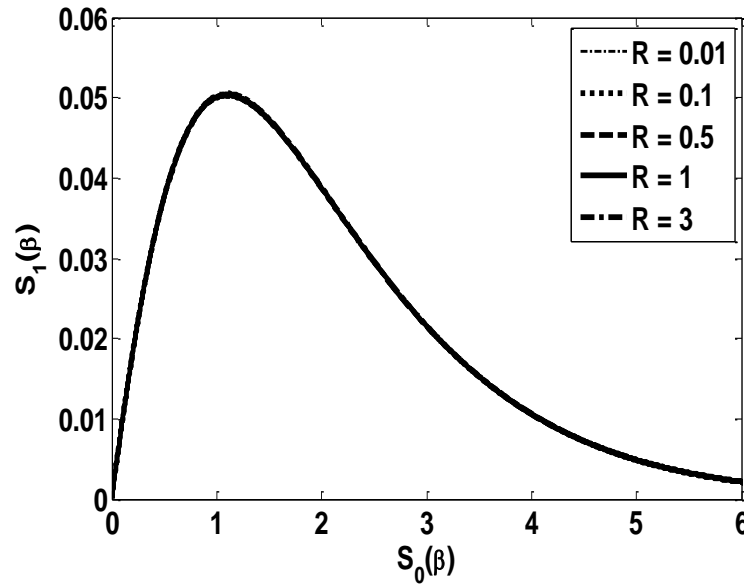


Figure 5.24 Perturbation in solidification front as a function of  $S_0(\beta)$  for selected values of  $R$  when  $H = 4$ ,  $U = 0.5$ ,  $\bar{R}' = -1$ ,  $\bar{R}'_m = -1$ ,  $\zeta_1 = 2$ ,  $\zeta_2 = 2$  and  $R_m = 0.01$

Figure 5.24 shows that the effect of the  $R$  on the growth of the perturbation in solidified shell when both thermal conductivity ratios between the solidified shell, coating and mold are equal to 2 ( $K^c > K^b > K^d$ ). The result shows that the variation in the thermal contact resistance does not have any effect on the growth instability. It means that if the solidified shell is more rigid than the coating and mold then the effect of the thermal contact resistance on the growth instability diminishes for weak coupling rates at shell/coating and coating/mold. It can be also seen by comparing this result with the previous results in Figure 5.21, Figure 5.22 and Figure 5.23 that increase in  $\zeta_1$  leads to decrease in the effect of  $\bar{R}$  on the growth instability. This means that when coating layer is become more distortive than the solidified shell regardless of the mold materials, the destabilizing effect of the thermal contact resistance at shell/coating interface eliminates for weak coupling at both interfaces. It is also seen that the amplitude of the growth

perturbation in solidified shell will be greatest when the values of  $\zeta_1$  and  $\zeta_2$  are greater than 1. Most uniform growth is obtained when  $R$  is selected smaller when the ranking of thermal conductivities of the solidified shell, coating and mold materials is  $K^d > K^b > K^c$ .

In order to investigate the effect of  $R$  on the growth of the perturbation in solidified shell when coupling rate at the upper surface of coating layer is strong, we increased magnitude of  $\bar{R}'$  to 100 while  $\bar{R}'_m$  is still equal to -1.

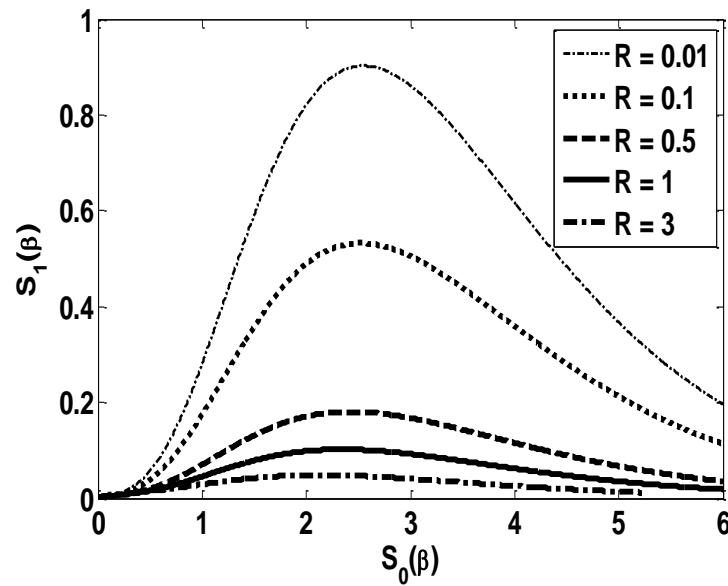


Figure 5.25 Perturbation in solidification front as a function of  $S_0(\beta)$  for selected values of  $R$  when  $H = 4$ ,  $U = 0.5$ ,  $\bar{R}' = -100$ ,  $\bar{R}'_m = -1$ ,  $\zeta_1 = 0.1$ ,  $\zeta_2 = 0.1$  and  $R_m = 0.01$

Figure 5.25 shows the effect of the thermal contact resistance at shell/coating interface when thermal conductivity ratios between materials of solidified shell, coating and mold are ranked as  $K^d > K^b > K^c$ . The destabilizing effect of  $R$  on the growth instability converts to stabilizing when the coupling between shell and coating is increased. It means that increase in the thermal contact resistance at shell/coating interface leads to decrease in the amplitude of the growth perturbation in solidified shell. Low values of  $R$  cause more rapid growth and the perturbation diminishes in a longer time. This result suggests that the thermal contact resistance at shell/coating interface should be selected high for more uniform growth in solidified shell. It can be seen by comparing the results in Figure 5.21 that the amplitude of growth perturbation in shell thickness increases for all selected values of  $R$  when we increased the coupling rate at shell/coating interface.

Additionally, the sensitivity of the growth of the perturbation to zeroth order thermal contact resistance at shell/coating interface increases under this conditions.

Figure 5.26 depicts the variation of the growth perturbation at moving interface as a function of mean shell thickness for selected values of  $R$  when  $\zeta_1$  is increased to 2. The result shows that the thermal contact resistance at shell/coating interface has stabilizing effect on the growth instability.

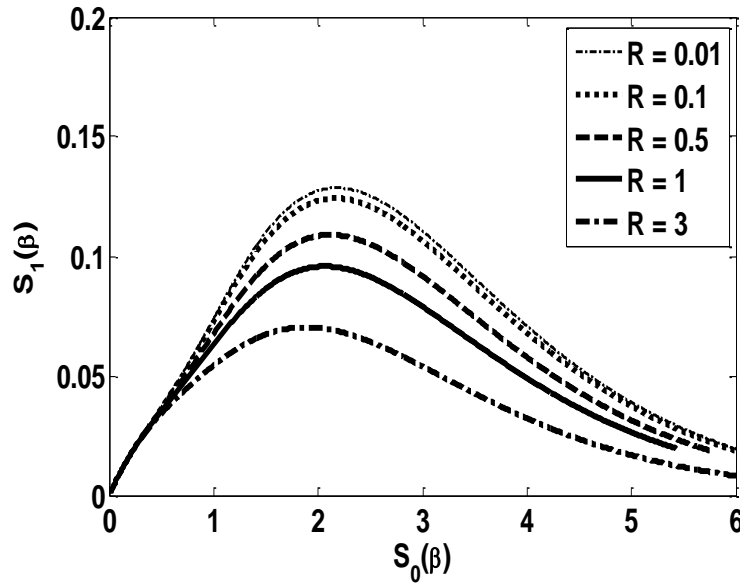


Figure 5.26 Perturbation in solidification front as a function of  $S_0(\beta)$  for selected values of  $R$  when  $H = 4$ ,  $U = 0.5$ ,  $\bar{R}' = -100$ ,  $\bar{R}'_m = -1$ ,  $\zeta_1 = 2$ ,  $\zeta_2 = 0.1$  and  $R_m = 0.01$

It can be remembered that the results in Figure 5.22 showed that  $R$  does not have significant effect on the growth of the perturbation at freezing front. However, it can be seen that increase in the coupling between solidified shell and coating layer leads to increase in the sensitivity of the growth instability to  $R$  during the solidification process. On the other hand, when we compared with the previous figure, we observed that if the thermal conductivities of the materials of solid layers are ranked as  $K^d > K^c > K^b$  ( $\zeta_1 = 2$  and  $\zeta_2 = 0.1$ ) then dependence of the process on  $R$  decreases. It means that the sensitivity of the process to  $R$  decreases for strong coupling rate at shell/coating interface when coating layer is become more distortive than the solidified shell. It is also noteworthy that increase in coupling rate leads to increase in the mean shell thickness when the perturbation reaches its maximum value.

Figure 5.27 shows the variation of perturbation in solidified shell for same parameters given in Figure 5.25 except the value of  $\zeta_2$ .  $\zeta_2$  is increased to 2 when the thermal and

mechanical problems are strongly coupled only at shell/coating interface. The results show that increase in  $R$  leads to decrease in the amplitude of the growth perturbation in solidified shell. When we compared these results with the results in Figure 5.25, we observed that increase in  $\zeta_2$  leads to decrease in the  $R$  dependence of the process for same coupling conditions. It means that when the coating layer is become more rigid than the mold, the effect of  $R$  on the process decreases when the solidified is the most distortive layer in the process. However, it can be seen by comparing this case and the previous case, the sensitivity of the growth instability to thermal contact resistance at the shell/coating interface increases for  $\zeta_1 = 0.1$ ,  $\zeta_2 = 2$ . This means that increase in the thermal conductivity of the coating layer leads to increase the effect of the  $R$  on the growth instability during solidification process when thermal conductivity ratio between shell and mold materials are constant.

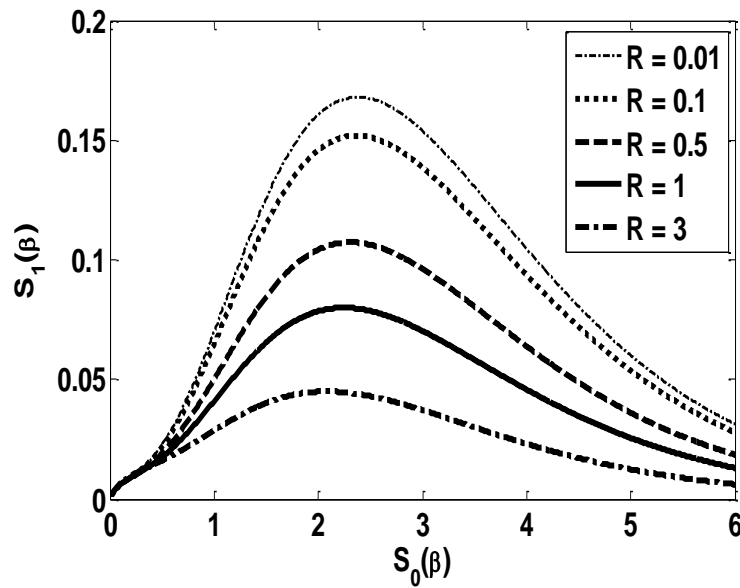


Figure 5.27 Perturbation in solidification front as a function of  $S_0(\beta)$  for selected values of  $R$  when  $H = 4$ ,  $U = 0.5$ ,  $\bar{R}' = -100$ ,  $\bar{R}'_m = -1$ ,  $\zeta_1 = 0.1$ ,  $\zeta_2 = 2$  and  $R_m = 0.01$

Figure 5.28 shows that effect of the contact resistance at shell/coating interface on the growth instability for similar coupling rates combination when  $\zeta_1 = 2$  and  $\zeta_2 = 2$ . Similar to Figure 5.24, the result shows that  $R$  has not any significant effect on the growth instability during the solidification process. The effect of the zeroth order thermal contact resistance at shell/coating interface eliminates when the thermal conductivities of the solidified shell, coating and mold materials are ranked as  $K^c > K^b > K^d$ . It means that when a material solidifies on a more distortive coating and mold than itself, coupling rate at shell/coating interface does not change the effect of  $R$

on the process. As a result, increase in the coupling rate at shell/coating interface leads to turns to destabilizing effect of  $R$  to stabilizing and increase in the sensitivity of the process to changes of thermal contact resistance at shell/coating interface except the case in which  $\zeta_1 = 2$  and  $\zeta_2 = 2$ . On the other hand, the amplitude of the growth perturbation at moving interface increases for all selected values of  $R$  except the same case, in which the thermal conductivity ratios between solidified shell, coating and mold materials are equal to 2, when coupling rate at shell/coating interface is increased.

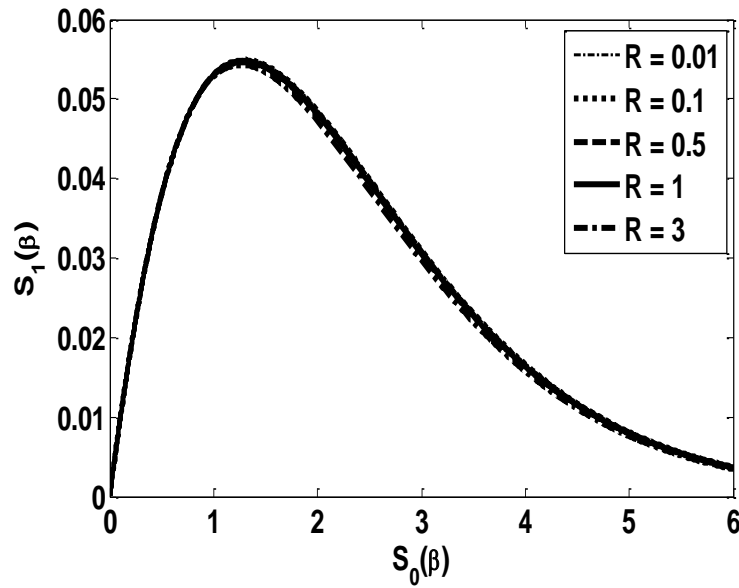


Figure 5.28 Perturbation in solidification front as a function of  $S_0(\beta)$  for selected values of  $R_0$  when  $H = 4$ ,  $U = 0.5$ ,  $\bar{R}' = -100$ ,  $\bar{R}'_m = -1$ ,  $\zeta_1 = 2$ ,  $\zeta_2 = 2$  and  $R_m = 0.01$

When we increased only the coupling rate at coating/mold interface or both upper and lower surfaces of coating layer in order to investigate the effects of thermal contact resistance at shell/coating interface on the growth instability, we obtained similar results with the previous considered cases in which the coupling is strong only at shell/coating interface. The thermal contact resistance at coating/mold interface has stabilizing effect on the growth of the perturbation at moving interface except the case in which the thermal conductivities of the materials of solidified shell, coating and the mold are ranked as  $K^c > K^b > K^d$ . Similarly,  $R$  has no effect on the process for this case. Additionally, we observed that the amplitude of the growth perturbation is smaller for all selected values of  $R$  when the coupling at coating/mold interface only is strong only than when the coupling is strong only at shell/coating interface. When the coupling rates at shell/coating and coating/mold interfaces are strong together, the amplitude of the

growth perturbation at moving interface reaches highest value and contact resistance sensitivity of the process increases for all thermal conductivity ratio combination except the combination of  $\zeta_1 = 2$  and  $\zeta_2 = 2$ . As a result, when the coupling rates at shell/coating and coating/mold interfaces are increased one by one or together the destabilizing effects of the thermal contact resistance at shell/coating interface on the growth instability turns to stabilizing for all considered cases except the case in which solidified shell is more rigid than the coating and mold.

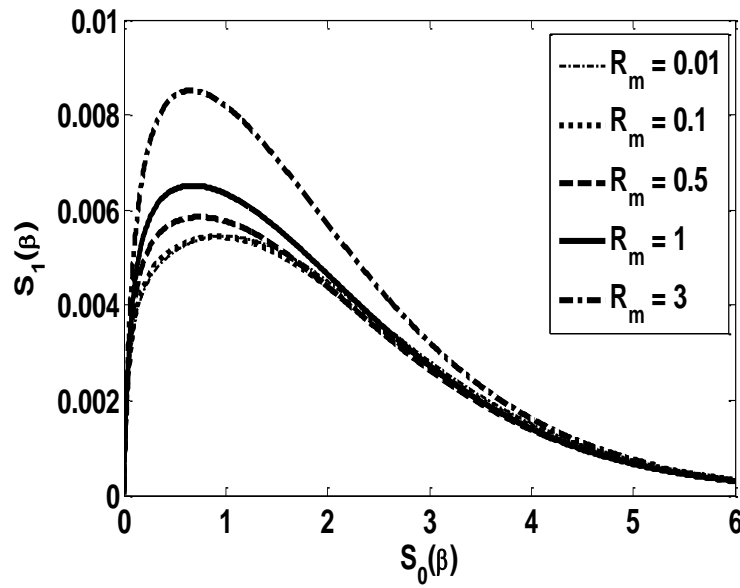


Figure 5.29 Perturbation in solidification front as a function of  $S_0(\beta)$  for selected values of  $R_m$  when  $H = 4$ ,  $U = 0.5$ ,  $\bar{R}' = -1$ ,  $\bar{R}'_m = -1$ ,  $\zeta_1 = 0.1$ ,  $\zeta_2 = 0.1$  and  $R = 0.01$

The effects of the thermal contact resistance at coating/mold interface,  $R_m$ , on the growth of the perturbation in solidified shell are investigated for the combinations of thermal conductivity ratios of materials and coupling rates at shell/coating and coating/mold interfaces. Figure 5.29 shows the variation of growth perturbation depending on the thermal contact resistance at coating/mold interfaces for  $\zeta_1 = 0.1$  and  $\zeta_2 = 0.1$  thermal conductivity ratios combination when coupling rates at upper and lower surfaces of the coating. The result shows that  $R_m$  has destabilizing effect on the growth of the perturbation in solidified shell. However, Figure 5.30 shows the results for same parameters given in previous figure except the coupling at shell/mold interface is increased only. It can be seen that the destabilizing effect of  $R_m$  turns to stabilizing and the maximum amplitude of the perturbation and mean shell thickness when the perturbation reaches its maximum value increase when the coupling rate at shell/coating

interface is increased. On the other hand, increase in the coupling rate at shell/coating interface leads to increase in the sensitivity of growth instability to  $R_m$ .

We observed that  $R_m$  has similar effects with  $R$  on the growth instability for all considered cases. Similarly, it has destabilizing effects on the growth of the perturbation at moving interface for  $\zeta_1 = \zeta_2 = 0.1$  and  $\zeta_1 = 0.1, \zeta_2 = 2$  thermal conductivity ratios combinations when the coupling rates are small at both upper and lower interface of coating layer. Under same coupling rates it has no significant effect for  $\zeta_1 = 2, \zeta_2 = 0.1$  and  $\zeta_1 = \zeta_2 = 2$  combinations. However, it has stabilizing effect on the growth instability for the combinations of  $\zeta_1 = \zeta_2 = 0.1$ ,  $\zeta_1 = 0.1, \zeta_2 = 2$  and  $\zeta_1 = 2, \zeta_2 = 0.1$  when the coupling rates at shell/coating and coating/mold are increased one by one or together. Similar to previous cases, the process is insensitive to changes of coupling rates and thermal contact resistance at coating/mold interface for  $\zeta_1 = \zeta_2 = 2$  thermal conductivity ratio combinations. This means that when the solidified shell is more distortive than the coating and mold, the variations in  $\bar{R}'$ ,  $\bar{R}'_m$ ,  $R$  and  $R_m$  do not affect the thermoelastic instability during the solidification process. The effects of the coupling rates on the growth of the perturbation in solidified shell are investigated in the following sections in detail.

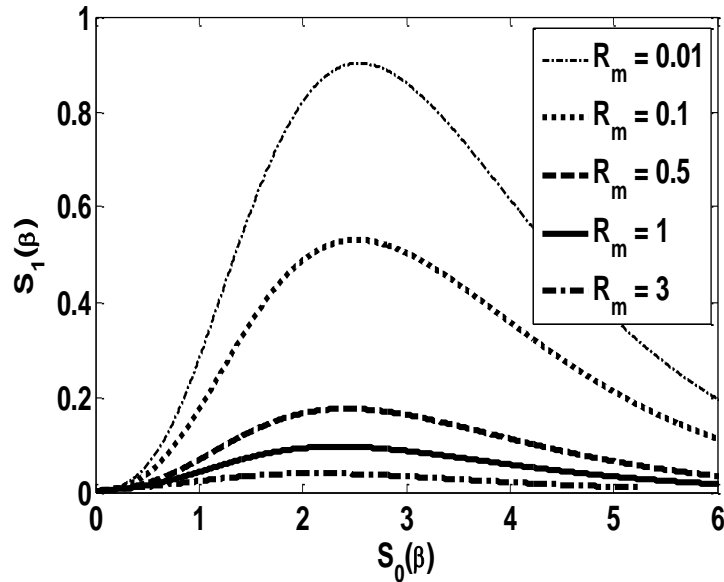


Figure 5.30 Perturbation in solidification front as a function of  $S_0(\beta)$  for selected values of  $R_m$  when  $H = 4$ ,  $U = 0.5$ ,  $\bar{R}' = -100$ ,  $\bar{R}'_m = -1$ ,  $\zeta_1 = 0.1$ ,  $\zeta_2 = 0.1$  and  $R = 0.01$

As a result of these considered cases, it can be seen that the contact resistances at the both upper and lower surfaces of coating layer have approximately similar effect on the

growth instability during the solidification process for all considered combinations of the thermal conductivity ratios between the solidified shell, coating and the mold materials and coupling rates.

#### 5.2.4 Effect of wavelength ( $\lambda$ )

In order to investigate the effect of the wavelength,  $\lambda$ , on the growth of the perturbation in solidified shell for fixed values of  $R$ ,  $R_m$ ,  $\bar{R}'$  and  $\bar{R}'_m$ , we describe a new dimensionless parameter for the magnitude of the perturbation in solidified shell, time, the coupling rate at shell/coating interface and the coupling rate at coating/mold interface as follows

$$\lambda = \frac{S_1(\beta)}{R} = \frac{s_1(t)}{K^c R_0} \quad (5.2)$$

$$\tau = \frac{\beta}{R^2} = \frac{T_m}{L^c \rho^c K^c R_0^2} t \quad (5.3)$$

$$\bar{R}'_h = \frac{\bar{R}'}{R} = \frac{E^c \alpha^c T_m}{(1 - \nu^c) K^c R_0} R'(P_o) \quad (5.4)$$

$$\bar{R}'_{hm} = \frac{\bar{R}'_m}{R} = \frac{E^c \alpha^c T_m}{(1 - \nu^c) K^c R_0} R'_m(P_o) \quad (5.5)$$

These are chosen to be independent of the wavenumber,  $m$ , when the other physical parameters are held constant. The effect of varying  $m$  will appear through the variation in the parameter  $R = mK^c R_0$ , which here rename  $M$  to highlight its present function of characterizing the wavenumber of the perturbation.

Figure 5.31 shows the effect of the wavenumber,  $M$ , on the variation of the perturbation amplitude  $\lambda(\tau)$  as a function of time,  $\tau$ , for the coupling rates at shell/coating and coating/mold interfaces are equal to each other as  $\bar{R}'_h = \bar{R}'_{hm} = -300$  and other selected system parameters. The initial condition for calculating amplitude of the perturbation at moving interface is assumed to be  $\lambda'(0) = 0.1$ . Large values of  $M$  correspond to short wavelengths. The results show that when the wavenumber is increased, the perturbation grows faster and reaches smaller peak amplitudes than decays its steady state value. Assuming a random distribution of wavelengths in the initial perturbation, shorter wavelengths have stabilizing effect on the solidification



process. Variation of the growth instability during the solidification depending on the wavenumber shows us the changing the surface topographies of coating layer or the mold has significant effect on the growth of the perturbation in solidified shell during the casting process. The effects of the other parameter such as thickness of the mold and coating layer, thermal contact resistances at the shell/coating and coating/mold interfaces are similar to the obtained results in previous studies and hence they no reported in this study.

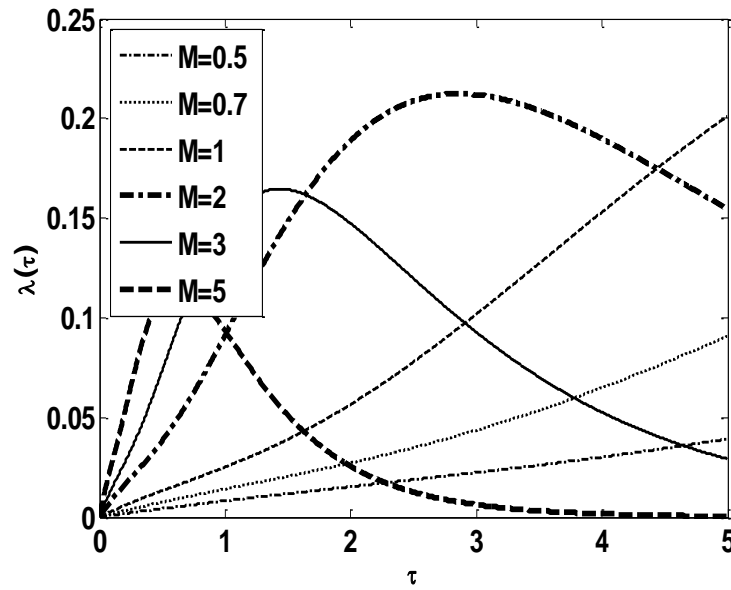


Figure 5.31 Effect of the wavelength on the growth of the perturbation when  $H = 4$ ,  $U = 0.5$ ,  $\zeta_1 = 2$ ,  $\zeta_2 = 0.1$ ,  $\bar{R} = 0.5$ ,  $\bar{R}_m = 0.5$ ,  $\bar{R}'_h = -300$  and  $\bar{R}'_{hm} = -300$

### 5.3 A case study

In this section we determine the effects of coating layer properties such as thickness and material of it and coupling rates at shell/coating and coating/mold interfaces on the uneven shell growth during casting of pure metals by using of the theoretical formulations discussed in previous chapters. We examine the variations of the growth perturbation at solidification front for specific material combinations and process parameter in dimensional form. We handled a special case for improving our knowledge about the thermo-elastic instability mechanism which contains the solidification of pure aluminum. Aluminum is one of the most used materials in casting industry and we determine the conditions for eliminating or minimizing growth instability and improve the quality and usability of the final aluminum casting.

### 5.3.1 Properties of selected Materials

We examine the effects of the properties of the coating layer on the growth instability for the system in which aluminum shell is solidified on a coated planar mold of finite thickness. We wish to determine the conditions in the process for obtaining the best quality final casting. Pure aluminum, iron and copper materials combinations are used as the coating and mold materials. The thermal and mechanical properties of these pure materials are listed in the Table 5.1.

Table 5.1 Material Properties at Fusion Temperature

	Aluminum		Iron		Copper	
Property	Value	Ref.	Value	Ref.	Value	Ref.
$T_m(^{\circ}C)$	660	[97]	1536	[166]	1084	[166]
$L (10^5 J/kg)$	3.9	[97]	2.7	[167]	2	[167]
$\rho(kg/m^3)$	2650	[97]	7265	[168]	7938	[172]
$E(10^{10} Pa)$	6	[97]	14.4	[169]	6.4	[173]
$K(W/m^{\circ}C)$	229.4	[97]	36.2	[170]	345.4	[170]
$\alpha (10^{-6} ^{\circ}C^{-1})$	37.8	[97]	23.4	[171]	26	[171]
$\nu$	0.33	[97]	0.33	[169]	0.37	[174]

These values of properties, which are measured values near fusion temperature of each material, are independent of temperature.  $T_m$ ,  $L$ ,  $\rho$ ,  $E$ ,  $K$ ,  $\alpha$  and  $\nu$  denote the melting temperature, latent heat of fusion, density, Young's modulus, thermal expansion coefficient and Poisson's ratio, respectively.

The thickness of the coating layer is changed from  $u = 1 \text{ mm}$  to  $u = 10 \text{ mm}$  in these simulations. These values of coating thickness represent the thinner and thicker coating layer respectively. On the other hand, the thermal and mechanical problems are coupled in our model and the effects of rates of the coupling at the shell/coating and coating/mold interfaces are determined via changing these values between the  $-10^{-14} \text{ m}^2 \text{ sec}^{\circ}C / J Pa$  and  $-10^{-12} \text{ m}^2 \text{ sec}^{\circ}C / J Pa$  which mean weak and strong coupling rates at the interfaces, respectively. Thermal contact resistances at these interfaces are assumed same and equal to  $R_0 = R_m^0 = 10^{-5} \text{ m}^2 \text{ sec}^{\circ}C / J$ . Finally we fix the thickness of the mold at  $h = 30 \text{ mm}$  in the following simulations. Each of following figures are shown the variation of the amplitude of the adding perturbation on the mean

shell thickness for different process conditions.  $s_1^m$ ,  $s_0^m$  and  $t^m$  denote the maximum amplitude of the perturbation at freezing front, mean shell thickness and elapsed time when the perturbation reaches the maximum value, respectively.

### 5.3.2 Effect of coating layer material

In order to examine the effects of coating material on the growth of the perturbation in solidified shell, we studied on the two cases in which the aluminum shell solidifies on a coated copper mold with different coating materials and then in order to investigate the effect of the mold material's thermal conductivity on the growth instability, the material of the mold is changed as iron. In this section, we will determine the best combinations of the coating and mold materials for selected pure materials to obtain the more uniform growth of the perturbation in solidified aluminum shell for different coupling rates at shell/coating and coating/mold interfaces. The following tables show the values of  $s_1^m$ ,  $s_0^m$  and  $t^m$  for the combinations of coating material and coupling rates during the solidification of pure aluminum on copper and iron molds. We use pure aluminum, iron and copper as coating material and the thermal conductivities of these materials are ranked as  $K^{Cu} > K^{Al} > K^{Fe}$ . In other words, their thermal distortivities are ranked as  $\delta_{Cu} < \delta_{Al} < \delta_{Fe}$ .

Table 5.2 shows the results for aluminum shell solidifies on iron, aluminum or copper coated copper mold for different coupling rates. It can be seen that the thermal conductivity of coating material has stabilizing effect on growth instability when thermal and mechanical problems are weakly coupled at both interfaces. It means that when we coated inside of the rigid mold with highly rigid material, the growth of the perturbation becomes more uniform and the quality of the final casting increases. This result suggests that the coating layer should be selected highly rigid for copper mold to improve the quality of the aluminum casting when the coupling rates are small at both upper and lower surfaces of the coating layer. It is also observed that increase in the thermal conductivity of the coating layer leads to increase in the values of  $s_0^m$  and  $t^m$ . It means that the perturbation reaches its maximum value thinner mean shell and more quickly for highly rigid coating layer.

In order to investigate the effects of the coupling rate at shell/coating interface on the variation of the maximum amplitude of the growth perturbation, we increased the value of  $R'$  to  $-10^{-12} \text{ m}^2 \text{ sec}^\circ \text{C} / \text{J Pa}$ .

Table 5.2 Coating material effect on  $s_1^m$ ,  $s_0^m$  and  $t^m$  values under different coupling rates for aluminum solidifies on a copper mold with coating of 1 mm thickness

	$R' = -10^{-14}, R'_m = -10^{-14}$			$R' = -10^{-12}, R'_m = -10^{-14}$		
Coating Material	$s_1^m [\text{mm}]$	$s_0^m [\text{mm}]$	$t^m [\text{sec}]$	$s_1^m [\text{mm}]$	$s_0^m [\text{mm}]$	$t^m [\text{sec}]$
Fe	0.2830	6.8	1.5913	0.4101	11	2.7220
Al	0.2072	6.2	1.2144	0.4232	12.6	2.7311
Cu	0.1958	6.1	1.1786	0.4114	12,6	2.7139
	$R' = -10^{-14}, R'_m = -10^{-12}$			$R' = -10^{-12}, R'_m = -10^{-12}$		
Coating Material	$s_1^m [\text{mm}]$	$s_0^m [\text{mm}]$	$t^m [\text{sec}]$	$s_1^m [\text{mm}]$	$s_0^m [\text{mm}]$	$t^m [\text{sec}]$
Fe	0.3994	10.7	2.6325	0.5922	12.8	3.2545
Al	0.3814	12	2.5835	0.7080	13.9	3.0933
Cu	0.3707	12.2	2.6007	0.7082	14.1	3.0920

The results show that the material of the coating layer does not have a significant effect on the maximum amplitude of growth perturbation at moving interface. This means that increase in the coupling rate at shell/coating interface diminishes the effect of the thermal conductivity of the coating material on the growth instability and the sensitivity of the growth perturbation to thermal conductivity of the coating layer decreases in comparison with the previous case. On the other hand, increase in the coupling rate at the upper surface of coating leads to increase in the values of  $s_0^m$  and  $t^m$  for all selected coating materials. In the previous case, decrease in the thermal distortivity of the coating layer decreases the value of  $s_0^m$ . However, strong coupling at shell/coating interface leads to increase in the mean shell thickness values depending on the increase the thermal distortivity of the coating layer. On the other hand, change of the coating material does not affect the time to reach maximum perturbation significantly when the coupling rate is become strong only at shell/coating.

When the coupling at coating/mold interface is increased while coupling between solidified shell and coating layer is weak, the copper coating leads to the most uniform

and the iron coating leads to most non-uniform growth in the solidified aluminum shell. It means that the thermal conductivity of the coating has stabilizing effect on the growth instability during the solidification of pure aluminum on a copper mold when the coupling at the lower surface of the coating is strong only. It can be seen by comparing the results in the case in which coupling rates are small that the thermal conductivity of the coating material dependence of the growth instability decrease. However, process is more sensitive to change of coating material for strong coupling at coating/mold interface than for strong coupling at the shell/coating interface. It can be also seen from comparison with the previous case that the amplitude of the perturbation decreases for all selected coating materials. On the other hand, the thermal conductivity of the coating material leads to increase in the values of  $s_0^m$  similar to previous case. This means that increase in the coupling rates at shell/coating and coating/mold one by one leads to increase in  $s_0^m$  when the thermal conductivity of the coating material is increased. The time for reaching maximum amplitude of the perturbation is longest for iron and shortest for aluminum coating layer. The values of  $s_0^m$  and  $t^m$  when coupling is only strong at coating/mold interface are smaller than the values when coupling is strong only at shell/coating interface for all selected coating material.

The effect of the thermal conductivity of the coating material on the growth of the perturbation in solidified shell turns the opposite when the thermal and mechanical problems are coupled strongly at both upper and lower surfaces of the coating layer. Thermal conductivity of the coating layer has destabilizing effect on the growth instability during the solidification of pure aluminum on a copper mold. This result suggests that the coating layer should be selected highly distortive to improve the quality of the aluminum casting on the copper mold when the coupling rates are strong at shell/coating and coating/mold interfaces. It can be seen that increase in the thermal conductivity of the coating material leads to increase in  $s_0^m$  and decrease in  $t^m$  for this coupling rates combination. On the other hand, the values of  $s_1^m$ ,  $s_0^m$  and  $t^m$  increase for all coating materials when the coupling rates are become strong together.

As seen in Table 5.2, most stable growth of the perturbation is observed for the case in which coating material is selected copper and couplings are weak at both interfaces. Also, the mean shell thickness and elapsed time is lowest for this case. However, the most unstable growth is observed in the same case when coupling rates are strong at both interfaces. As a results, the highly rigid coating layer on a highly rigid mold leads

to completely opposite effects on the growth of the perturbation in solidified aluminum shell depending on the coupling rates at shell/coating and coating/mold interfaces. It means that the coating material is selected depending on the coupling rates at the interface for highly rigid mold. The results suggest that the coating layer and the coupling rates should be selected highly rigid and weak respectively for obtaining most uniform growth during solidifying aluminum shell on a highly rigid copper mold.

In order to investigate the effects of the mold distortivity on the variation of the above quantities depending on the coating material, the distortivity of the mold is increased by selecting its material as iron. Table 5.3 shows the effects of the coating material on  $s_1^m$ ,  $s_0^m$  and  $t^m$  for different coupling rates at upper and lower surfaces of the coating layer. It can be seen that when the coupling rates are weak at shell/coating and coating/mold interfaces, the thermal conductivity of the coating material has a stabilizing effect on growth instability. Most stable growth is observed when copper is used as coating material. Similar to the result of the same case in Table 5.2, more rigid coating material leads to more uniform growth in the solidified aluminum shell. This result suggests that the thermal conductivity of the coating material should be selected higher for both mold materials to provide more uniform growth in the solidified shell. On the other hand, mean shell thickness and the time when the perturbation reaches its maximum value become smaller when thermal conductivity of the coating material is increased.

If we compared the results for iron and copper mold when coupling rates are small, we observed that decrease in the thermal conductivity of mold leads to increase in the values of  $s_1^m$ ,  $s_0^m$  and  $t^m$  for all selected coating materials. In other words, increasing the mold distortivity leads to increase in the amplitude of the perturbation at moving interface and therefore, the thermal conductivity of the mold has stabilizing effect on the growth instability. However, it is found in Yigit [107] that thermal conductivity of the mold material has destabilizing effect on growth of perturbation when coupling are weak at casting/mold interface. It can be seen that the effect of the thermal conductivity of the mold material turns to opposite when it is coated with a layer regardless of its material. It is also noteworthy that the values of  $s_0^m$  and  $t^m$  increase for all selected coating materials when the thermal conductivity of the mold material is decreased.

When we increased the coupling rate at shell/coating interface for highly distortive mold, the coating material has stabilizing effect on the growth perturbation in solidified

aluminum shell similar to previous case. It means that selecting highly rigid coating layer leads to more uniform growth in the solidified shell. It can be seen that increase in the coupling rate does not increase the amplitude of the growth perturbation in comparison with the previous case. However, it is shown in Table 5.2 that the maximum amplitude of the perturbation increases significantly for highly rigid mold when the coupling rate at shell/coating is increased. This result indicates that the sensitivity of maximum amplitude of the perturbation in solidified shell to coupling rate at shell/coating interface decreases very much when the thermal conductivity of the mold material is decreased. Additionally, increase in mold distortivity leads to decrease in the values of  $s_1^m$  for all selected coating materials when the coupling rate is strong only at shell/coating interface. This result shows the stabilizing effect of the thermal conductivity of the mold material on the growth instability clearly.

Table 5.3 Coating material effect on  $s_1^m$ ,  $s_0^m$  and  $t^m$  values under different coupling rates for aluminum solidifies on an iron mold with coating of 1 mm thickness

	$R' = -10^{-14}, R'_m = -10^{-14}$			$R' = -10^{-12}, R'_m = -10^{-14}$		
Coating Material	$s_1^m$ [mm]	$s_0^m$ [mm]	$t^m$ [sec]	$s_1^m$ [mm]	$s_0^m$ [mm]	$t^m$ [sec]
Fe	0.3735	7.4	10.2784	0.3798	7.6	10.5924
Al	0.3375	7.1	9.6976	0.3477	7.5	10.2825
Cu	0.3210	7	9.5273	0.3326	7.5	10.2188
	$R' = -10^{-14}, R'_m = -10^{-12}$			$R' = -10^{-12}, R'_m = -10^{-12}$		
Coating Material	$s_1^m$ [mm]	$s_0^m$ [mm]	$t^m$ [sec]	$s_1^m$ [mm]	$s_0^m$ [mm]	$t^m$ [sec]
Fe	0.3788	7.5	10.5522	0.3859	7.8	10.9388
Al	0.3424	7.3	9.9674	0.3538	7.8	10.6580
Cu	0.3253	7.2	9.7904	0.3383	7.8	10.6154

Thermal conductivity of the coating material has no significant effect on the mean shell thickness when the perturbation reaches its maximum value for this case. On the other hand, increase in thermal conductivity of the coating material leads to decrease in the values of  $t^m$  for these coupling rates. Similar to previous case, It can be seen from the comparison with the results in Table 5.2 that increase in the thermal conductivity of the mold material increases the values of  $s_0^m$  and  $t^m$  for all selected coating materials.

In order to investigate the effects of the coupling rate at coating/mold interfaces, we increased  $R'_m$  to  $-10^{-12} \text{ m}^2\text{sec}^0\text{C}/\text{J Pa}$ . The results depict that the thermal conductivity of the coating material has similar effects on  $s_1^m$ ,  $s_0^m$  and  $t^m$  with the results when the coupling rates are small. The most uniform and non-uniform growths are observed for copper and iron coating, respectively. It means that the thermal conductivity of the coating layer has stabilizing effect on the growth instability during the solidification of aluminum on an iron mold for this coupling rates combination. On the other hand, increase in the thermal conductivity of the coating leads to decrease in the values of  $s_0^m$  and  $t^m$ . It can be seen that the mean shell thickness when the perturbation reaches its maximum decreases for all selected materials of coating layer in comparison with the case in which the copper mold is used for same coupling rates combination at the interfaces. Additionally,  $t^m$  increases when the thermal conductivity of the mold is decreased for same couplings.

When the thermal and mechanical problems are coupled at the upper and lower surfaces of the coating layer, the thermal conductivity of the coating has stabilizing effect on the growth instability. When we compared the results for highly rigid and distortive mold, we observed that increase in the distortivity of mold turns opposite the destabilizing effect of the thermal conductivity of coating material on the growth of perturbation for high coupling rates at the both shell/coating and coating/mold interfaces. The most uniform growth is observed when the coating material is selected as iron for copper mold but however, copper coating leads to more uniform growth in solidified shell for iron mold. This means that the thermal conductivity of the coating material should be selected small for highly rigid mold and should be selected high as possible for highly distortive mold when coupling rates are strong at both upper and lower surfaces of the coating layer. It can be also seen that increase in the coupling rates does not have significant effect on the maximum amplitude of the growth perturbation for highly distortive mold. On the other hand, it can be seen that coating material does not have significant effect on the values of the mean shell thickness when the maximum perturbation is occurred. This means that increase in coupling rates reduces the sensitivity of  $s_0^m$  to coating material during solidification on a more distortive mold. The values  $t^m$  decrease when the thermal conductivity of the coating material is increased but its sensitivity to thermal conductivity of coating material decreases similar to sensitivity of  $s_0^m$ .



It is also noteworthy that the effects of the coupling rates at the shell/coating and coating/mold interfaces on  $s_1^m$  decrease for all considered coating material when the thermal conductivity of the mold material is decreased. On the other hand, the coupling rate effects on  $s_0^m$  also decrease when the distortivity of the mold is increased and the time to reach maximum perturbation is become longer for highly distortive mold.

### 5.3.3 Effect of Thickness of the Coating Layer

Thickness of the coating is an important parameter for the solidification process due to its thermal and mechanical effects on the thermoelastic instability. The value of the coating layer thickness affects the mechanical stiffness of the layer and the temperature distribution in the layer. An increase in the thickness of the layer leads to increase in the stiffness and decrease in the slope of temperature distribution. These two contrary effects of thickness have an important role on the growth instability when the material of the coating layer is selected highly distortive.

The effects of coating thickness are investigated for solidification of pure aluminum on a copper mold with different coating materials in the following figures when the coupling rates between shell/coating and coating/mold are changed. In the following section, the effects of coating thickness are investigated firstly for Al-Fe-Cu combination as solidified shell, coating and mold materials and after that Al-Al-Cu materials combination are considered.

*Case 1: Shell Material: Al – Coating Material: Fe – Mold Material: Cu*

Figure 5.32 and Figure 5.33 shows the effects of the coating thickness on the growth of the perturbation in solidified shell thickness for Al-Fe-Cu materials combination when the coupling rate between solidified shell and coating is equal to  $-10^{-14} m^2 sec^{\circ}C / J.Pa$  and  $-10^{-12} m^2 sec^{\circ}C / J.Pa$  while coupling rate between the coating and mold equals to  $-10^{-14} m^2 sec^{\circ}C / J.Pa$ .

Figure 5.32 indicates the variation of the amplitude of the growth perturbation in solidified shell as a function of mean shell thickness when the thermal and mechanical problems are weakly coupled at both lower and upper surfaces of the coating layer ( $R' = R'_m = -10^{-14} m^2 sec^{\circ}C / J.Pa$ ). The results show that thinner coating layer leads

to slow growth of the perturbation at moving interface and reaches the smallest amplitude. This means that thickness of the coating layer has destabilizing effect on the growth instability. In order to interpret physical meaning of this behavior, we must dwell on the thermal distortivity of a material which identifies the formed curvature in a body due to flowing heat through it (readers refer to [165] for more detail). So, the stabilizing effect of stress relaxation due to highly distortive coating layer overcomes the destabilizing effect of less cooling rate for small thickness. The result suggests that coating thickness should be selected thinner for coating material of less thermal conductivity than solidified shell. As seen in the figure, after perturbation reaches its maximum, it starts to fall down its steady state value because dependence of the conditions at solid/liquid interface on the conditions at shell/coating and coating/mold interfaces becomes less when mean shell thickness increases sufficiently. On the other hand, coating thickness does not have significant effect on the mean shell thickness when the perturbation in solidified shell reaches its maximum amplitude,  $s_0^m$  when coupling rates are weak.

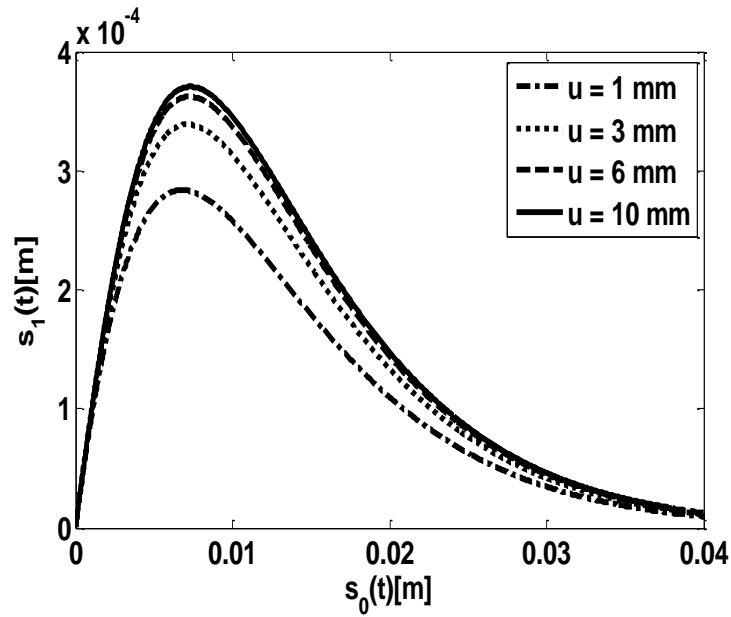


Figure 5.32 Perturbation in the solidification front as a function of  $s_0(t)$  for various values of  $u$  and Al-Fe-Cu material combination when  $R' = R'_m = -10^{-14} m^2 sec^{\circ}C / J.Pa$

In order to investigate the effect of coating thickness on the growth instability when the coupling rate between the shell and coating layer is changed, we increased the value of  $R'$  in Figure 5.33. The results show that maximum amplitude of the perturbation decreases when the thickness of the coating layer is increased. In other words, coating

thickness has stabilizing effect on growth instability. It can be seen that growth perturbation at moving interface shows two different behaviors during the process. For highly distortive coating layer, the conditions at the freezing front are highly dependent on the conditions at shell/coating and coating/mold interfaces when mean shell thickness is sufficiently small. For this reason, perturbation grows more rapidly for thicker coating due to dominance of the destabilizing effect of the high stiffness of the coating layer at early stages of solidification. As the time progressed, increase in the mean shell thickness gives a positive contribution to the stabilizing effect of less cooling rate on the process and it overcomes the destabilizing effect of the stiffness after a time and hence the perturbation grows slowly. As a result, perturbation has lower amplitude at moving interface for thicker coating layer. It is also noteworthy that the sensitivity of the process to the coating thickness decreases for Al-Fe-Cu materials combination when coupling rate at shell/coating interface is increased. On the other hand, thicker coating layer causes that the maximum amplitude of the perturbation occurs at smaller mean shell thickness and sensitivity of  $s_0^m$  to thickness of the coating increases under these conditions.

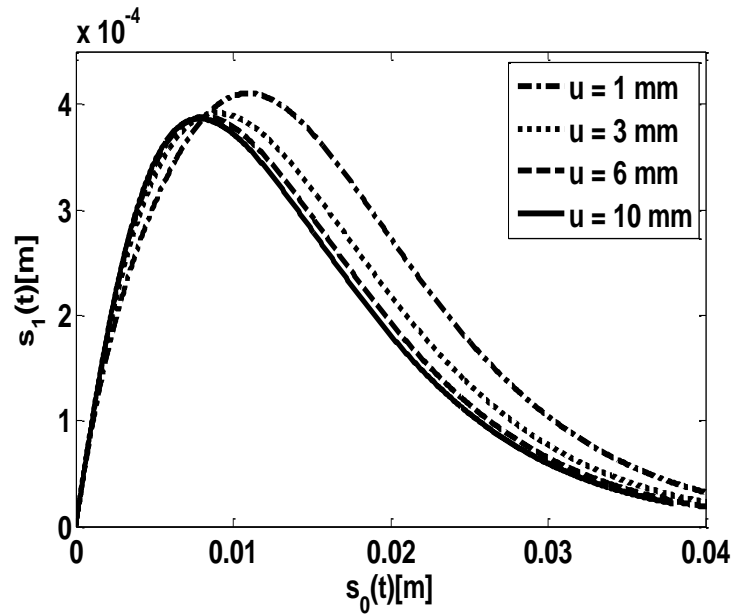


Figure 5.33 Perturbation in the solidification front as a function of  $s_0(t)$  for various values of  $u$  and Al-Fe-Cu material combination when  $R' = -10^{-12} m^2 sec^{\circ}C / J.Pa$  ,  
 $R'_m = -10^{-14} m^2 sec^{\circ}C / J.Pa$

Figure 5.34 shows the variations of the amplitude of growth perturbation in solidified shell for selected values of coating thickness when coupling rate is increased only at lower surface of the coating layer. Similar to Figure 5.33, coating thickness has

stabilizing effect on the growth instability and perturbation changes its behavior depending on the coating thickness due to two contrary effects of stiffness and cooling rate. Stabilizing effects of less cooling rate and high stress relaxation are not dominant at early stages and therefore, thicker coating leads to more non-uniform growth due to its stiffness. When mean shell thickness becomes large enough, stabilizing effect due to less cooling rate becomes dominant and growth rate of perturbation starts to decrease. Similarly, coating thickness leads to decrease in the mean shell thickness when perturbation reaches its maximum. It can be seen by comparison with the previous figure that the effect of coating thickness on the growth of the perturbation in solidified shell does not change significantly for highly distortive coating layer when the coupling at shell/coating or coating/mold became strong enough.

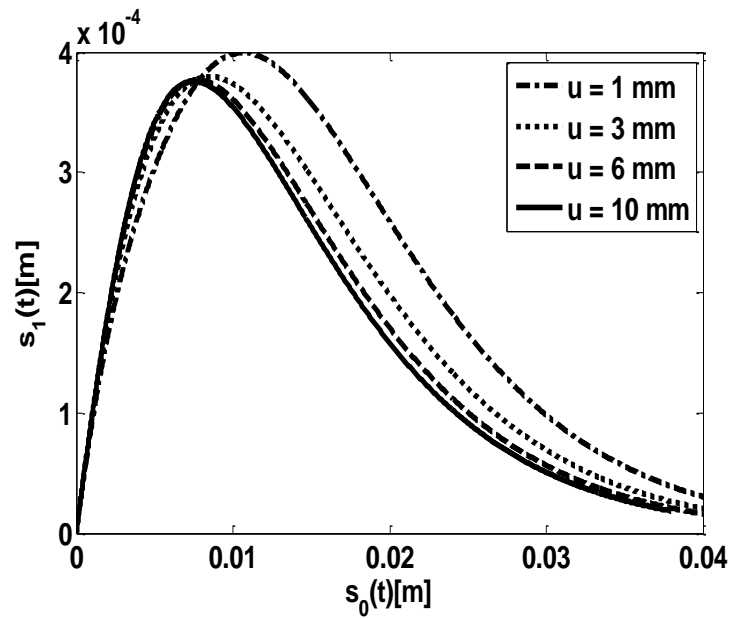


Figure 5.34 Perturbation in the solidification front as a function of  $s_0(t)$  for various values of  $u$  and Al-Fe-Cu material combination when  $R' = -10^{-14} m^2 secoC / J.Pa$ ,  $R'_m = -10^{-12} m^2 secoC / J.Pa$

When thermal and mechanical problems are strongly coupled at the surfaces between shell/coating and coating/mold, the variation of  $s_1(t)$  as a function of  $s_0(t)$  for selected values of coating thickness is illustrated in Figure 5. The results show that the thickness of coating layer has stabilizing effect on the growth instability. The combined effects of coupling rates between shell/coating and coating/mold lead to an increase in the sensitivity of the growth perturbation to coating thickness in comparison with the results in previous figures. Similarly, thicker coating leads to more non-uniform growth at the early stages however, the stabilizing effects due to high stress relaxation and less

cooling rate becomes more significant as the time progressed. The perturbation at moving interface reaches smaller amplitude and diminishes faster for thicker coating layer. In addition, the mean shell thickness when the perturbation reaches its maximum amplitude decreases depending on an increase in the coating thickness. Its sensitivity to coating thickness does not change significantly when both coupling rates at upper and lower surfaces of coating becomes strong.

Additionally, it can be seen for the above cases that increase in the coupling rates at shell/coating and coating/mold interfaces one by one or together leads to an increase in the amplitude of the growth perturbation in the solidified shell. This behavior is examined in the following section in detail.

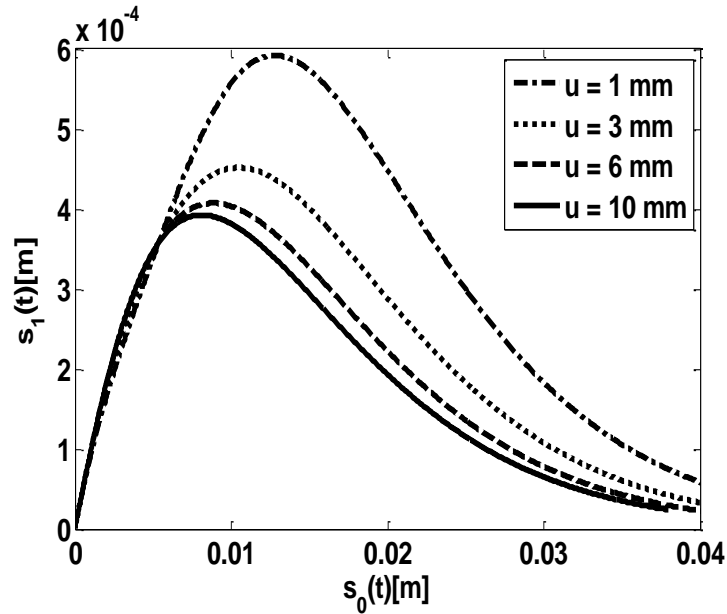


Figure 5.35 Perturbation in the solidification front as a function of  $s_0(t)$  for various values of  $u$  and Al-Fe-Cu material combination when  $R' = R'_m = -10^{-12} m^2 sec^\circ C / J.Pa$

The discussed results in previous figure involve the effects of coating thickness when aluminum is solidified on a highly distortive coating layer which is made of iron. After that, we investigated the effects of the thickness of highly rigid coating layer on the growth instability during the solidification of aluminum on a planar copper mold in the following section.

*Case 2: Shell Material: Al – Coating Material: Al – Mold Material: Cu*

Similar to Figure 5.32, we observed that thickness of the coating layer leads to more non-uniform growth of the perturbation in solidified shell when the thermal and mechanical problems are weakly coupled at upper and lower surfaces of coating layer. However, the destabilizing effect of mold coating thickness when couplings are weak is greater for coating material of high thermal distortivity than coating layer of low thermal distortivity. On the other hand, mean shell thickness when the perturbation reaches its maximum amplitude does not change depending on the coating thickness under these conditions. As a result, the coating thickness has no significant effect on the  $s_m^0$  regardless of the material of the coating layer when coupling rates are small at both interfaces of coating layer.

The destabilizing effect of the coating thickness on the growth instability during the solidification of pure aluminum on copper mold turns to stabilizing when the thermal and mechanical problems are strongly coupled at shell/coating and coating/mold interfaces one by one or together for highly rigid coating layer similar to the cases in which highly distortive coating layer is used. The destabilizing effect of the coating layer on the growth of the perturbation due to its stiffness reduces owing to high rigidity.

Therefore, thermal problems play more important roles than the mechanical ones on the process for less distortive coating layer. The perturbation grows rapidly due to destabilizing effect of less stress relaxation at the early stages of solidification process for thicker and highly rigid coating layer. However, the stabilizing effect of less cooling rate dominates the process behavior after a period of time and growth of the perturbation in solidified shell reaches smaller amplitude.

When the coupling rate at upper surface of the coating layer between solidified shell and mold is increased alone, we observed similar behavior with the results in Figure 3. The variations of the growth of perturbation depending on the thickness of coating are approximately similar for highly rigid and highly distortive coating layers. It means that, coating material does not change the effect of the coating thickness on the growth of perturbation significantly for this coupling rate combination. It can be also noted that an increase in  $u$  leads to decrease in the values of  $s_0^m$  also for highly rigid coating layer.

Figure 5.36 shows the variation of the amplitude of growth perturbation at the freezing front when the coupling rate is increased only at the lower surface of the coating layer. It is observed that coating thickness has stabilizing effect for highly rigid coating layer due to dominance of the stabilizing effect of less cooling rate and this effect becomes greater in comparison with the case in which coupling rate between shell and coating is increased only. This result suggests that an increase in the coupling rate between coating and mold is more preferable for thicker coating material of high thermal conductivity to improve the quality of the casting. On the other hand, it can be seen by comparing the results in Figure 5.34 and Figure 5.36 that increase in the thermal conductivity or rigidity of coating material leads to more uniform growth regardless of the coating thickness. Additionally, the mean shell thickness, when the amplitude of the growth perturbation reaches its maximum value, decreases depending on an increase in coating thickness. The sensitivity of  $s_0^m$  to coating thickness does not change depending on the material of the coating layer when coupling is strong only at coating/mold interface.

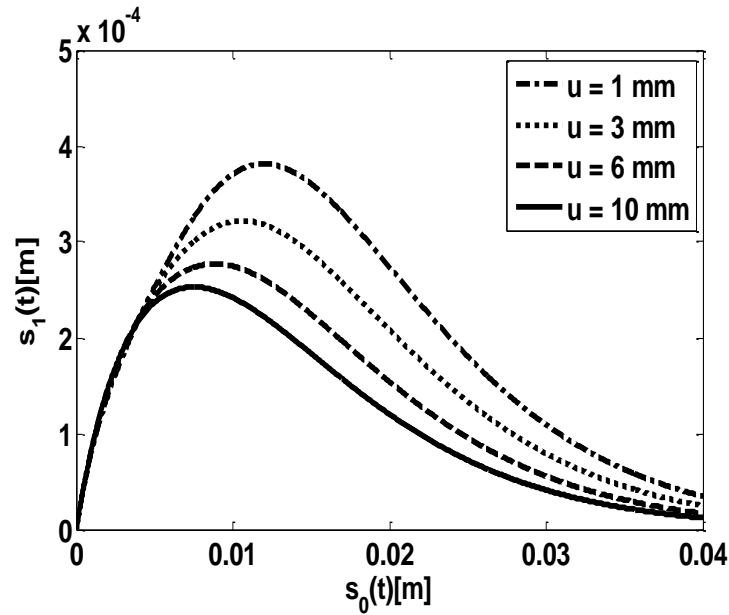


Figure 5.36 Perturbation in the solidification front as a function of  $s_0(t)$  for various values of  $u$  and Al-Al-Cu material combination when  $R' = -10^{-14} \text{ m}^2 \text{ sec}^\circ \text{C} / \text{J} . \text{Pa}$  ,  
 $R'_m = -10^{-12} \text{ m}^2 \text{ sec}^\circ \text{C} / \text{J} . \text{Pa}$

Figure 5.37 depicts the variation of the maximum amplitude of the periodic undulations at the solidification front depending on the coating thickness when thermal and mechanical problems are strongly coupled at both surfaces of coating layer. It can be seen that uneven shell growth reduces when thickness of coating is increased and

combined effects of strong coupling rates leads to increase the effect of coating thickness on growth instability for less distortive coating layer. However, it can be seen by comparing the Figure 5.35 and Figure 5.37 that for less distortive coating layer, the variation of the maximum of the perturbation is more sensitive to changes in thickness of coating than for highly distortive coating. On the other hand, coating thickness has similar decreasing effect on  $s_0^m$  but the sensitivity of  $s_0^m$  to coating thickness decreases when the thermal conductivity of the coating layer material is increased for these coupling rates. It is also observed that increase in the coupling rate at the shell/coating interface while the coupling between coating layer and mold is strong leads to reduce the sensitivity of  $s_0^m$  to the thickness of coating for highly rigid coating layer. Similarly, coupling at the coating/mold interface reduces the coating thickness sensitivity of the  $s_0^m$  when thermal and mechanical problems are highly coupled at shell/coating interfaces.

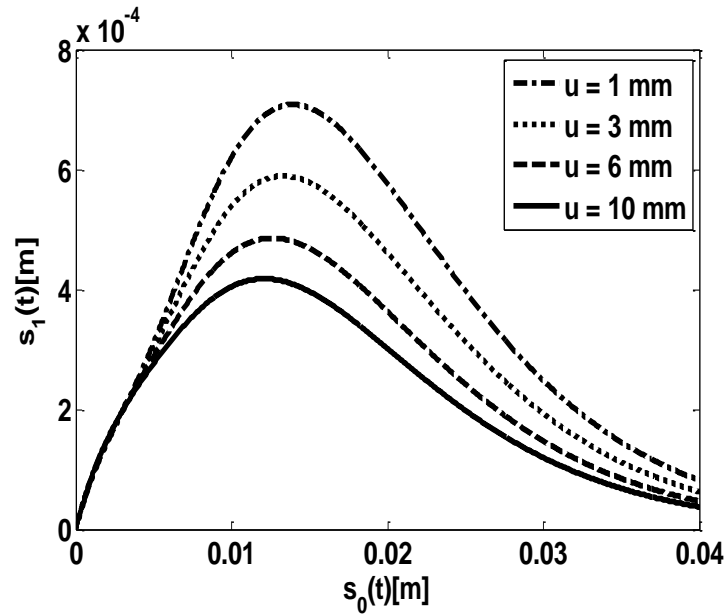


Figure 5.37 Perturbation in the solidification front as a function of  $s_0(t)$  for various values of  $u$  and Al-Al-Cu material combination when  $R' = R'_m = -10^{-12} m^2 sec^\circ C / J.Pa$

### 5.3.4 Effect of Coupling Rates

For two dissimilar or similar bodies are placed in contact with each other, heat transfer rate along the contact surface depends considerably occurring thermal and mechanical events in these bodies. There are three solid bodies in solidification process modeled in the present study such as solidified shell, coating layer and mold. The thermal and mechanical events in these solid layers affect each other through contact pressure



dependent thermal contact resistances at shell/coating and coating/mold interfaces during the solidification. When the coupling is weak, dependence between the thermal and mechanical problems reduces then thermal problem dominates the behavior of the process. However, if the coupling rate is increased then thermal and mechanical properties of each body become important to analyze uneven shell growth during the solidification. Similarly, we handled some cases such as Al-Fe-Cu and Al-Al-Cu materials combinations for solidified shell, coating and mold. The effects of coupling rates at the lower and upper surfaces of coating on the growth of the perturbation at moving interface are investigated for two different coating thickness ( $u = 1 \text{ mm}$  and  $u = 10 \text{ mm}$ ) in the following simulations.

Firstly, the variation of the amplitude of the growth perturbation as a function of mean shell thickness for thin highly distortive coating layer for selected values of  $R'$  and  $R'_m$  are investigated. Figure 5.38 shows the variation of the amplitude of the growth perturbation as a function of mean shell thickness for thin and highly distortive coating layer for selected values of  $R'$  while coupling between coating and mold is still weak.

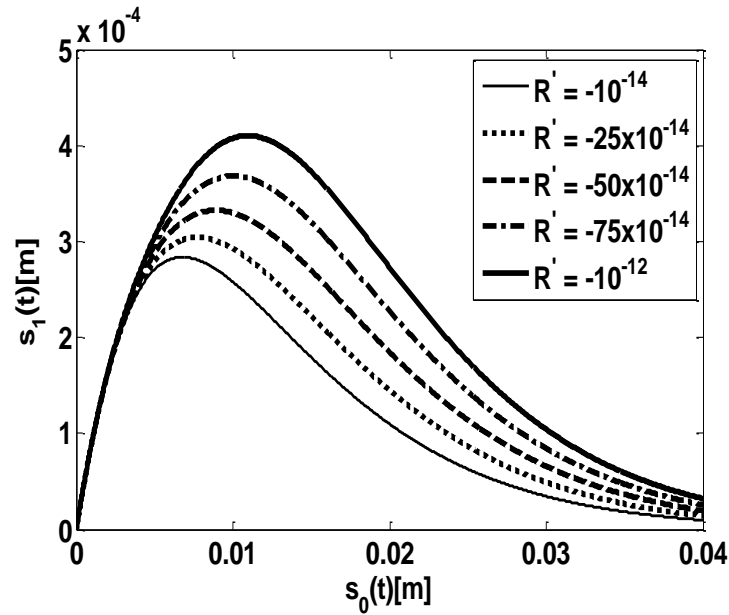


Figure 5.38 Perturbation in the solidification front as a function of  $s_0(t)$  for various values of  $R'$  and Al-Fe-Cu material combination when  $u = 1 \text{ mm}$  and  $R'_m = -10^{-14} \text{ m}^2 \text{ sec}^\circ \text{C} / \text{J} . \text{Pa}$

The results show that increase in the coupling between the shell and coating leads to increase in the maximum amplitude of the growing perturbation. In other words, it has destabilizing effect on the growth of the perturbation in solidified shell. As seen in the figure, at early stages of the solidification coupling between the each layer has no

significant effect on the process. But as the time progress, when mean shell thickness becomes thick enough the destabilizing effect of the coupling dominates the process. For the same case when the thickness of the coating is increased, the destabilizing effect of coupling rate at shell/coating interface diminishes and it does not have significant effect on the growth instability. These results suggest that thickness of the coating layer reduces the effect of this coupling rate on the solidification process when highly distortive coating layer is used. It can be seen that the usage of thicker distortive coating eliminates the destabilizing effect of coupling rate between shell and coating. It is also noteworthy that  $s_0^m$  increases when this coupling rate is increased for thin and highly distortive coating layer. However,  $s_0^m$  becomes insensitive to changes of coupling rate for highly distortive and thicker coating layer.

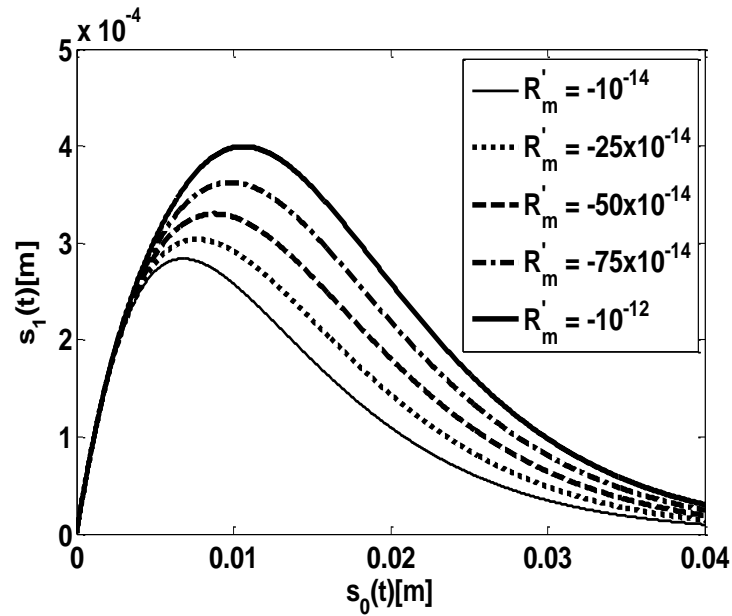


Figure 5.39 Perturbation in the solidification front as a function of  $s_0(t)$  for various values of  $R'_m$  and Al-Fe-Cu material combination when  $u = 1 \text{ mm}$  and  $R' = -10^{-14} \text{ m}^2 \text{ sec}^\circ \text{C} / \text{J} \cdot \text{Pa}$

Figure 5.39 shows the effect of coupling between coating and mold on the growth of perturbation in solidified shell for thin and highly distortive coating layer. It can be seen that  $R'_m$  has destabilizing effect on the growth of the perturbation in solidified shell similar to the one observed in the previous figure. However, destabilizing effect of  $R'_m$  is less than the coupling effect between the solidified shell and coating layer. Physically, coupling at the lower surface of the coating leads to more uniform growth than the coupling at upper surface for thin coating layer. It can be seen that  $s_0^m$  increases when the coupling rate at coating/mold is increased. Similar to the effect of coupling between

the shell and coating, coupling at the coating/mold has not significant effect on the growth instability for thicker and highly rigid coating layer. This result suggests that the thickness of the coating should be increased to eliminate the effects of the coupling rates at the shell/coating and coating/mold when more distortive coating layer than solidified shell is used.

In order to investigate the effects of the coupling rates on the growth instability for the coating layer of high thermal conductivity, we changed the coating material with aluminum in Figure 5.40 and Figure 5.41. Firstly, we investigated the effect of the coupling at shell/coating interface on the growth instability in Figure 5.40. The results indicate that coupling between shell and coating has destabilizing effect on the growth instability similar to the one observed in Figure 8.a for thin and highly rigid coating layer. However, it can be seen by comparing these figures that  $R'$  dependence of the growth instability increases for thin and highly rigid coating layer because the separation between the maximum amplitudes of perturbation for smallest and largest values of  $R'$  becomes larger as seen in Figure 5.40. This behavior of the process can clearly be seen in Figure 5.41.

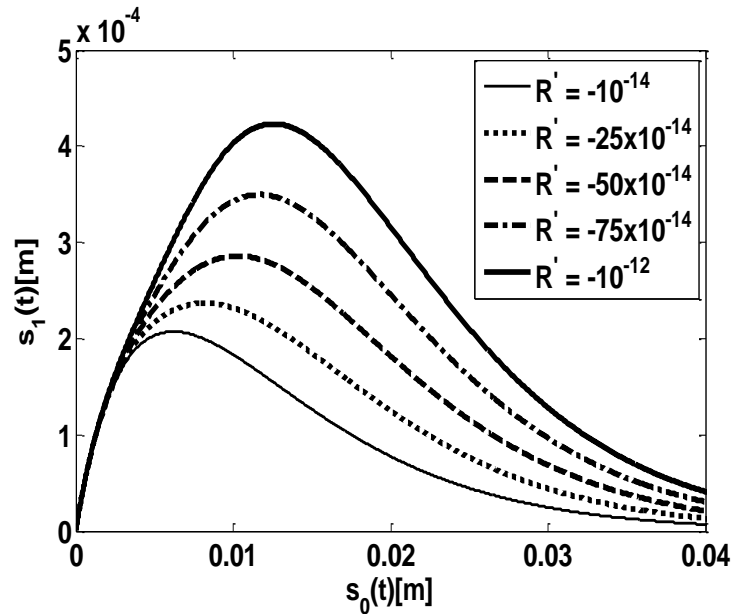


Figure 5.40 Perturbation in the solidification front as a function of  $s_0(t)$  for various values of  $R'$  and Al-Al-Cu material combination when  $u = 1 \text{ mm}$  and  $R'_m = -10^{-14} \text{ m}^2 \text{ sec}^\circ \text{C} / \text{J} . \text{Pa}$

As it can be remembered, coupling between shell and coating has no effect on the growth instability when thicker and highly distortive coating layer is used. The effect of

the coupling at shell/coating interface on the growth instability is shown in Figure 5.41 for thicker and highly rigid coating layer. The result shows that  $R'$  has destabilizing effect on the growth of the perturbation in solidified shell. On the other hand,  $R'$  dependence on  $s_0^m$  increases for thicker and highly rigid coating layer in comparison with the result for thicker and highly distortive coating layer. In other words, decrease in the thermal conductivity of the coating material leads to decrease in the destabilizing effect of coupling at shell/coating interface on the growth instability for thicker coating layer. Comparison of Figures 5.40 and 5.41 with each other shows that increase in the thickness of the coating reduces the sensitivity of  $s_1(t)$  to coupling rate at shell/coating interface for less distortive coating similar to for high distortive coating layer.

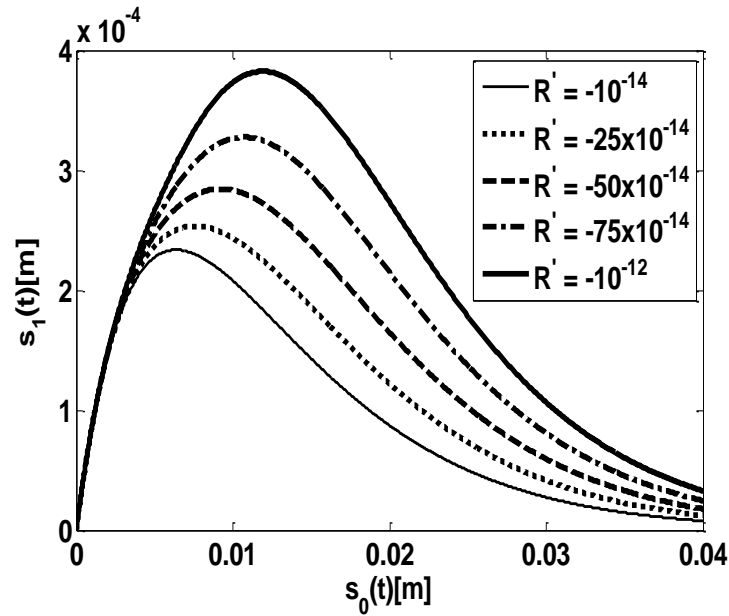


Figure 5.41 Perturbation in the solidification front as a function of  $s_0(t)$  for various values of  $R'$  and Al-Al-Cu material combination when  $u = 10 \text{ mm}$  and  $R'_m = -10^{-14} \text{ m}^2 \text{ sec}^\circ \text{C} / \text{J} . \text{Pa}$

When we investigated the effect of coupling between coating and mold for highly rigid coating layer, it is observed that this coupling rate has destabilizing effect on growth instability for thinner coating layer similar to the one observed in Figure 5.39. This destabilizing effect of coupling becomes more significant for highly rigid coating than more distortive one. Similarly,  $R'_m$  leads to increase in  $s_0^m$  for highly rigid thin coating layer. For thicker and highly rigid coating layer, coupling at coating/mold interface does not create the same remarkable effect on growth instability likewise the effect of coupling at shell/coating interface for thicker coating in Figure 5.41.  $R'_m$  has no effect on the growth of the perturbation and  $s_0^m$  for thicker and highly rigid coating layer

similar to the thicker and highly distortive coating layer. This result shows that coupling between coating and mold does not have any effect on the growth of the perturbation in solidified shell regardless of the thermal conductivity of coating material when the coating layer is selected thick enough. Additionally, increase in the coating thickness weakens the effect of the coupling between coating and mold.

### SUMMARY AND CONCLUSIONS

#### 6.1 Summary

A mathematical model is developed in this dissertation to investigate the thermoelastic instability mechanism during the solidification of pure metals on a coated mold of finite thickness. This study extends the previous works on growth instability during solidification process by investigating the effects of an added coating layer theoretically. The unstable growth of the shell during the solidification due to non-uniform heat extraction causes severe defects such as cracks in the casting. These defects lead to decrease in the quality and usability of the final casting product. Mold coating is one of the most important factors controlling the heat transfer rate and hence, it has a very important role on the solidification rate and the development of microstructure. The other important effects of mold coating are that it protects the mold, improves the quality of the mold surface and helps separation of the final cast from the mold.

Non-uniform heat extraction from the process depends on the thermal and mechanical events in the solidified shell, coating layer and mold. The thermal and mechanical problems are coupled through the contact pressure dependent thermal contact resistances at shell/coating and coating/mold interfaces. Stability analysis of the solidification process involves determination of the temperature fields and the development of the associated thermal stresses in the solidified shell, coating and mold. The thermal diffusivities of the solidified shell, coating layer and mold materials are assumed to be infinitely large. Physical meaning of this assumption is thermal capacity of these materials are zero and this assumption provides us to solve the heat conduction

and thermal stress problems analytically. Dependence of thermal stresses on the temperature field necessitates the solution of the heat conduction problem first. A linear perturbation method is used to reduce the spatial dimension of the problem from two to one.

Two second order differential equations with variable coefficients are obtained after modelling. They involve magnitude of the growth perturbation in solidified shell and residual stress function and their derivatives. These governing differential equations are written in state-space form and a variable step variable order predictor-corrector algorithm suitable for stiff problems is used to solve the final coupled governing equations numerically.

Finally in Chapter 5, the effects of the coating properties on the instability mechanism in the solidification process during casting of pure metals are investigated. The conditions which eliminate or minimize the profile defects in the casting associated with the coupled thermo-mechanic events are also determined in this chapter. The effects of the system parameters such as thickness of the coating layer, thermal conductivity ratio between the solidified shell and coating materials, thermal conductivity ratio between the coating and mold materials, wavelength of the perturbation in extracting heat at the bottom of the mold and thermal contact resistances at the interfaces on the growth instability during solidification process are analyzed in dimensionless form.

A case study is done which involves the solidification of pure aluminum on the different combinations of coating layer and mold materials. The effects of coating properties such as material and thickness and coupling rates between solidified shell/coating and coating/mold interfaces are investigated for real material combinations.

## **6.2 Conclusions**

The main goals of the present work are showing the effects of mold coating on the dynamics of the solidification process and suggesting design criteria to manufacturer for metal casting process to increase the quality of casting. For this purposes, the evolution of the growth perturbation in solidified shell is investigated for different process parameters such as properties of coating layer, coupling rates at shell/coating and coating/mold interfaces, thermal conductivity ratios between the solidified shell, coating layer and mold materials etc. The conditions for eliminating or minimizing the

growth instability during the solidification process are also determined. General results are summarized as follows:

The selection of the material of coating layer depending on the materials of solidified shell and mold and other system parameters is very important for improving the quality of the casting. The results show that decrease in the thermal conductivity of the coating material leads to more non-uniform growth regardless the values of coating thicknesses and material combinations of solidified shell and mold when the couplings are weak. When the coupling rates are increased, there are critical thermal conductivity ratios between the solidified shell and coating materials for leading most unstable or stable growth in the solidified shell depending on the conditions of coating thickness and materials of each solid layer.

When the solidified shell is more distortive than mold, the thermal conductivity of the coating material must be chosen far enough away from the thermal conductivity of shell material regardless of coating thickness to obtain more uniform growth in solidified shell in case where the coupling rate at the shell/coating interface is strong. On the other hand, when coupling between the coating and mold is increased, thermal conductivity of the coating material shows stabilizing effect on the growth of the solidifying shell for relatively thicker coating layer. For relatively thinner coating layer, the effects of thermal conductivity of coating material on the growth instability are changed depending on the thermal conductivity ratio between the shell and mold materials.

Thermal contact resistances at the shell/coating and coating/mold interfaces have similar effects on the growth instability during the solidification process. Under weak coupling rates they have destabilizing effect on the growth of the perturbation in solidified shell when solidified shell material is more distortive than the coating and mold. However, under same coupling rates, if the solidified shell is more rigid than the coating layer without noticing the distortivity of the mold then the growth instability becomes insensitive to changes of these thermal contact resistances. When the coupling rates are increased individually or together, the effects of the thermal contact resistances turns from destabilizing to stabilizing for the cases in which solidified shell is the most distortive layer in the process. Additionally, if the rigid mold is coated more distortive coating layer than itself and solidified shell, thermal contact resistance insensitiveness of the growth instability changes and they have stabilizing effect on the process for this case. When the distortivity of the solidified shell is less than the distortivities of the



mold and coating layer, the process is insensitive to changes of thermal contact resistances for all coupling rates combinations.

The effects of the wavelength of the added perturbation on the growth of the perturbation in solidified shell are also investigated in this study by using the wavenumber parameter. Wavenumber has an inverse proportion with the wavelength. When the wavenumber is increased, the perturbation grows faster and reaches smaller peak amplitudes than decays its steady state value. Assuming a random distribution of wavelengths in the initial perturbation, shorter wavelengths have stabilizing effect on the solidification process. Variation of the growth instability during the solidification depending on the wavenumber shows us the changing the surface topographies of coating layer or the mold has significant effect on the growth of the perturbation in solidified shell during the casting process.

Thickness of coating has different effects on the growth instability during solidification depending on the thermal conductivities of solidified shell, coating layer and mold materials and coupling rates at shell/coating and coating/mold interfaces.

When the thermal and mechanical problems are weakly coupled at the shell/coating and coating/mold interfaces, the coating thickness has destabilizing effect on the growth instability regardless of the coating material. The destabilizing effect of coating thickness turns to stabilizing when the coupling rates at shell/coating and coating/mold interfaces are increased one at a time or together.

Combined effects of coupling rates at the upper and lower surfaces of coating lead to increase in the sensitivity of the growth perturbation to the thickness of the coating. Both coupling rates between the solidified shell and coating and coating and mold have destabilizing effect on the growth instability for thin and highly distortive coating layer. These destabilizing effects of coupling rates diminish when the thickness of coating is increased. For highly distortive coating layer, increase in the coating thickness causes to reduce the sensitivity of the process to coupling between the solidified shell and coating and coating and mold. This result suggests that the thickness of the coating should be increased to eliminate the effects of the coupling rates at the shell/coating and coating/interfaces when more distortive coating layer is used.

Both coupling rates have destabilizing effect on the growth instability for thin highly distortive coating layer. However, the destabilizing effects of coupling rates diminish

when the thickness of coating is increased when the coating layer is selected highly distortive. On the other hand, an increase in the coating thickness causes to reduce the sensitivity of the process to coupling rates between the solidified shell and coating, and coating and mold for highly distortive coating layer. This result suggests that the thickness of the coating should be increased for eliminates the effects of the coupling rates at the shell/coating and coating/interfaces when more distortive coating layer is used.

Similarly, both coupling rates leads to more non-uniform growth of the perturbation in solidified shell for thin and highly rigid coating layer. It is observed that coupling between the shell and coating has significant destabilizing effect on the growth instability when the thermal conductivity of the coating material is increased. However, variation of thermal conductivity of coating layer does not change the effect of the coupling between the coating layer and mold on the growth instability for thicker coating layer. This means that coupling between coating and mold does not have any effect on the growth of the perturbation in solidified shell regardless of the thermal conductivity of coating material when the coating layer is selected thick enough.

### **6.3 Future Works**

The developed model in this study does not involve the effects of the thermal diffusivities of the solidified shell, coating layer and mold materials. This assumption is only valid for early stages of solidification. This study is extended by adding the effect of thermal diffusivities of the materials in the future study to analysis the full model of the solidification process during the casting of pure metals. The obtained results in this study are used as initial conditions in the solution of this full solidification problem.

On the other hand, the thermal and mechanical properties of the materials do not change depending on the temperature in this study. But however, in practice temperature is really affected the material properties such as thermal conductivity, density etc. Therefore the temperature dependence functions of the material properties are added to the model in the future.

The sensitivity of the thermal contact resistance to contact pressure is constant in our model. But the experimental works in the literature show that thermal contact resistance changes not linearly depending on the contact pressure. The mathematical relations

between thermal contact resistance and contact pressure can be taken into account in the future studies.

The inelastic deformations at the early stages of the solidification are neglected in the present work. When most of the solidified layer is still near the melting temperature, inelastic strains are occurred in the solidified layer and this may be sufficient to affect the stability behavior during the solidification.

The present mathematical model is restricted to the solidification of pure metals. The solidification of an alloy involving the presence of a mushy zone between the solid/liquid moving boundary is another challenging problem for future researchers. Additionally, the effect of densitiy change between the solid and liquid phase of shell material is also considered in the future studies.

Finally, this work involves the solidification of pure metals on a coated planar mold. In addition to mold coating, the non-uniform heat extraction is controlled also by adjusting the surface topography of the mold. The effects of the coating layer on the growth instability during the solidification of metals on the sinusoidal mold are the one of the cases to be investigated in the future works.

## REFERENCES

- 
- [1] Mazo A.B., Snegirev B.A., (1995). "Mathematical models of purification of a melt centrifuged at high temperatures", *Journal of Engineering Physics and Thermophysics*, 68(1):103-109.
  - [2] Hill J.M., Wu Y.H., (1994). "On a nonlinear Stefan problem arising in the continuous casting of steel", *Acta Mechanica*, 107(1-4):183-198.
  - [3] Davis M., Kapadia P., (1985). "Solution of a Stefan problem in the theory of laser welding by the method of lines", *Journal of Computational Physics*, 60(3):534–548.
  - [4] Huan Z., He S., Ma Y., (2003). "Numerical simulation and analysis for quick-frozen food processing", *Journal of Food Engineering*, 60(3): 267-273.
  - [5] Rabin Y., Shitzer A., (1997). "Combined solution of the inverse Stefan problem for successive freezing/thawing in non-ideal biological tissues", *Journal of Biomedical Engineering*, 119(2):146-52.
  - [6] Wang X. Q., Mujumdar A. S., Yap C., (2007). "Effect of orientation for phase change material (PCM)-based heat sinks for transient thermal management of electric components", *International Communications in Heat and Mass Transfer* 34(7): 801–808.
  - [7] Verdier D., Falcoz Q., Ferriere A., (2014). "Design of a protection thermal energy storage using phase change material coupled to a solar receiver", *High Temperature Materials and Processes*, 33(6):509-523.
  - [8] Stefan J., (1891). "Über die theorie der eisbildung inbesondee über die eisbindung im polarmeere", *Annalen der Physik.*, 42: 269-286.
  - [9] Evans G.W., (1951). "A note on the existence of a solution to a problem of Stefan", *Quarterly of Applied Mathematics*, 9:185-193.
  - [10] Douglas J., (1957). "A uniqueness theorem for the solution of a Stefan problem", *Proc. Amer. Math. Soc.*, 8:402-408.
  - [11] Junyi L., Mingyu X., (2009). "Some exact solutions to Stefan problems with fractional differential equations", *Journal of Mathematical Analysis and Applications*, 351(2):536–542.
  - [12] Crank, J (1984) *Free and moving boundary problem*. Oxford University Press, Oxford, UK.
  - [13] Hill, JM (1987) *One-dimensional Stefan problems, An Introduction*. Longman Scientific and Technical. New York, USA.

- [14] Barry S. I., Caunce J., (2008). "Exact and numerical solutions to a Stefan problem with two moving boundaries", *Applied Mathematical Modelling* 32:83–98.
- [15] Song T., Upreti K., Subbarayan G., (2015). "A sharp interface isogeometric solution to the Stefan problem", *Computer Methods in Applied Mechanics and Engineering*, 284:556–582.
- [16] Reutskiy S. Y., (2011). "A meshless method for one-dimensional Stefan problems", *Applied Mathematics and Computation*, 217:9689–9701.
- [17] Juric D., Tryggvason G., (1996). "A front-tracking method for dendritic solidification", *Journal of Computational Physics*, 123:127–148.
- [18] Murray W.D., Landis F., (1959). "Numerical and machine solutions of transient heat-conduction problems involving melting or freezing", *Journal of Heat Transfer*, 81:106–112.
- [19] Segal G., Vuik C., Vermolen F., (1998). "A conserving discretization for the free boundary in a two-dimensional Stefan problem", *Journal of Computational Physics*, 141:1–21.
- [20] Kutluay B, Bahadir AR, Ozdes A., (1997). "The numerical solution of one-phase classical Stefan problem", *Journal of Computational and Applied Mathematics*, 81:135 –144.
- [21] Caldwell J, Kwan Y.Y., (2002). "Nodal integral and enthalpy solution of one-dimensional Stefan problem", *Journal of Mathematical Sciences*, 13(2):99 –109.
- [22] Caldwell J, Savovic S, Kwan Y.Y. (2003). "Nodal integral and finite difference solution of one-dimensional Stefan problem", *Journal of Heat Transfer*, 125:523–527.
- [23] Caldwell J, Chiu C.K., (2000). "Numerical solution of one-phase Stefan problems by the heat balance integral method, Part I—cylindrical and spherical geometries", *Communications in Numerical Methods in Engineering*, 16:569 – 583.
- [24] Caldwell J, Chiu C.K., (2000). "Numerical solution of one-phase Stefan problems by the heat balance integral method, Part II—special small time starting procedure", *Communications in Numerical Methods in Engineering*, 16:585 –593.
- [25] Caldwell J., Kwan Y., (2004). "Numerical methods for one-dimensional Stefan problems", *Communications in Numerical Methods in Engineering*, 20:535–545.
- [26] Tarwidi D., Pudjaprasetya S. R., (2013). "Godunov Method for Stefan Problems with Enthalpy Formulations", *East Asian on Applied Mathematics*, Vol. 3, No. 2: 107-119.
- [27] Savovic S., Caldwell J., (2003). "Finite difference solution of one-dimensional Stefan problem with periodic boundary conditions", *International Journal of Heat and Mass Transfer*, 46:2911–2916.
- [28] Javierre E., Vuik C., Vermolen F. J., Van der Zwaag S., (2006). "A comparison of numerical model for one-dimensional Stefan problems", *Journal of Computational and Applied Mathematics*, 192:445-459.

- [29] Voller V. R., (1987). "An implicit enthalpy solution for phase change problems: with application to a binary alloy solidification", *Applied Mathematical Modelling*, 11:110-116.
- [30] Nedjar B., (2002). "An enthalpy-based finite element method for nonlinear heat problems involving phase change", *Computers and Structures*, 80: 9–21.
- [31] Chen S., Merriman B., Osher S., Smereka P., (1997). "A Simple Level Set Method for Solving Stefan Problems", *Journal Of Computational Physics* 135: 8–29.
- [32] Gibou F., Fedkiw R., Caflisch R., Osher S., (2003). "A Level Set Approach for the Numerical Simulation of Dendritic Growth", *Journal of Scientific Computing*, 19:1–3.
- [33] Mackenzie J. A., Robertson M. L., (2002). "A Moving Mesh Method for the Solution of the One-Dimensional Phase-Field Equations", *Journal of Computational Physics*, 181:526–544.
- [34] Sun Y., Beckermann C., (2007). "Sharp interface tracking using the phase-field equation", *Journal of Computational Physics*, 220:626–653.
- [35] Voller V. R., Falcini F., (2013). "Two exact solutions of a Stefan problem with varying diffusivity", *International Journal of Heat and Mass Transfer*, 58:80–85.
- [36] Esen A, Kutluay S., (2004). "A numerical solution of the Stefan problem with a Neumann-type boundary condition by enthalpy method", *Applied Mathematics and Computation*, 148:321–329.
- [37] Asaithambi A., (2007). "Numerical solution of Stefan problems using automatic differentiation", *Applied Mathematics and Computation*, 189:943–948.
- [38] Yang H., He Y., (2010). "Solving heat transfer problems with phase change via smoothed effective heat capacity and element-free Galerkin methods", *International Communications in Heat and Mass Transfer*, 37:385–392.
- [39] Vynnycky M., Mitchell S.L., (2015). "On the numerical solution of a Stefan problem with finite extinction time", *Journal of Computational and Applied Mathematics*, 276:98–109.
- [40] Mitchell S.L., Vynnycky M., (2014). "On the numerical solution of two-phase Stefan problems with heat-flux boundary conditions", *Journal of Computational and Applied Mathematics*, 264:49–64.
- [41] Myers T. G., Mitchell S. L., (2011). "Application of the combined integral method to Stefan problems", *Applied Mathematical Modelling*, 35:4281-4294.
- [42] Zabaras N., Ruan Y., (1990). "Moving and deforming finite-element simulation of two-dimensional Stefan problems", *Communications in Applied Numerical Methods*, 6:495-506.
- [43] Voller V. R., Swenson J. B., Paola C., (2004). "An analytical solution for a Stefan problem with variable latent heat", *International Journal of Heat and Mass Transfer*, 47:5387–5390.
- [44] Zhou Y., Wang Y., Bu W., (2014). "Exact solution for a Stefan problem with latent heat a power function of position", *International Journal of Heat and Mass Transfer* 69:451–454.

- [45] Salva N. N., Tarzia D. A., (2011). "Explicit solution for a Stefan problem with variable latent heat and constant heat flux boundary conditions", *Journal of Mathematical Analysis and Applications*, 379:240-244.
- [46] Natale M. F., Marcus E. A. S., Tarzia D., (2010). "Explicit solutions for one-dimensional two-phase free boundary problems with either shrinkage or expansion", *Nonlinear Analysis Real World Applications* 11(3):1946-1952.
- [47] Zabaras N., Mukherjee S., (1987). "An analysis of solidification problem by the boundary element method", *International Journal for Numerical Methods in Engineering*, 24:1879-1900.
- [48] Z. Dursunkaya, S. Nair, "Solidification of a finite medium subject to a periodic variation of boundary temperature", *Journal of Applied Mechanics* 70 (2003) 633-637
- [49] Skrzypczak T., Wegrzyn- Skrzypczak E., (2012). "Mathematical and numerical model of solidification process of pure metals", *International Journal of Heat and Mass Transfer*, 55:4276-7284.
- [50] Caldwell J., Kwan Y.Y., (2003). "On the perturbation method for the Stefan problem with time-dependent boundary conditions", *International Journal of Heat and Mass Transfer*, 46:1497–1501.
- [51] Pedroso R.I., Domoto G.A., (1973). "Exact solution by perturbation method for planar solidification of a saturated liquid with convection at the wall", *International Journal of Heat Mass Transfer*, 16:1816–1819.
- [52] Huang C.L., Shih Y.P., (1975). "Shorter communications: perturbation solution for planar solidification of a saturated liquid with convection at the wall", *International Journal of Heat Mass Transfer*, 18:1481–1483.
- [53] Pedroso R.I., Domoto G.A., (1973). "Perturbation solutions for spherical solidification of saturated liquids", *International Journal of. Heat Transfer* 95:42–46.
- [54] Stephan K., Holzknecht B., (1976). "Perturbation solutions for solidification problems", *International Journal of. Heat Mass Transfer* 19:597–602.
- [55] Yu Z. T., Fan L. W., Hu Y. C., Cen K. F., (2010). " Perturbation solution to heat conduction in melting or solidification with heat generation", *International Journal of. Heat Mass Transfer*, 46:479–483.
- [56] Yigit F., (2007). "A simplified analytical solution of a two-dimensional Stefan problem with a periodic boundary condition", *International Review of Mechanical Engineering* 1:703-714.
- [57] Yigit F., (2007). "Perturbation solution for solidification of pure metals on a sinusoidal mold surface", *International Journal of Heat and Mass Transfer*, 50:2624–2633.
- [58] Yigit F., (2008). "Approximate analytical and numerical solutions for a two-dimensional Stefan problem", *Applied Mathematics and Computation*, 202:857–869.
- [59] Yigit F., (2008). "Sinusoidal perturbation solution for solidification of pure materials on a planar mold of finite thickness", *International Journal of Thermal Sciences*, 47:25–34.

- [60] Yigit F., (2008). "Approximate analytical solution of a two-dimensional heat conduction problem with phase-change on a sinusoidal mold", *Applied Thermal Engineering*, 28:1196–1205.
- [61] Yigit F., (2011). "One-dimensional solidification of pure materials with a time periodically oscillating temperature boundary condition", *Applied Mathematics and Computation*, 217:6541–6555.
- [62] Hu H., Argyropoulos S. A., (1996). "Mathematical modelling of solidification and melting: a review", *Modelling and Simulation in Material Science and Engineering*, 4:371-396.
- [63] Zabaras N., Ruan Y., Richmond O., (1992). "Design of two-dimensional Stefan processes with desired freezing front motions", *Numerical Heat Transfer Part B*, 21:307-325.
- [64] Onyejekwe O. N., (2014). "The Solution of One-Phase Inverse Stefan Problem by Homotopy Analysis Method", *Applied Mathematical Sciences*, 8(53):2635 – 2644.
- [65] Zabaras N., Liu J. C., (1988). "An analysis of two dimensional linear inverse heat transfer problems using an integral method", *Numerical Heat transfer*, 13:527-533.
- [66] Zabaras N., Mukherjee S., Richmond O., (1988). "An analysis of inverse heat transfer problems with phase changes using an integral method *International Journal of Heat and Mass Transfer*, 110:554-561.
- [67] Zabaras N., Ruan Y., (1989). "A deforming FEM analysis of inverse Stefan problems", *International Journal for Numerical Methods in Engineering*, 28: 295-313.
- [68] Yang G. Z., Zabaras N., (1998). "An adjoint method for the inverse design of solidification processes with natural convection", *International Journal for Numerical Methods in Engineering*, 42:1121-1144.
- [69] Zabaras N., Yuan K., (1994). "Dynamic programming approach to the inverse Stefan design problem", *Numerical Heat Transfer Part B* 26: 97-104.
- [70] Sampath R., Zabaras N., (2001). "Inverse design of directional solidification processes in the presence of strong external magnetic field", *International Journal for Numerical Methods in Engineering*, 50:2489-2520.
- [71] Tien R. H., Koump V., (1969). "Thermal stresses during solidification on basis of elastic model", *Journal of Applied Mechanics*, 36(4):763-767.
- [72] Richmond O., Tien R. H., (1971). "Theory of thermal stresses and iar-gap formation during the early stages of solidification in rectangular mold", *Journal of the Mechanics and Physics of Solids*, 19:273-284.
- [73] Heinlein M., Mukherjee S., Richmond O., (1986). "A boundary elemnt method analysis of temperature fields and stresses during solidification", *Acta Mechanica*, 59:59-81.
- [74] Chen X. J., Nakano S., Liu L. J., Kakimoto K., (2008) "Study on thermal stress in a silicon ingot during a unidirectional solidification process", *Journal of Crystal Growth*, 310:4330–4335.



- [75] Zhang L., Shen H. F., Rong Y., Huang T. Y., (2007). "Numerical simulation on solidification and thermal stress of continuous casting billet in mold based on meshless methods", *Materials Science and Engineering A*, 466:71–78.
- [76] Liu B. C., Kang J. W., Xiong S. M., (2001). "A study on the numerical simulation of thermal stress during the solidification of shaped castings", *Science and Technology of Advanced Materials*, 2:157-164.
- [77] Risso J. M., Huespe A. E. and Cardona A., (2000). "Thermal stress evaluation in the steel continuous casting process", *International Journal for Numerical Methods in Engineering*, 65(9):1355 – 1377.
- [78] Meng Y., Li C., Parkman J., and Thomas B. G., "Simulation of shrinkage and stress in solidifying steel shells of different grades", *Solidification Processes and Microstructures: A symposium in honor of Wilfried Kurs*, TMS, March 15-18, 2004, Charlotte, NC.
- [79] Xue X., Wang Y. P., (2013). "Numerical simulation of casting thermal stress based on finite difference method", *Reviews On Advanced Materials Science*, 33:410-415.
- [80] Sadrossadat S. M., Johansson S., (2009). "The effects of casting parameters on residual stresses and microstructure variations of an Al. Si cast alloy", *Int. Centre for Diffraction Data*: pp, 553-560
- [81] Uehara T., Fukui M., Ohno N., (2008). "Phase field simulations of stress distributions in solidification structures", *Journal of Crystal Growth* 310:1331–1336.
- [82] Farhangi H., Norouzi S., Nili-Ahmadabadi M., (2004). "Effects of casting process variables on the residual stress in Ni-base superalloys", *Journal of Materials Processing Technology*, 153:209-212.
- [83] Uehara T., (2011). "A phase field modelling for multi-scale deformation mechanics of polycrystalline metals", *Procedia Engineering*, 10:1779–1784.
- [84] Thomas B. G., Samarasekera I. V., Brimacombe J. K., (1987). "Mathematical model of the thermal processing of steel ingots: Part II. Stress model", *Metallurgical Transactions B*, 18:131-147.
- [85] Singh S., Blazek K., (1974). "Heat Transfer and Skin Formation in a Continuous Casting Mold as a Function of Steel Carbon Content", *J. Metals*, 17-27
- [86] Cisse J., Cole G., Bolling G., (1971). "Freezing Front Asymmetry During Ingot Solidification of Aluminum and Its Alloys," *AFS Cast Metals Research Journal*, 7:158-161.
- [87] Wray P. J., (1977). "Nonuniform Growth of a Plate Solidifying on a Chilled Surface," *Presentation Notes, Proceedings of the AIME Conference*, Atlanta, GA
- [88] Wray P. J., (1981). "Geometric Features of Chill-Cast Surfaces", *Metallurgical and Materials Transactions B*, 12:167–176.
- [89] Hanao M., Kawamoto M., Yamanaka A., (2009). "Growth of solidified shell just below the meniscus in continuous casting mold", *ISIJ International* 49:365-374.

- [90] Yamaguchi R., Suzuki M., Katuhiko M., (1995). "Control of uneven shell formation of stainless in early stages of solidification", *Material Science and Technology*, 13: 3-11.
- [91] Sigutani Y., Nakamura M., Okuda M., Kawasaki M., Miyahara S., (1992). "Control of Uneven Solidified Shell Formation of Hypo-peritectic Carbon Steels in Continuous Casting Mold", *Trans. Iron Steel Inst. Jpn*, B-91.
- [92] Konishi J., Militzer M., Brimacombe J. K., Samarasekera I. V., (2002). "Modeling the formation of longitudinal facial cracks during continuous casting of hypoperitectic steel", *Metall. and Mate. Trans. B: Process Metall. and Mate. Processing Sci.*, 33:413-423.
- [93] Suzuki M., Yamaoka Y., (2003). "Influence of carbon content on solidifying shell growth of carbon steels at the initial stages of solidification", *Materials Transactions*, 44:836-844.
- [94] Yamaguchi R., Suzuki M., Katuhiko M., (1995). "Control of uneven shell formation of stainless in early stages of solidification" *Metall. Sci. and Tech.*, 13:3-11.
- [95] Richmond O., Huang N. C., (1977). "Interface stability during unidirectional solidification of a pure metal", *Proc 6<sup>th</sup> Canadian Congress of Applied Mechanics*, Vancouver.
- [96] Li N. Y., Barber J. R., (1989). "Sinusoidal perturbation solutions for planar solidification", *International Journal of Heat and Mass Transfer*, 32:935-941.
- [97] Richmond O., Hector L. G., Fridy J. M., (1990). "Growth Instability During Non-Uniform Directional Solidification of Pure Metals", *Journal of Applied Mechanics*, 57:529-536.
- [98] Zabaras N., Ruan Y., Richmond O., (1990). "Front tracking thermo mechanical model for hypoelastic-viscoplastic behavior in a solidifying body", *Computer Methods in Applied Mechanics and Engineering*, 81:333-364.
- [99] Zabaras N., Ruan Y., Richmond O., (1991). "On the calculation of deformations and stresses during axially symmetric solidification", *Journal of Applied Mechanics*, 58:865-871.
- [100] Li N.-Y., Barber J. R., (1991). "Thermoelastic Instability in Planar Solidification", *International Journal of Mechanical Science*, 33:945-959.
- [101] Yigit F., Li N.Y., Barber J.R., (1993). "Effect of Thermal Capacity on Thermoelastic Instability During the Solidification of Pure Metals", *Journal of Thermal Stresses*, 16:285-309.
- [102] Yigit F. Barber J.R., (1994). "Effect of Stefan Number on Thermoelastic Instabilities in Unidirectional Solidification", *International Journal of Mechanical Science*, 36:707-723.
- [103] Zabaras N., Kang S., (1990). "Thermomechanical final state design of unidirectional solidification processes", *Journal of Materials Processing and Manufacturing Science*, 2:141-157.
- [104] Hector Jr. L.G., Li N.Y., Barber J.R., (1994). "Strain rate relaxation effect on freezing front growth instability during planar solidification of pure metals, part 1 Uncoupled theory", *Journal of Thermal Stresses*, 17(4):619-645.

- [105] Li N.Y., Hector L.G., Barber J.R., (1995). "Strain rate relaxation effect on freezing front growth instability during planar solidification of pure metals, part 2 Coupled theory", *Journal of Thermal Stresses*, 18(1):69-85.
- [106] Hector Jr L.G., Kim W.S., Richmond O, (1996). "Freezing range effect on shell growth instability during alloy solidification," *Journal of Applied Mechanics*, 63:594-602.
- [107] Yigit F., (1998). "Effect of mold properties on thermoelastic instability in unidirectional planar solidification", *J. Thermal Stresses*, 21: 55-81.
- [108] Murakami H., Suzuki M., Kitagawa T., Miyahara S., (1992). "Control of Uneven Solidified Shell Formation of Hypo-peritectic Carbon Steels in Continuous Casting Mold," *Transaction of Iron and Steel Institute Japan.*, 78:105–112.
- [109] Anyalebechi P. N., (2007). "Undulatory solid shell growth of aluminum alloy 3003 as a function of the wavelength of a grooved mold surface topography", *Material Processing Fundamentals*, 31-47.
- [110] Anyalebechi P. N., (2007). "Ungrooved mold surface topography effects on cast subsurface microstructure", *Material Processing Fundamentals.*, 49-62.
- [111] Laki R.S., Beech J., Davies G. J., (1985). "Surface Structures of Chill and Continuously Cast Stainless Steels," *Ironmaking Steelmaking*, 12:233–241.
- [112] Morales A., Glicksman M. E., Biloni H., (1997). "Influence of Mould Wall Microgeometry on Casting Structure," *Proc. Int. Conf. on Solidification*, Sheffield Metallurgical Eng. Assn., Univ. Sheffield, and The Metals Society, Sheffield, U.K.
- [113] Zhao K., Shen M., Wang, X. (2005). "Simulation of inside-grooved mould improving heat transfer of original shell of casting slab", *Journal of University of Science and Technology Beijing: Mineral Metallurgy Materials*, 12:23-25.
- [114] Zhang L. F. Shen M. G. Miao X. C. Xu H. L. Chen Z. W. (2008) "Thermo-mechanical coupled simulation of initial shell formation in grooved mold of slab caster", *Kang T'ieh/Iron and Steel (Peking)*, 43 (6): 35-37.
- [115] Haga T., Motomura M., (1994). "Effect of Polishing Condition on the Roll of the Surface of Foils of Pure Aluminum and Al-Si Alloy Manufactured by Single Roll Rapid Solidification," *Journal of Japan Institute of Light Metals*, 44:22–27.
- [116] Hector L.G., Kim W.S., Howarth J., (1999). "Thermomechanical models of pure metal solidification on a periodic mold surface", *Journal of Thermal Stresses*, 22 (2):125-158.
- [117] Yigit F., Hector Jr. L. G., (2002). "Solidification of a pure metal with finite thermal capacitance on a sinusoidal mold surface", *Journal of Thermal Stresses*, 25:663-690.
- [118] Yigit F., (1999). "Growth instability during planar solidification with a mold of finite thermal capacity", *Journal of Thermal Stresses*, 22:757-779.
- [119] Hector Jr L.G., Howarth J.A., Richmond O., Kim,W.S., (2000). "Mold Surface Wavelength Effect on Gap Nucleation in Solidification," *Journal of Applied Mechanics*, 67:155-164.

- [120] Yigit F., Hector L.G., (2000). "Critical Wavelengths for Gap Nucleation in Solidification. Part 1: Theoretical Methodology", *Journal of Applied Mechanics* , 67:66-76.
- [121] Yigit F., Hector L. G., (2000). "Critical Wavelengths for Gap Nucleation in Solidification. Part 2: Results for selected mold-shell material combinations", *Journal of Applied Mechanics* , 67:77-86.
- [122] Howarth J. A., Hector Jr. L.G., (2001). "A thermomechanical model of solidification on a plane wall with a single asperity of arbitrary shape", *Journal of Thermal Stresses*, 24:753-778.
- [123] Howarth J. A., Hector Jr. L. G., (2001). "A thermomechanical model of solidification on a mold moving with constant velocity", *Journal of Thermal Stresses*, 24:937-985.
- [124] Yigit F., Hector L. G., Richmond O.,(2002). "A theoretical investigation of pure metal solidification on a deformable mold in the absence of interfacial coupling", *Journal of Thermal Stresses*, 25(8):773-809.
- [125] Yigit F., (2004). "Existence of critical wavelength for gap nucleation in solidification on a rigid mold",*Journal of Applied Mechanics.*, 71:96-108.
- [126] Yigit F., (2005). " Combined effects of mold deformation and shell thermal capacity on growth instability during unidirectional solidification of pure metals", *Journal of Thermal Stresses*, 28(12):1199-1226.
- [127] Yigit F., (2007). "Role of the mold properties on gap nucleation in solidification", *Journal of Thermal Stresses*, 30(11):1137-1158.
- [128] Samanta D., Zabaras N., (2005). "Numerical study of macrosegregation in Aluminum alloys solidifying on uneven surfaces", *International Journal of Heat and Mass Transfer*, 48:4541–4556.
- [129] Lewis R., Ransing R., (1998). " A correlation to describe interfacial heat transfer during solidification simulation and its use in the optimal feeding design of castings",*Metallurgical and Materials Transactions B*, 29:437-448.
- [130] Tan L., Zabaras N., (2004). "Modeling the effects of mold topography on aluminum cast surfaces", *Solidification of Aluminum Alloys*, Edited by TMS.
- [131] Samanta D., Zabaras N., (2004). "Solidification and macrosegregation in aluminum alloys on uneven surfaces", *CFD Modeling and Simulation in Materials Processes*, TMS.
- [132] Tan L., Zabaras N., (2005). "A thermomechanical study of the effects of mold topography on the solidification of aluminum alloys", *Materials Science and Engineering: A*, 404:197-207.
- [133] Samanta D., Zabaras N., (2005), " A coupled thermomechanical, thermal transport and segregation analysis of the solidification of aluminum alloys on molds of uneven topographies", *Materials Science and Engineering: A*, 408:211-226.
- [134] Sanz A., (2001). "Tribological behavior of coatings for continuous casting of steel", *Surface and Coating Technology*, 146-147:55-64.
- [135] Chen X., Ji Y., Zhang S., Li J., (2015). " Increasing the cooling rate of Cu mold by liquid alloy coating", *Materials Letters*, 151:35-37.

- [136] Jafari H., Idris M. H., Ourdjini A., Karimian M., Payganeh G., (2010). "Influence of gating system, sand grain size, and mould coating on microstructure and mechanical properties of thin-wall ductile iron", *Journal of Iron and Steel Research*, 17 (12):38-45.
- [137] Chen S. C., Chang Y., Chang Y. P., Chen Y. C., Tseng C. Y., (2009). "Effects of cavity surface coating on mold temperature variation and the quality of injection molded parts", *International Communications in Heat and Mass Transfer*, 36:1030-1035.
- [138] Salas O., Kearns K., Carrera S., Moore J. J., (2003). "Tribological behavior of candidate coatings for Al die casting dies, *Surface and Coatings Technology*", 172:117-127.
- [139] Karimian M., Ourdjini A., Idris M. H., Jafari H., (2012). "Effect of pattern coating thickness on characteristics of lost foam Al-Si-Cu alloy casting", *Trans. Nonferrous Met. Soc. China*, 22:2092-2097.
- [140] Acimovic-Pavlovic Z. S., Prstic A. K., Andric L. D., ) (2007). "The characterization of TALC –based coating for application for Al-Si alloy casting", *Chemical Industry & Chemical Engineering Quarterly*, 13:138-40.
- [141] Hamasaiid A., Dargusch M. S., Davidson C. J., Tovar S., Loulou T., Rezai-Aria F., Dour G., (2007). "Effects of mold coating materials and thickness on heat transfer in permanent mold casting of aluminum alloys", *Metallurgical and Materials Transactions A*, 38:1303-1316.
- [142] Lu H. S., Yaokawa J., Anzai K., (2006). "Effect of die-surface treatment on magnesium alloys fluidity", *Materials Transactions*, 27:883-888.
- [143] Borouni M., Niroumand B., Fathi M. H., (2014). "Effect of a nano-ceramic mold coating on the fluidity length of thin-wall castings in A14-1 alloy gravity sand casting", *Materials and technology* 48(4):473–477.
- [144] Zhang W., Yu Y., Fang Y., Li J. G., (2011). "Effect of coating on instantaneous interfacial heat transfer during near-rapid solidification", *Journal of Iron Steel Research*, 18:67-73.
- [145] Lee K. Y., Cho G. S., Choe K. H., Jo H. H., Ikenaga A., Koroyasu S., (2006). "Effects of reduced pressure and coat permeability on casting characteristics of magnesium alloy in evaporative pattern casting process", *Materials Transactions* 47:2798-2803.
- [146] Srivastava A., Vivek J., Shivpuri R., Bhattacharya R., Dixit S., (2003). "A multilayer coating architecture to reduce heat checking of die surfaces", *Surface and Coatings Technology*, 163:631–636.
- [147] Shivpuri R., Chu Y. L., Venkatesan , Conrad J. R., Sridharan K., Shamim M., Fetherston R. P., (1996). "An evaluation of metallic coatings for erosive wear resistance in die casting applications, *Wear*, 192:49-55.
- [148] Sulaiman S., Ariffin M. K. A. M., Tang S. H., Saleh A., (2013). "Influence of pattern coating thickness on porosity and mechanical properties of lost foam casting of Al-Si (LM6) alloy", *Applied Mechanics and Materials V. 333-301*:1281-1284

- [149] Sands M., Shivkumar S., (2003). "Influence of coating thickness and sand fineness on mold filling in the lost foam casting process", *Journal of Material Science*, 38:667-673.
- [150] Nwaogu U. C., Tiedje N. S., (2011). "Foundry coating technology: A review", *Materials Science and Applications*, 2:1143-1160.
- [151] Turgut M. N., Demir M. H., Yigit F., (2012). "Effect of mold coating on shell morphology in solidification", *Advanced Materials Research* , 445:325-330.
- [152] Hanna M. D., Kleber R. M., inventors; GM Global Technology Operations, Inc., assignee. Rotor assembly and method. US patent 7,594,568 B2. 2009 Sep 29.
- [153] Hanna M. D., Sung S. H., inventors; GM Global Technology Operations, Inc., assignee. Damped product with an insert having a layer including graphite thereon and methods of making and using the same. US patent 8,758,902 B2. 2014 Jun 24.
- [154] Schroth J. G., Hanna M. D., Hamma R. H., Dessouki O. S., Lowe B. D., Riefe M. T., Short J. W., Verbrugge M. W., inventors; GM Global Technology Operations, Inc., assignee. Method of casting components with inserts for noise reduction. US patent 7,644,750 B2. 2010 Jan 12.
- [155] Hanna M. D., Schroth J. G., Dessouki O. S., inventors; GM Global Technology Operations, Inc., assignee. Bi-metal disc brake rotor and method of manufacturing. US patent 7,775,332 B2. 2010 Aug 17.
- [156] Agarwal P., Sachdev A. K., Sundurraj S., inventors; GM Global Technology Operations, Inc., assignee. Insert with tabs and damped products and methods of making the same. US patent 7,836,938 B2. 2010 Nov 23.
- [157] Golden M. A., Ulieny J. C., Hanna M. D., inventors; GM Global Technology Operations, Inc., assignee. Insert with filler to dampen vibrating components. US patent 8,104,162 B2. 2012 Jan 31.
- [158] Hanna M. D., Sundar M., Schertzer A., inventors; GM Global Technology Operations, Inc., assignee. Casting noise-damped, vented brake rotors with embedded inserts. US patent 8,118,079 B2. 2012 Feb 21.
- [159] Hanna M. D., Schroth J. G., inventors; GM Global Technology Operations, Inc., assignee. Coulomb damped disc brake rotor and method of manufacturing. US patent 8,245,758 B2. 2012 Aug 21.
- [160] Hanna M. D., Sundar M., Schertzer A., inventors; GM Global Technology Operations, Inc., assignee. Method of casting damped part with insert. US patent 7,950, 441, B2. 2011, May 31.
- [161] Fletcher L. S., (1988), "Recent developments in contact conductance heat transfer", *ASME Journal of HEat Transfer*, 110, 4B, 1059-1070.
- [162] Barber J. R., Dundurs J., Comninou, (1980), " Stability considerations in thermoelastic contact", *ASME Journal of Applied Mechanics*, 47, 229-232
- [163] Zhang, R., Barber J. R., (1990), "Effect of material properties on the stability of static thermoelastic contact", *ASME Journal of Applied Mechanics*, 57, 365-369.

- [164] Byrne, G. D., Hindmarsh, A. C., (1975), "A polyalgorithm for the numerical solution of ordinary differential equations", *ACM Trans. On Math. Soft.*, 1, 71-96.
- [165] Dundurs, J., (1974), "Distortion of a Body Caused by Free Thermal Expansion", *Mech. Res. Commun.*, 1, 121-124.
- [166] Boltz, R. E., Tuve, G. L., (1984), "CRC Handbook of Tables for Applied Engineering and Science", CRC Press, Boca Raton, FL.
- [167] Baumeister, T., Avallone, E. A., Baumeister, T. III., (1978), "Marks' Standard Handbook for Mechanical Engineers, 8th ed.", McGraw-Hill, New York.
- [168] L. D. Lucas, L. D., (1972), "Density of Metals at high temperatures in the solid and molten states, Part 2", *Mem. Sci. Rev. Met.*, 69, (6), 479-492.
- [169] Wawra, H. H., (1974), "The Elastomechanical Properties of Pure Iron and FeS<sub>2</sub> in Different Crystallographic Directions as a Function of Temperature and Pressure", *Arch. Eisenhuettenwes.*, 45, (5), 317-320.
- [170] Touloukian, Y. S., Powell, R. W., Ho, C. Y., Klemens, P. G., (1970), "Thermophysical properties of matter: thermal conductivity", Vol. 1, IFI/Plenum, New York.
- [171] Touloukian, Y. S., Kirby, R. K., Taylor, R. E., Desai, P. D., (1978), "Thermophysical properties of matter: thermal expansion", Vol. 12, IFI/Plenum, New York.
- [172] Lucas, L. D., (1972), "Density of Metals at high temperatures in the solid and molten states, Density of Metals at High Temperatures in the Solid and Molten States, Part 1", *Mem. Sci. Rev. Met.*, 69, (5), 395-409.
- [173] Ledbetter, H. M., Naimon, E. R., (1974), "Elastic Properties of Metals and Alloys, II. Copper," *J. Phys. Chem. Ref. Data*, 3, 897-935.
- [174] Wawra, H. H., (1978), "Accurate Elastomechanical Values of Copper Materials," *Metall.*, 32, 346-348.

## CURRICULUM VITAE

---

### PERSONAL INFORMATION

**Name Surname** : MEHMET HAKAN DEMİR  
**Date of birth and place** : 15.09.1986 ÇAYELİ  
**Foreign Languages** : English  
**E-mail** : [mehmethakandemir@yahoo.com](mailto:mehmethakandemir@yahoo.com)

### EDUCATION

Degree	Department	University	Date of Graduation
Master	Mechatronics Engineering	Istanbul Technical University	2012
Undergraduate	Mechatronics Engineering	Kocaeli University	2009
High School	Hamdi Bozbağ Anatolian High School		2004

### WORK EXPERIENCE

Year	Corporation/Institute	Enrollment
2009	Yıldız Technical University	Research Assistant



## PUBLISHERMENTS

### Papers

1. Turgut, M.N.,**Demir, M.H.**,Yigit, F., 2012, “Effect of Mold Coating on Shell Morphology in Solidification”, Advanced Materials Research,Vol:445, page: 325-330.
2. **Demir, M.H.**, Yigit, F.,2016,”Early Time Perturbation Solution of Solidification on a Coated Sinusoidal Mold of Finite Thickness”, Journal of Adv. Mater. Pro. Tech. Vol: (1) Issue:3-4 327-337.

### Under Review Journal Papers

1. **Mehmet Hakan Demir** and Faruk Yigit, “A Theoretical Heat Transfer Model for Solidification of Pure Metals on a Coated Sinusoidal Mold of Finite Thickness”, *International Journal of Heat and Mass Transfer*, Under Review
2. **Mehmet Hakan Demir** and Faruk Yigit, “Effect of Coating Material on the Growth Instability in Solidification of Pure Metals on a Coated Planar Mold of Finite Thickness”, *Journal of Solids and Structures*, Under Review
3. **Mehmet Hakan Demir** and Faruk Yigit, “Thermoelastic Stability Analysis of Solidification of Pure Metals on a Coated Planar Mold of Finite Thickness”, *Journal of Manufacturing Processes*, Under Review

### Conference Papers

1. **Demir, M.H.**, Yigit, F.,2014, “Dynamic Analysis and Fuzzy Logic Based Control of a Cantilever Pipe Conveying Fluid”, AMPT 2014, Dubai, United Arab Emirates,16-20 November 2014
2. **Demir, M.H.**, Yigit, F.,2014,”Early Time Perturbation Solution ofSolidification on a Coated Sinusoidal Mold of Finite Thickness”, AMPT 2014, Dubai, United Arab Emirates,16-20 November 2014
3. Kırılı,A., **Demir, M.H.**, Büyükşahin, U., Tüfekçi C. S., Yiğit, F.,2013,”Çift Sarkaç (Pendubot) Sisteminin Dinamik Analizi ve Görüntü Geri Beslemeli Kontrolü”,TOK 2013 ,26-28 Eylül 2013, Malatya

4. **Demir, M. H.**, Yesildirek, A., Yigit, F., 2015, “ Control of a cantilever pipe conveying fluid using Neural Network”, IEEE Conference ICMSAO15, Istanbul, Turkey
5. **Demir, M.H.**, Yigit, F.,2016,” Effects of Coating Properties on the Growth Instability during the Early Stages of Solidification of Pure Metals on a Coated Planar Mold”, Thermal Stresses Congress, 5-9 June 2016, Salerno, Italy

#### **Book Chapter**

1. Akdoğan E.,**Demir M.H.**: "Rehabilitation Technologies: Biomechatronics Point of View", A Roadmap of Biomedical Engineers and Milestones, InTech - Open Access Publisher, ISBN 979-953-307-731-3, 2012.

#### **Projects**

1. Avrupa Birliği, LEONARDO DA VINCI PROGRAMI YENİLİK TRANSFERİ (ToI) PROJESİ, *Implementation of artificial intelligent technologies in rehabilitation engineering: Training for vocational rehabilitation counsellors (INTECH)*, Proje No: 2010-1-TR1-LEO05-16695, **Araştırmacı**, Bitti
2. BAP Projesi, *Eksenli Router’larda Yazıcı Ana Kartının Hareket Kontrol Kartı Olarak Kullanılması*, **Araştırmacı**, Devam Ediyor
3. TÜBİTAK 1512, *Acil hasta transferinde hastayı darbelerden korumaya ve konforunu arttırmaya yönelik ambulans içi pasif ve aktif süspansiyon sistemleri tasarımlarının geliştirilmesi*, **Proje Sahibi**, Devam Ediyor